東海大学大学院　令和2年度 博士論文

Research of Coastal Erosion in Thailand and Rational Methods for Planning Suitable Countermeasures

(タイ国における海岸侵食と適切な対策を立案するための合理的手法の研究)

指 導　山 本 吉 道 教 授

東海大学 大学院 総合理工学研究科

総合理工学専攻

Kornvisith Silarom

Research of Coastal Erosion in Thailand and Rational Methods for Planning Suitable Countermeasures

Kornvisith Silarom

Table of Contents

List of Tables

List of Figures

List of abbreviations and symbols

Chapter 2

Abbreviations and symbols	Description
b	subscription b denotes the breaking point
c	the overtopping coefficient
C_g	the wave celerity
C_s	the settling rate of the suspended materials
C_{ut}	the uptake rate of the suspended materials
d	the instantaneous water depth
D_B	the height of berm (from mean sea level)
D_C	the depth of closure
E	the wave energy
f_c	the bed friction coefficient
g	the gravitational acceleration
H	the incident wave height
h	the still water depth
H_0	the offing wave height
H_s	the significant wave height
K_1	the calibration coefficient
K_2	the calibration coefficient
L_0	the wavelength in deep water
M_{bx}	the wave energy loss due to wave breaking in x-direction
M_{by}	the wave energy loss due to wave breaking in y-direction
q (in the one-line model)	the offshore (on-off) sediment transport rate
q (in Yamamoto and Horikawa's formula)	the irregular or regular wave overtopping rate
Q (in Ca et al.'s model)	the total discharge
Q (in the one-line model)	the longshore sediment transport rate
q (in Van da meer's formula)	the irregular wave overtopping rate
q_{bx}	the bed load transportation rate in x-direction
q_{by}	the bed load transportation rate in y-direction
q_x	the depth integrated flow discharge in x-direction
q_y	the depth integrated flow discharge in y-direction
R in Equation (2.14)	the wave run-up height
R in Equation (2.16)	the vertical length from the still water level to the wave run-up height

R_c	the crown height of a dike
$R_{u2\%}$	the 2 % run-up level above the still water line
S_{op}	the wave breaking parameter
tanβ	the beach slope
x	the longshore distance
X_0	the horizontal length of the shape of the wave run-up profile
y	the offshore distance
α	the equivalent slope of a dike
α in Equation (2.14)	the hypothetical slope
α in Equation (2.16)	the surface slope
α_b	the incident wave breaking angle
β	the beach slope
γ_b	the reduction factor for the influence of a berm
γ_f	the reduction factor for the slope roughness
γ_r	the reduction factor for the surface roughness
γ_β	the reduction factor for oblique wave attack
ε_s	the porosity coefficient of the bed load
ζ	the bottom elevation
η	the water surface elevation
λ	the porosity coefficient
ρ_s	the density of sand
ρ_w	the density of water

Chapter 3

Abbreviations and symbols	Description
c in Equation (3.4)	the fluid force coefficient
C_D	the drag force coefficient
C_d	the reduction coefficient for the changing of the layer thickness
C_{D50}	the modification coefficient for the median grain size
C_M	the coefficient of inertia
C_x	the reduction coefficient for the inner length inside a structure
d	the thickness of the backfilling materials
d in Equations (3.24)–(3.25)	the representative size of the wave dissipation unit
d	the thickness of the backfilling materials
D_{50}	the median grain size of the backfilling materials

D_{50} in Equation (3.1)	the median grain size of the bed
d_{max}	the maximum thickness of the backfilling materials
d_t	the thickness of the backfilling materials
d_t (in Ioroi and Yamamoto's formula)	the layer thickness at the lowest edge of the structure
f	the outflow coefficient
F	the VOF function
g	the gravitational acceleration
h	the still water depth
H	the incident wave height
h_t	the water depth at the front of the structure
i	subscription i denotes the mesh number in x-direction
m	a coefficient in Equation (3.1)
p	the excess pore water pressure
p^*	the water pressure
P_{CAD}	the calculated pressure from CADMAS-SURF
p_{MOD}	the modified pressure
P_{obmax}	the maximum excess pore water pressure during all return flows
q in Equation (3.1)	the bed load transportation rate
q in Equation (3.7)	the outflow rate of the backfilling materials (included porosity)
R_x	the drag force in the horizontal direction
R_z	the drag force in the vertical direction
t	the elapsed time
T	the incident wave period
t	superscript t donates time
u in Equation (3.3)	the return flow velocity
u in Equations (3.14)–(3.15)	the velocity in the horizontal direction
U_{CAD}	the calculated velocity in the horizontal direction from CADMAS-SURF
v	the flow velocity
V_{max}	the maximum return flow velocity in the horizontal direction
w	the velocity in the vertical direction
w_s	the settling velocity
x	the horizontal coordinate
x	the inner length inside a structure
x_{max}	the total length of a structure
z	the vertical coordinate
α_0	the coefficient for D–F method
β	the proportional coefficient
β_0	the coefficient for D–F method
γ_v	the porosity

γ_x	the sectional permeability in the horizontal direction
γ_z	the sectional permeability in the vertical direction
Δt	the time step
Δx	the mesh size in the horizontal direction
Δz	the mesh size in the vertical direction
θ	the Shield parameter (dimensionless shear stress acting on the backfilling materials)
θ in Equation (3.1)	the Shield parameter (dimensionless shear stress acting on the bed)
θ_c	the critical Shield parameter (dimensionless shear strength of the backfilling materials)
θ_c in Equation (3.1)	the critical Shield parameter (dimensionless shear strength of the bed)
θ_{repose}	the repose angle of the backfilling materials
ν_e	the kinematic viscosity
ρ_s	the density of the backfilling materials
ρ_w	the density of water
τ_f	the shear stress acting on the backfilling materials generated by the return flow
τ_r	the shear strength of the backfilling materials
ϕ	the friction angle of the backfilling materials

List of Publications

This dissertation is based on the following publications:

1. Silarom, K., Yamamoto, Y., and Yoshizawa, S. (2019). “Numerical Model for Predicting the Sand Outflow Rate of Backfilling Materials from a Coastal Dike,” Journal of Japan Society of Civil Engineers, Vol. 7(1), pp. 63-71. doi:10.2208/journalofjsce.7.1_63

2. Silarom, K., and Yamamoto, Y. (2019). “The Reproduction Ability of a Numerical Model for Simulating the Outflow Rate of Backfilling Materials from a Coastal Structure,” Journal of Marine Science and Engineering 2017, 7(12), 447, 17p. doi:10.3390/jmse7120447

3. Yamamoto, Y., Silarom, K., and Yoshizawa, Y. (2017). “Investigation on Coastal Erosion and Examination of Coastal Protection Facilities at Chumphon Coast in Thailand,” Journal of Japan Society of Civil Engineers, Ser. B2 (Coastal Engineering) 2017, Vol 73(2), pp. I_1585-I_1590. doi:10.2208/kaigan.73.I_1585

4. Silarom, K., Yamamoto, Y., and Charusrojthanadech, N. (2017). “Analysis of Coastal Erosion in Khlong Wan Coast,” Proceedings of the 27th International Ocean and Polar Engineering Conference, 25-30 June 2017, San Francisco, California, USA, pp. 1519-1526.

5. Silarom, K., Yamamoto, Y., Yoshizawa, S., and Charusrojthanadech, N. (2018). “Development of a numerical simulation model for suction rate using CADMAS-SURF,” Proceedings of the 4th International Conference on Engineering, Applied Sciences and Technology, 4-7 July 2018, Phuket, Thailand, 4p. doi: 10.1051/matecconf/201819202063

6. Silarom, K., and Yamamoto, Y. (2019). “Examinations on Sand Outflow Phenomenon by Using a Numerical Model,” Proceedings of the 29th International Ocean and Polar Engineering Conference, 16-21 June 2019, Honolulu, Hawaii, USA, pp. 3783-3790.

I. Introduction

1.1 Coastal erosion in Thailand—overview

1.2 Researches on coastal erosion in Thailand

1.3 Destruction of coastal structures constructed in very shallow areas

1.4 Objectives and outline of the research

1.1 Coastal erosion in Thailand—overview

In Thailand, there are many usages of the coasts. Department of Marine and Coastal Resources, Ministry of Natural Resources and Environment [1], classified usages of Thai coasts into nine categories including 1) Tourist, 2) Industry, 3) Aquaculture, 4) Salt farming, 5) Community and city resources, 6) Mangrove Forest, 7) Mineral mining and sand mining, 8) Watershed, and 9) Transportation. Thus, Thailand has been binding to the coasts. Thai costs have approximately shorelines length of 3,100 kilometers, which consist of about 2,000 kilometers on the Thai Gulf and 1,100 kilometers on the Andaman Sea. About 700 kilometers of the shorelines suffered or have been suffered coastal erosion for many decades [2]. Figure 1.1 show the coastal erosion situation extracted from Central Database System and Data Standard for Marine and Coastal Resources, Department of Marine and Coastal Resources [3]. Coastal erosion causes many problems, both direct and indirect ways, for example, problems on environment, economy, and social. Nearly 180 km^2 of coastal areas were eroded, which was estimated to be about 0.1 billion baht [2]. Since the impact of coastal erosion is enormous, it is necessary to implement coastal erosion prevention and mitigation plans in Thailand.

Department of Marine and Coastal Resources [4] concluded causes of coastal erosion in Thailand as follows:

1) Inappropriate usage of coastal areas: this includes seashore poaching, infrastructure developments, mangrove forest deforestations. Seashore poaching structures such as villas and bungalows directly affect circulations of currents in their areas and usually block the longshore sediments transport. Infrastructures constructed in coastal areas, for example, seaside roads, were sometimes constructed on dunes or swash zones and affected coastal morphodynamic processes. Mangrove deforestations devastate natural coastal barriers and cause coastal erosion. In Thailand, many mangrove forests were deforested to produce charcoals and to construct shrimp farms.

2) Lack of sediments: naturally: coastal sediments come from the weathering of sedimentary rocks. These sediments transport through rivers and river mouths. Some structures, such as a dam, can block riverine sediments and result in coastal erosion.

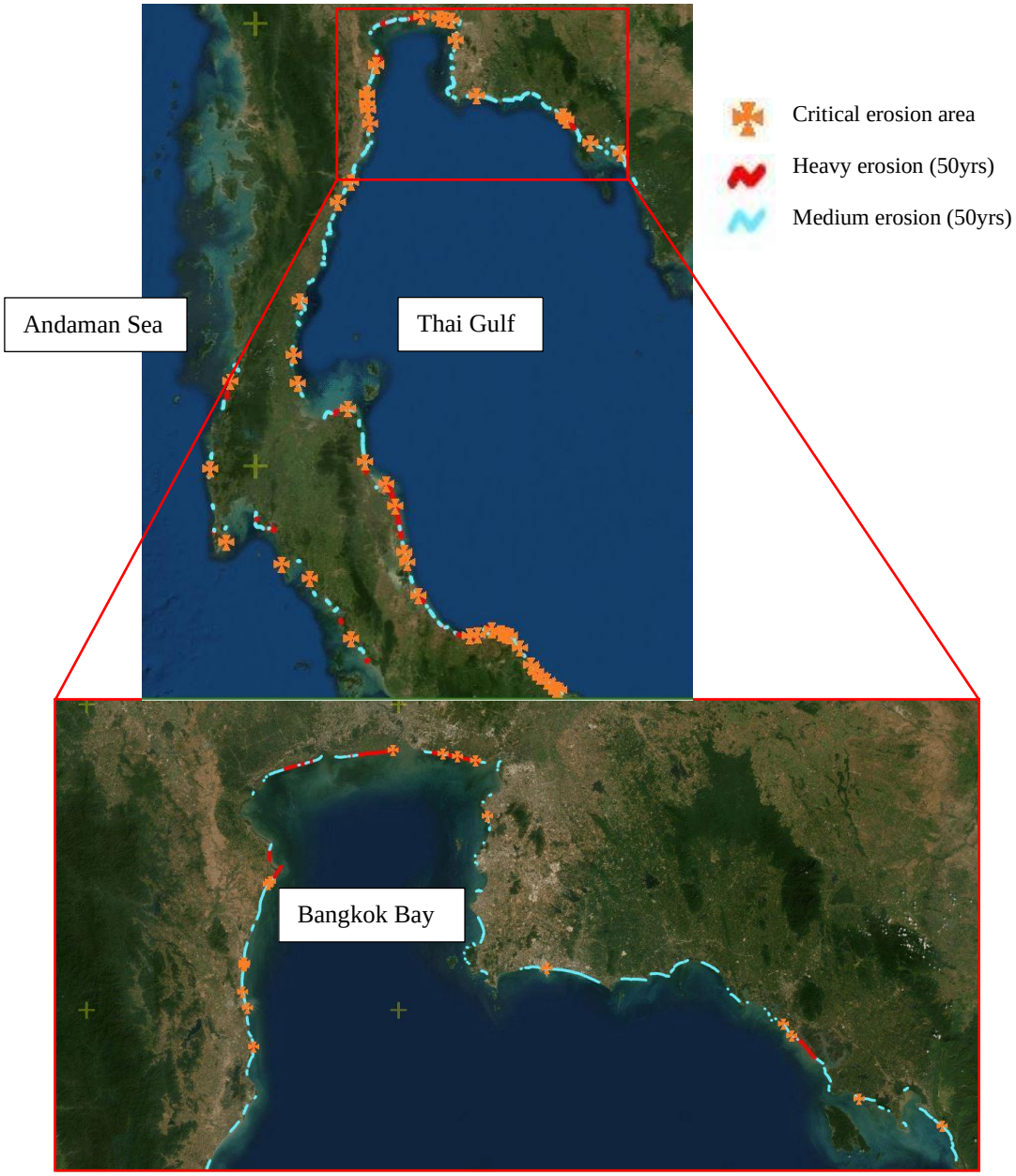

Figure 1.1. An erosion situation in Thailand (modified from Central Database System and Data Standard for Marine and Coastal Resources, Department of Marine and Coastal Resources [3]).

3) Development of coastal projects: big projects such as industrial estates and ports constructed in coastal areas may have substantial effects to coastal process in their adjacent areas. Frequently, heavy depositions of sediments occur in upstream sides of the projects, and heavy erosion occurs in downstream sides of the projects.

4) Natural coastal processes: coastal erosion can be naturally caused by the effects of natural forces, which including the waves force, the current force, the tidal force, and the wind force. In Thailand, waves tend to be higher in the lower south part,

where is an open area. Thus, when a typhoon hits Thailand, damage on the lower south coasts tend to be higher than the others.

5) Lack of databases: a database is one of the essential tools for planning coastal projects; data—such as wave records, historical bathymetries, historical shorelines, and typhoon or storm surge records—is used for planning and investigating coastal projects. However, in Thailand, there are only a few wave observations stations. Moreover, production frequencies of bathymetry maps, aerial photographs, and satellite images is low. Lack of database affects the accuracy of simulations and the evaluation of projects.

There are many government authorities working on coastal erosion, for example, Department of Marine and Coastal Resources, Ministry of Natural Resources and Environment, Marine Department, Ministry of Transport; Department of Public Works and Town & Country Planning, Ministry of Interior; and Local Governments. Since there are some overlying duties, many coastal erosion protection projects were conducted by various departments. Since the sediment transportation is affected by every structure (and non-structure) in a littoral cell—the area isolated from its adjacent coasts in terms of sedimentology—lack of integration and redundancy between organizations may lead to unbalance of sediment transport and results in more or additional problems.

Various measurements were used in Thailand, that is, setbacks, beach restorations, edgings, vegetations, seawalls, dikes, revetments, breakwaters, groins, jetties where 2/3 of them are revetments and seawalls [2], as shown in Table 1.1. Some of them have achieved their goals; however, some of them did not. From the field surveys, cases that erosion is induced by a coastal protection project were founded, for example, toe scours were formed near seawalls and dikes; sediments were blocked by jetties or industrial estates resulted in heavy erosion in downstream areas. In addition, several dikes and seawalls were broken because their backfilling materials flowed out from their bodies.

Table 1.1. Coastal erosion countermeasures in each coastal province in Thailand [2].

	Trat	Chanthaburi	Rayong	Chonburi	Chachoengsao	Samut Prakan	Bangkok	Samut Sakhon	Samut Songkhram	Phetchaburi	Prachuap Khiri Khan	Chumphon	Surat Thani	Nakhon Si Thammarat	Songkhla	Pattani	Narathiwat	Ranong	Phang Nga	Phuket	Krabi	Trang
1. Beach restoration	-	-	-	-	-	-	-	-	-	1	-	-	-	-	1	-	-	-	-	-	-	-
2. Edging	-	4	2	3	2	9	2	12	5	1	-	-	1	-	-	1	-	3	-	1	2	-
3. Offshore breakwater	-	-	11	3	4	1	-	3	-	4	2	-	-	9	3	5	8	-	-	-	-	-
4. Groin	2	-	2	4	-	-	-	-	-	2	-	-	1	10	6	3	31	-	-	-	-	-
5. Revetment	12	7	6	11	7	6	1	-	1	16	3	6	5	15	27	14	1	-	5	5	9	-
6. Seawall	2	9	10	23	-	1	-	-	-	22	15	3	-	10	11	6	2	-	-	7	6	6
Total	16	20	31	44	13	17	3	15	6	46	20	9	7	44	48	29	42	3	5	13	17	6

1.2 Researches on coastal erosion in Thailand

There are numerous researches on coastal erosion in Thailand, especially in the Bangkok Bay and the lower Gulf of Thailand. Back to 1996, Vongvisessomjai et al. [5] analyzed coastal erosion in the Gulf of Thailand by utilizing navigation charts and topographic maps. They were able to find severe erosion on the west of Chao Phraya River mouth, Phetchaburi Province, and Hua Hin District, and Prachuap Khiri Khan Province; additionally, accretion was found on the east of Chao Phraya River mouth and the south of Songkhla Lagoon inlet. Remote sensing technologies became a useful tool for analyzing shoreline changes. Siripong [6] used remote sensing to investigate coastline changes in Thailand and mentioned that economic development since the 1970s, which led to the industrialization in coastal areas, connected to coastal erosion problems. The author also mentioned that mangrove deforestations increase erosion while preservations of such a forest can enhance accretion. Charusrojthanadech and Yamamoto [7] implemented shoreline change analysis in Sangchan Beach using satellite images. The results show that coastal structures in the area—that is, Y-type groins and detached breakwaters—were the cause of heavy erosion. Thampanya et al. [8] studied the relationship between coastal erosion and mangroves in Southern Thailand using in-situ transects and remote sensing. -They found that there is significantly different erosion characteristic between coasts with- and without-mangroves, that is, coasts with mangroves were found less erosion than the coasts

without mangroves. They mentioned that mangrove deforestations, usually for shrimp farming, induce coastal erosion by increasing fetches; moreover, constructions of dams have blocked riverine sediments and therefore cause erosion. The mechanism of mangroves was studied by Rattanarama et al. [9]. They performed hydraulic model experiments to investigate wave dissipation rates and an erosion protection ability of mangroves. Then, they could reproduce the effects of mangroves with acceptable accuracy by using Ca et al. [10] model, a numerical model based on the Volume of Fluid (VOF) technique, the shallow water equation of Boussinesq, and the bed transportation rate equation of Ribberink [11]. Thereafter, the effective width of the mangroves woods was proposed.

There are researches utilized beach evolution models to analyze coastal erosion. Doungpan and Charusrojthanadech [12], for example, analyzed the safety of Sanchan Beach to a storm surge by using a numerical model. A bathymetry change model proposed by Ca et al. [10] was used. They confirmed that existing erosion countermeasures are not able to assure the beach from a storm surge of 10 years of the return period. They used the same model to find the best solution for the beach; they concluded that a beach nourishment is the most proper solution. Silarom et al. [13] used a line model to predict long-term beach evolution in Chumphon Beach, Chumphon Province. They found that jetties for a navigation channel in the study area induced coastal erosion in the short-term by blocking littoral drifts; however, in the long-term, the beach can maintain the equilibrium shape. Saengsupavanich et al. [14] studied coastal erosion in Southern Thailand. They applied the Integrated Coastal Zone Management (ICZM) in the study. Aerial photographs and satellite images were used to determine historical changes of the study area. They mentioned that the mangrove forest in the area was deforested for shrimp farming; this was the cause of erosion in the area. A line model was used to evaluate the suitable countermeasure. By the contribution of stakeholders in the selection of measurements, a combination of detached breakwaters and a beach nourishment is the most suitable countermeasures for the area.

According to the pieces of literature, types of coastal erosion can be classified into two groups. One is deforestations of mangrove forests. Although many coasts in Thailand had been covered by mangroves, a number of mangroves have been rapidly

deforested for dozens of years. Consequently, several coasts have been not able to trap sediment supplies resulted in heavy erosion. The other is stoppages of sediment supplies due to huge facilities—such as dams, breakwaters, groins, and jetties—and sand dredges, such as aggregate extractions, and channel maintenance dredges.

1.3 Destructions of coastal structures constructed in very shallow areas

Dikes and seawalls are conventional measures for stopping retreat of a shoreline due to their ability to prevent wave overtopping. However, even these structures are constructed far away from shorelines, many times, heavy coastal erosion occurred, shorelines retreated, and the structures were exposed to the sea. Under this condition, incident waves are broken closer to the structures and wash away sediments at their fronts during return flows—this phenomenon is called scour at the front of a structure. Scour diminishes the stability at the front of the structures and be the main cause for overturns and slides of armor surfaces of the structures. Additionally, when the scouring depth reaches the lowest edge of a structure (usually, the sheet pile), waves can infiltrate the body of the structure and flow out the backfilling materials; this flow of the backfilling materials is called outflow or suction. Consequently, since the supporting materials for the shells (covering parts of the structures, such as the crown part, the seaward slope, and the landward slope) flowed out, the structure become weaker and are easy to be damaged by waves smaller than their design wave. An illusion of an outflow mechanism is shown in Figure 1.2. Since damage induced by erosion, scour and outflow is high, it is important to carefully consider the effects of them when designing a coastal structure constructed in a very shallow area.

Mechanisms of beach transformations can be divided into two parts: the long-term and the short-term changes. The long-term change is evolution induced by normal waves. The cross-shore sediment transportation in such a change can be neglected because beach evolution induced by this transportation is periodic in the long-term. The reason that this transportation is periodic is that although high waves generated by strong winds can carry sediments to offshores, when strong winds stop, sediments can be carried to shores by normal waves. Thus, it can be concluded that the main cause of the long-term change is the longshore sediment transport. This principle is one of the

important assumptions of the line model, which will be explained in chapter 2. As for the short-term change, this change is beach evolution induced by strong waves. As mentioned above, high waves can carry sediment to offshores and generate scour in front of coastal structures. Scour increases the water depth in front of the structures and therefore induces the incident wave height (the incident wave height becomes higher when the water depth becomes deeper). When the incident wave exceeds the crown height of the structures, the wave may transmit or pass an amount of water through the crown. These phenomena are called wave overtopping and wave run-up, which can damage the structures and areas behind the structures. Thus, since either normal waves or high waves can induce damage, both the long-term change and the short-term change must be considered in order to ensure the safety of planning areas.

Scouring depths in front of coastal structures induced by waves can be evaluated by many methods. For example, an empirical equation of Fowler [15] can evaluate the maximum scour depth induced by irregular waves in front of a vertical seawall. There are numerical models to simulate scour; for example, Ca et al. [10] proposed a numerical model that can reproduce scouring depths induced by waves.

However, there are a few evaluation methods to outflow rates, for example, an empirical formula of Ioroi and Yamamoto [16] could reproduce the outflow rate with acceptable accuracy. There are a few numerical models, which were designed for a specific shape of a structure. Maeno et al. [17] and Kotani et al. [18] proposed a numerical model to simulate cyclic water pressure, which could calculate the cyclic pressure acting on a simple seawall. Another model is a model of Nakamura et al. [19]. This model was able to simulate the outflow rate from the lowest edge of a rubble revetment. Since these models are limited by the shapes of structures, a numerical model that can calculate the outflow rates from a structure of arbitrary sections would be a useful tool for designing coastal structures in very shallow areas.

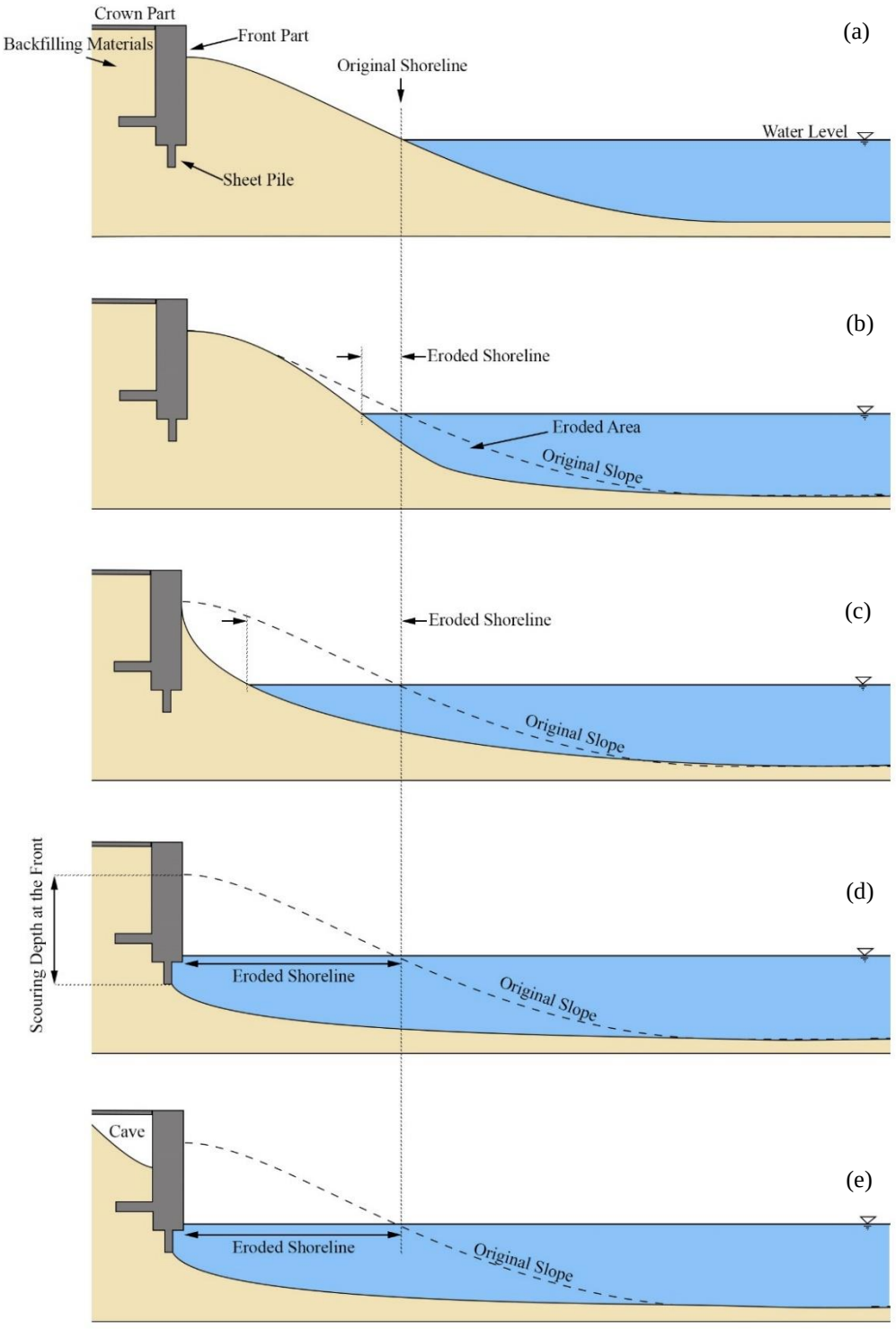

Figure 1.2. Beach profiles during erosion, scour, and outflow. The original beach profile (**a**) continual erodes (**b**-**c**). When the eroded shoreline reaches the structure (**c**) and the scouring depth reaches the tip of the sheet pile (**d**), the backfilling materials can flow out from the structure (**e**).

1.4 Objective and outline of the research

This research aims to propose rational methods for planning suitable countermeasures to coastal erosion, scour and out-flow of backfilling materials by using pieces of literature, field surveys, and numerical simulation models.

This article consists of four chapters. Chapter one introduces an overview of coastal erosion in Thailand, researches on coastal erosion in Thailand, problems on coastal structures constructed in very shallow areas, and the objectives and outline of the research. Chapter two describes existing numerical models for predicting beach evolution and their applications on field cases in Thailand. Chapter three explains the development of a numerical model for simulating the outflow rates of backfilling materials from a coastal structure of arbitrary sections and applications of the model to field cases. Chapter four concludes the research. A method for designing countermeasures to prevent coastal erosion and damage due to it is given in this chapter.

References

[1] Department of Marine and Coastal Resources. “Coastal Land Resources Utilization,” available online at https://km.dmcr.go.th/th/c_56/s_82 (in Thai)

[2] Department of Marine and Coastal Resources. “Guidelines for Project Development and Coastal Erosion Prevention and Resolution Plans”, available online at https://www.dmcr.go.th/detailLib/3712 (in Thai)

[3] Department of Marine and Coastal Resources. “Central Database System and Data Standard for Marine and Coastal Resources,” available online at https://marinegiscenter.dmcr.go.th/gis/ (in Thai)

[4] Department of Marine and Coastal Resources. “Strategies for Managing and Solving Coastal Erosion Problems,” ISBN 978-974-286-451-4, available online at https://www.dmcr.go.th/detailLib/272 (in Thai)

[5] Vongvisessomjai S., Polsi R., Manotham C., Srisaengthong D., and Charulukkana S. (1996). “Coastal Erosion in the Gulf of Thailand,” In: Milliman J.D., Haq B.U. (eds) Sea-Level Rise and Coastal Subsidence. Coastal Systems and Continental Margins, vol 2. Springer, Dordrecht.

[6] Absornsuda Siripong. (2010) “Detect the Coastline Changes in Thailand by Remote Sensing,” International Archives of the Photogrammetry, Remote Sensing and Spatial Information Science, Volume XXXVIII, Part 8, Kyoto Japan 2010, pp.992-996.

[7] Charusrojthanadech, N., and Yamamoto, Y. (2013). “Assessment of Coastal Erosion and Coastal Protection with Hybrid Y-Type Groyne/Detached Breakwater in Sangchan Beach,” Proceedings of the 21st Engineering, Applied Sciences, and Technology Conference, Thailand.

[8] Thampanya, U., Vermaat, J., Sinsakul, S., and Panapitukkul, N. (2006). “Coastal erosion and mangrove progradation of Southern Thailand,” Estuarine, Coastal and Shelf Science, 68(1-2), pp. 75–85. doi: 10.1016/j.ecss.2006.01.011

[9] Rattanarama, P., Charusrojthanadech N., Yamamoto, Y. (2015). “Prediction of Surface Elevation Change in Mangrove Forest and Evaluation of Coastal Erosion Prevention by Mangrove Forest,” Proceedings of the Twenty-fifth International Ocean and Polar Engineering Conference, 21-26 June, Kona, Hawaii, USA.

[10] Ca, V.T.; Yamamoto, Y.; Tanimoto, K.; and Arimura, J. (2002). “Simulation of Wave Dynamics and Scouring Near Coastal Structures by a Numerical Model,” Coastal Engineering 2002, pp. 1817–1829, doi:10.1142/9789812791306_0153.

[11] Ribberink, J.S. (1998) “Bed-load transport for steady flows and unsteady oscillatory flows,” Coastal Engineering, Vol. 34, pp. 59-82.

[12] Satawat, D., and Charusrojthanadech, N. (2015). “Study on Safety to a Storm Surge at Sangchan Beach,” Proceedings of the Twenty-fifth International Ocean and Polar Engineering Conference, 21-26 June, Kona, Hawaii, USA.

[13] Silarom K., Charusrojthanadech N., Sirikaew U., and Yamamoto Y. (2016). “Effect of Beach Change in Respond to Imposed Wave Condition and Coastal Structures in Chumphon Province,” Proceedings of the 21th National Convention on Civil Engineering, June 28 - 30, 2016, BP Samila Beach Hotel, Songkhla. (in Thai)

[14] Saengsupavanich, C., Chonwattana, S., and Naimsampao, T. (2009). “Coastal Erosion through Integrated Management: A Case of Southern Thailand,” Ocean & Coastal Management, 52(6), pp. 307–316. doi: 10.1016/j.ocecoaman.2009.03.005

[15] Fowler, J.E. (1992). “Scour Problems and Methods for Prediction of Maximum Scour at Vertical Seawall,” Technical Report, CERC-92-16; U.S. Army Corps of Engineers: Vickberg, MS, USA, 1992.

[16] Ioroi, M.; and Yamamoto, Y. (2013). “Formula for Evaluating Suction Rate of Backfilling Materials from a Coastal Dike by Big Waves,” Proceedings of the Twenty-Third International Offshore and Polar Engineering Conference, Anchorage, AK, USA, 30 June–5 July 2013; pp. 1210–1216.

[17] Maeno, S.; Kotani, Y.; Hoshiyama, C. Outflow limit of backfilling sand of revetment under cyclic loading of water pressure. Annu. J. Coast. Eng. Journal of Japan Society of Civil Engineers 2000, 47, pp. 926–930. (in Jpn)

[18] Kotani, Y., Yoshimura, C., Maeno, S., and Nago, H. (2002). “Flow Out of Back-Filling Sand Behind Sea Wall Under Cyclic Water Pressure Variation,” Journal of Japan Society of Civil Engineers 2002, 712, pp. 97–106, doi:10.2208/jscej.2002.712_97. (in Jpn.)

[19] Nakamura, T., Hur, D.S., Mizutani, N. (2006). “Suction Mechanism of Reclaimed Sand Behind a Rubble Seawall,” Journal of Japan Society of Civil Engineers Ser. B2 (Coastal Engineering) 2006, 62, pp. 150–162, doi:10.2208/jscejb.62.150. (in Jpn.)

II. Coastal erosion simulations

2.1 Conventional procedure for designing disaster prevention countermeasures

2.2 Existing beach evolution models

2.3 Applications of numerical models in Khlong Wan Coast

2.4 Applications of numerical models in Chumphon Coast

2.5 Conclusions

2.1 Conventional procedure for designing disaster prevention countermeasures

Many coasts in Thailand have been meliorated [1]—as for the 2015, about 565 kilometers of shoreline length has been protected. Almost of coastal erosion problems have been solved; however, some of them remain. Many times, coastal protection facilities could not work effectively or affected their adjacent areas. To handle this problem, the Department of Coastal and Marine Resources proposed a procedure for designing coastal erosion protection and mitigation [1] as follow:

1) Evaluate the erosion situation: in this process, coastal erosion on a target area is evaluated to classify the degree of erosion. If there is no heavy erosion, the area will be classified as a monitored area, and no countermeasures are needed. This classification aims to preserve the coastal resources and coastal process. However, if there is heavy erosion, the importance of the area is examined. In the case of high population areas or important economic areas, the importance of coastal erosion protection and mitigation is classified as high, and urgently actions are needed.

2) Determine appropriate countermeasures: firstly, the aim of the countermeasures must be determined by selecting one from these aims: 1) coastal equilibrium by natural processes, 2) coastal erosion protection, 3) coastal erosion solution, and 4) coastal rehabilitation. After the aim is determined, the countermeasures are selected by considering the effects of these to the economy and environment, the importance of the target area, and public opinions. Then, a plan, including costs, a construction plan, and an environmental impact assessment (EIA) report, must be proposed. This plan must be approved by authorized services. After the plan is approved, the construction can be started.

There is a standard table provides information on each countermeasure. However, there is no concrete method on the designing of these structure.

3) Maintenances and post-construction evaluations: after the construction, regular maintenances and post-construction evaluations must be implemented. If erosion still exists, further countermeasures are required.

The flow chart of this procedure is shown in Figure 2.1.

Since it may difficult to evaluate the causes of coastal erosion, and it is difficult to predict and evaluate beach evolution induced by proposed coastal facilities using the standard table, the author adapted a conventional procedure of design of coastal facilities using numerical models to Thai coasts in order to evaluate the applicability of the models. The adapted procedure is as follow:

1) Selection of planned protection line: in this process, the limit size of a target area is defined by its littoral cell (the area that active sediment can transport). In Thailand, the government have categorized the coasts into several littoral cells.

2) An evaluation of the long-term shoreline change. The shoreline change in duration of several decades can be determined by many numerical models. This analysis can indicate the causes of erosion and indicate the degree of erosion.

3) An evaluation on the safety from big typhoons: serious erosion may occur during the time of big typhoons. The evaluation of the topographical change induced by big waves can be done by using numerical models. At this stage, a wave condition corresponding to a typhoon of an imposed return period (usually, 20-50 years) is used. In addition, wave overtopping rate is evaluated to ensure the safety of the area. In this process, a conventional procedure of Design Manual for Coastal Facilities 2000 [2] is adapted; the procedure is shown in Figure 2.2.

By using numerical models, it is convenience to predict beach evolution in different scenarios. Thus, numerical models would be an appropriate tool for designing a coastal structure.

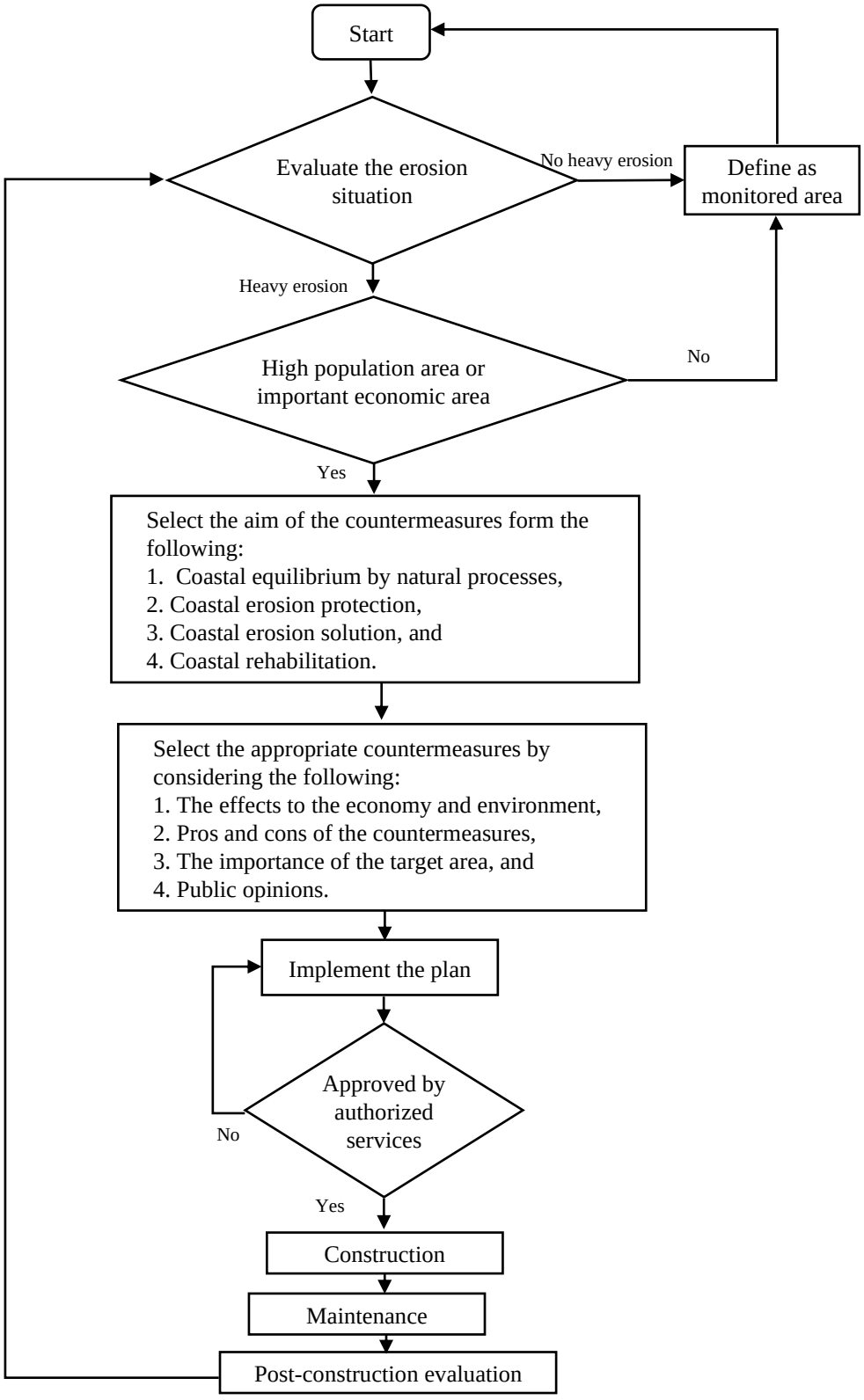

Figure 2.1. A design procedure for countermeasures in Thailand [1].

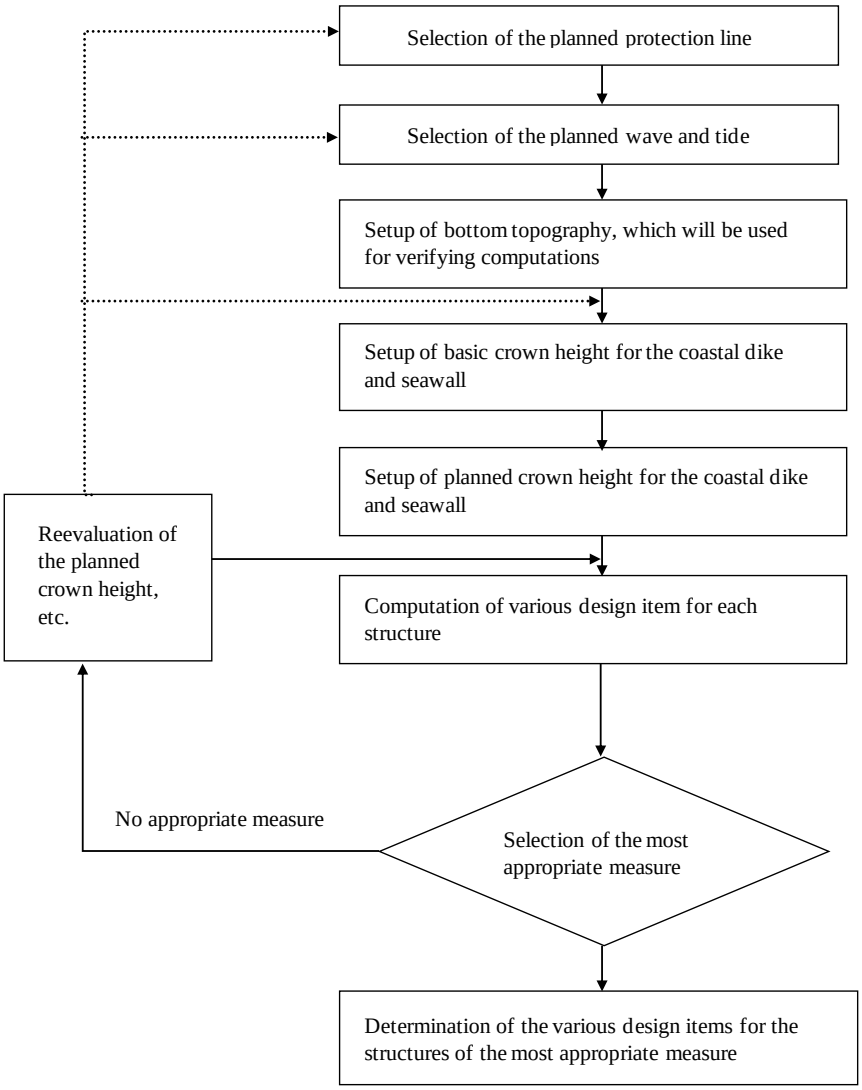

Figure 2.2. A design procedure of coastal facilities for storm surge or tsunami protection [2] (extracted from a report of Yamamoto [3]).

2.2 Existing beach evolution models

According to the rapid development of the calculation ability of computers, numerical models for simulating coastal processes become more accessible. These numerical models become a useful tool for planning and design coastal projects because they can consider coastal morphology with acceptable accuracy. There are many models for simulating coastal processes, which can be used in various proposes, for

example, line models for evaluating the shoreline change for the duration of decades, or bathymetry change models which can simulate scour depths induced by big waves for the duration of a half-day or a day. In this chapter, existing numerical models that can be used in Thai coasts are introduced. Moreover, applications of these models to field cases in Thailand are given.

2.2.1 Line models

Line models can be divided into two categories [2]—the one-line model and the n-lines model. The one-line model is used to predict the shoreline change, while the n-line model is used to predict the change of imposed contour lines. The main assumption of these models is that the shoreline change in the long-term depends on the longshore sediment transport rate, which can be expressed as a function of the wave height and the wave direction at the wave breaking point. Since the models consider that the longshore sediment transport is uniform in the offshore direction, the topographical change near structures cannot be calculated. However, the models can calculate the interception ability of coastal structures to the longshore sediment transport rate, which can be used to evaluate the effect of the structures, with fair accuracy and good calculation time. Thus, these models are practical. In this article, the one-line model is used.

A governing equation of the one-line model is obtained by using three assumptions, which are:

1) The cross-shore sediment transportation in such a long-term change can be neglected because the beach change induced by this transportation is periodic in the long-term. The reason that this transportation is periodic is that although high waves generated by strong winds can carry sediments to offshores, when strong winds stop, sediments can be carried to shores by normal waves. Thus, it can be concluded that the main cause of the long-term change is the longshore sediment transport.

2) The transportation of active sediments is limited to a constant value called "the berm crest height + the closure depth", $D_B + D_C$, as shown in Figure 2.3.

3) In long-term changes, beaches can maintain the same slope.

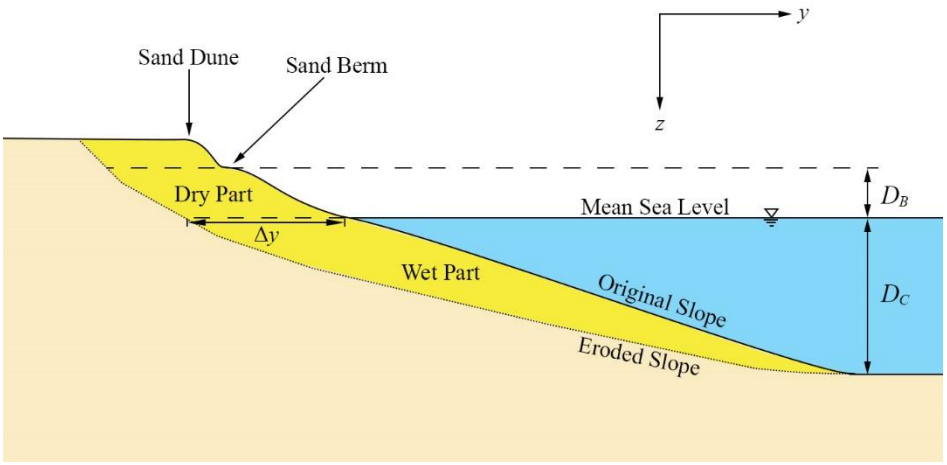

Figure 2.3. Profiles of an eroded beach. Where y-direction is the offshore direction; z-direction is the elevation; and Δy is the eroded shoreline length.

By using these assumptions, a cell of shoreline and its components can be obtained, as shown in Figure 2.4. The changing volume of a shoreline cell can be calculated by using Equation (2.1). By converting Equation (2.1) to Equation (2.2), the rate of shoreline change ($\Delta y/\Delta t$) induced by the longshore sediment transport rate (Q) can be simulated.

$$\Delta y \Delta x (D_B + D_C) = \left(Q + \frac{\partial Q}{\partial x} \Delta x \right) \Delta t - Q \Delta t \tag{2.1}$$

Then,

$$\frac{\Delta y}{\Delta t} = \frac{1}{(D_B + D_C)} \cdot \frac{\Delta Q}{\Delta x} \tag{2.2}$$

Where, D_C is the depth of closure; D_B is the height of the berm crest (from mean sea level); Δy is the change of the shoreline length; Δt is the time step; Q is the longshore sediment transport rate (the longshore drift) and the porosity of the sediment must be considered in this value; Δx is the mesh size in x-direction (=alongshore direction).

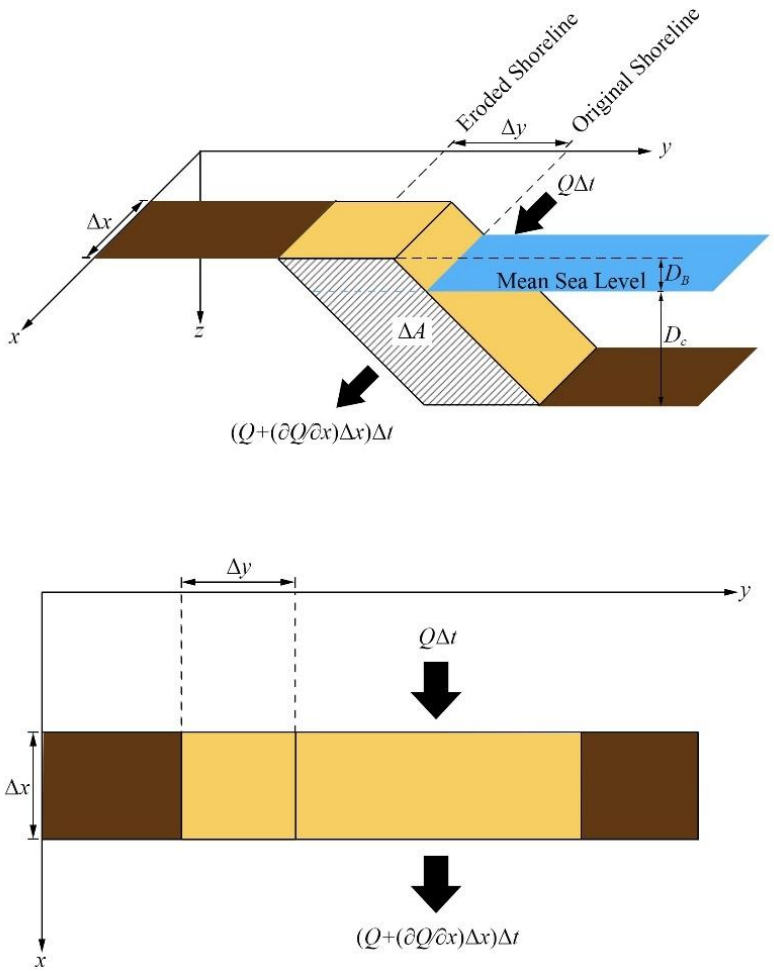

Figure 2.4. A simplified shoreline cell in the one-line model. Where Q is the longshore sediment transport rate (the longshore drift, included the porosity of the sediment); x-direction is the alongshore direction; y-direction is the offshore direction; z-direction is the elevation of the beach; Δx is the mesh size in x-direction; and Δy is the change of shoreline length during a time step, Δt.

Concerning the longshore sediment transport rate (Q), there are some well-known equations, for example, an equation of Hanson et al. [4], as expressed in Equations (2.3)–(2.5), or an equation of Osaza and Brampton [5], as expressed in Equation (2.6). The first term of Equations (2.3) and (2.6) calculate the longshore sediment transport rate induced by incident waves, while the second term considers the rate induced by wave energy in the longshore direction. The calibration on the coefficients K_1 and K_2 is needed in each field. To calibrate these coefficients, verification simulations are necessary. These simulations are implemented by trial and error the values of K_1 and K_2 until the simulated shoreline close to the measured shoreline.

$$Q = (H^2 C_g)_b (a_1 \sin 2\alpha_b + a_2 \cos \alpha_b \frac{\partial H}{\partial x}) \tag{2.3}$$

$$a_1 = \frac{K_1}{16(\rho_s / \rho_w - 1)(1-\lambda)(1.416)^{5/2}} \tag{2.4}$$

$$a_2 = \frac{K_2}{8(\rho_s / \rho_w - 1)(1-\lambda)\tan\beta(1.416)^{5/2}} \tag{2.5}$$

$$Q = \frac{(EC_g)_b}{(\rho_s - \rho_w)(1-\lambda)} \times \left(K_1 \sin(\alpha_b)\cos(\alpha_b) - K_2 \cos(\alpha_b)\cot\left(\beta \frac{\partial H_b}{\partial x}\right)\right) \tag{2.6}$$

Where Q is the longshore sediment transport rate; H is the incident wave height; C_g is the wave celerity; subscription b denotes the breaking point; a_1 and a_2 are coefficients calculated by Equations (2.4) and (2.5), respectively; α_b is the incident wave breaking angle; x is the longshore distance; ρ_s is the density of the sediment; ρ_w is the density of water; tanβ is the beach slope; K_1 and K_2 are the calibration coefficients; E is the wave energy; and λ is the porosity coefficient.

As for the effects of coastal structures, excepted for seawalls, which will be explained later, the model considers the effects of the structures to the wave height and the wave direction (the parameters H_b and α_b in Equation (2.3) or (2.6)). Since the wave used in the longshore sediment transport rate calculation is the breaking wave, the transformations of waves from the offing boundary must be considered. A function for calculating wave transformation must be included in the model. Typically, in the case that waves directly hit the structures, the wave transmission coefficient is used for converting the incident wave height to the transmitted wave height. The wave directions of the offing waves can be affected by the wave diffraction induced by the structures. The wave diffraction near the structures can be considered by using the diffraction coefficient. The transformation of waves passing through the gap between breakwaters can also be calculated by using the diffraction coefficient. Therefore, by determining the values of the transmitted and diffraction coefficients, the effects of the structures

(excepted for seawalls) can be considered.

For the effect of seawalls, the existence of seawalls in the model is to set the maximum retreated shoreline. If the calculated eroded shoreline reaches the seawalls, there will be no more erosion in the section.

Therefore, the main components of the one-line model are the governing equation, Equation (2.2), the longshore sediment transport rate formula, for example, Equation (2.3) or (2.6), and a wave transformation subroutine.

2.2.2 Topographical change models

The wave field calculation, the near-shore current field calculation, and the topographical change calculation are included in this kind of model. The wave field and the near-shore current field calculated are used to evaluate the external forces acting on the bottom. Then, the movement of the bottom is calculated by using these external forces. Thus, the on-off sediment transport can be considered by using these models. The accuracy of these models is better than the line models because more detailed physical mechanisms are considered. However, according to the complexity of the models, the calculation time of this model is high; therefore, this model is suitable for short duration simulations. In this article, a topographical change model of Ca et al. [6] is used.

Ca et al. [6] proposed a numerical model that can simulate the nearshore wave dynamic and the bottom topographical change. In this model, the topographical change can be simulated by using Equations (2.7) and (2.8). Equation (2.7) evaluates the rate of the bed elevation change by considering the bed load transport rates in the plane—including the bed load transport rates in x- and y-directions (q_{bx} and q_{by}, respectively), and the settling and the uptake rates of the suspended load (C_s and C_{ut}, respectively). The bed load transport rate is calculated by using Riberink's formulae [7], expressed in Equation (2.8), while the settling and the uptake rates can be evaluated by using the concentration rate of the suspended load.

$$\frac{\partial \zeta}{\partial t} = -\frac{1}{1-\varepsilon_s}\left(\frac{\partial q_{bx}}{\partial x} + \frac{\partial q_{by}}{\partial y} - C_s + C_{ut}\right) \tag{2.7}$$

$$\frac{q_{bi}}{\sqrt{\Delta g D_{50}}} = \begin{cases} m\left(|\theta_s| - \theta_{sc}\right)^n \cdot \dfrac{\theta_{si}}{|\theta_s|} & \text{when } \theta_s \geq \theta_{sc} \\ 0 & \text{when } \theta_s < \theta_{sc} \end{cases} \tag{2.8}$$

Where ζ is the bottom elevation; ε_s is the porosity coefficient of the bed load; q_{bx} and q_{by} are the bed load transportation rates in x- and y-directions, respectively; C_s is the settling rate of the suspended load; C_{ut} is the uptake rate of the suspended load; q_{bi} is the bed load transportation rate in i-th direction; Δ is the relative density of the bed (=(ρ_s–ρ_w)/ρ_w); ρ_s is the density of the bed; ρ_w is the density of water; g is the gravitational acceleration; D_{50} is the median gain size of the bed; m(=11) and n(=1.5) are coefficients; θ_s is the Shield parameter (dimensionless shear stress) calculated by Equation (2.9); θ_{si} is a component of θ_s in i-th direction; and θ_{sc} is the critical Shield parameter (critical shear stress) calculated by a formulae of Van Rijn [8], expressed in Equation (2.10).

$$\theta_s = \frac{0.5\rho_w f_w' |V_b| V_b}{\left(\rho_s - \rho_w\right) g D_{50}} \tag{2.9}$$

$$\theta_{sc} = \frac{\tau_{bc}}{\left(\rho_s - \rho_w\right) g D_{50}} = \begin{cases} 0.24 D_*^{-1} & \text{when } 1 < D_* < 4 \\ 0.14 D_*^{-0.64} & \text{when } 4 \leq D_* < 10 \\ 0.04 D_*^{-0.1} & \text{when } 10 \leq D_* < 20 \\ 0.013 D_*^{0.29} & \text{when } 20 \leq D_* < 150 \\ 0.055 & \text{when } 150 \leq D_* \end{cases} \tag{2.10}$$

$$D_* = D_{50}\left(\frac{g\Delta}{\nu^2}\right)^{1/3} \tag{2.11}$$

Where f_w'is the bed friction coefficient of Riberink [7]; V_b is the flow velocity at the top of the bed (=$\sqrt{u^2 + v^2}$, where u and v are the components of the flow velocity in x- and y-directions, respectively); τ_{bc} is the critical shear stress at the bed; D_* is the dimensionless grain size calculated by Equation (2.11); and ν is the kinematic viscosity coefficient.

In Ca et al.'s model, the depth integrated flow discharges simulation is used to simulate components for the unknown values—q_{bi}, C_s, and C_{ut}. These discharges can be simulated by using the nearshore fluid dynamic model based on depth integrated Boussinesq equations for nearshore wave transformation, as expressed in Equations (2.12)–(2.14), where Equation (2.12) is the governing equation. A numerical scheme of Crank–Nicholson is used. A cell of the bottom in this model is shown in Figure 2.5. By using this model, the scour depths induced by big waves can be simulated.

$$\frac{\partial q_x}{\partial x}+\frac{\partial q_y}{\partial y}+\frac{\partial \eta}{\partial t}=0 \tag{2.12}$$

$$\begin{aligned}&\frac{\partial q_x}{\partial t}+\frac{\partial}{\partial x}\left(\frac{q_x^2}{d}\right)+\frac{\partial}{\partial y}\left(\frac{q_x q_y}{d}\right)+gd\frac{\partial \eta}{\partial x}+\frac{h^3}{6}\left[\frac{\partial^3}{\partial x^2\partial t}\left(\frac{q_x}{h}\right)+\frac{\partial^3}{\partial x\partial y\partial t}\left(\frac{q_y}{h}\right)\right]\\&-\frac{h^2}{2}\left(\frac{\partial^3 q_x}{\partial x^2\partial t}+\frac{\partial^3 q_y}{\partial x\partial y\partial t}\right)-M_{bx}+\frac{f_c}{d^2}Qq_x=0\end{aligned} \tag{2.13}$$

$$\begin{aligned}&\frac{\partial q_y}{\partial t}+\frac{\partial}{\partial x}\left(\frac{q_x q_y}{d}\right)+\frac{\partial}{\partial y}\left(\frac{q_y^2}{d}\right)+gd\frac{\partial \eta}{\partial y}+\frac{h^3}{6}\left[\frac{\partial^3}{\partial y^2\partial t}\left(\frac{q_y}{h}\right)+\frac{\partial^3}{\partial x\partial y\partial t}\left(\frac{q_x}{h}\right)\right]\\&-\frac{h^2}{2}\left(\frac{\partial^3 q_y}{\partial y^2\partial t}+\frac{\partial^3 q_x}{\partial x\partial y\partial t}\right)-M_{by}+\frac{f_c}{d^2}Qq_y=0\end{aligned} \tag{2.14}$$

Where q_x is the depth integrated flow discharge in x-direction; q_y is the depth integrated flow discharge in y-direction; η is the water surface elevation; d is the instantaneous water depth; h is the still water depth; M_{bx} and M_{by} are wave energy losses due to wave breaking in x- and y-directions, respectively; f_c is the bed friction coefficient; Q is the total discharge (= $\sqrt{q_x^2+q_y^2}$).

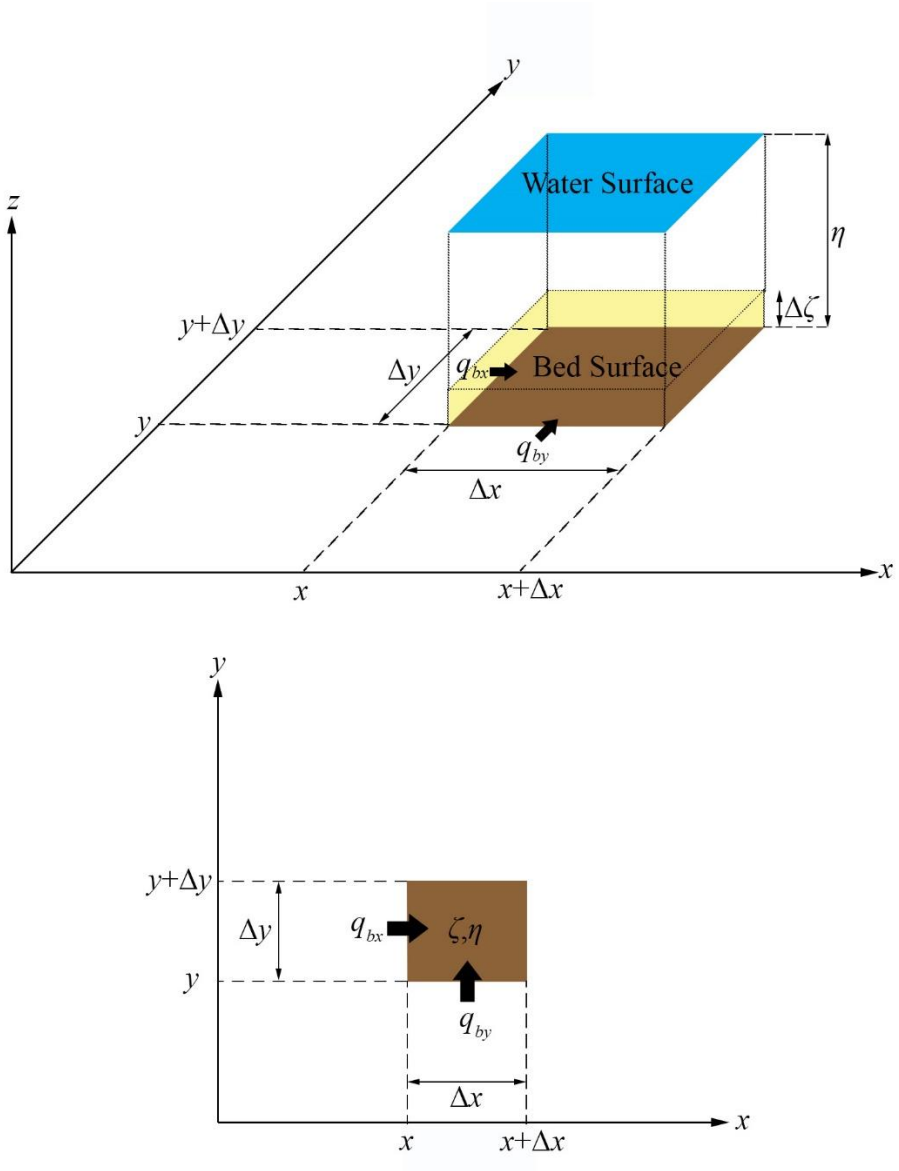

Figure 2.5. A cell of the bottom of Ca et al.'s model in the case of the initial bed elevation (ζ) is zero. Where Δx and Δy are the mesh sizes in x- and y-directions, respectively; $\Delta\zeta$ is the topographical change of the bed; η is the water surface elevation; and q_{bx} and q_{by} are the bed load sediment transport rates in x- and y-directions, respectively.

2.2.3 Wave overtopping analysis

Wave overtopping is one of the important parameters to evaluate the safety from a storm surge of non-submerge coastal facilities, especially of seawalls. Wave overtopping can damage structures and area behind the structures, which can cause the failure to the structures. An illustration of the wave overtopping rate and the wave run-

up height is shown in Figure 2.6. Generally, wave overtopping is evaluated by two parameters—the wave overtopping rate (q), and the wave run-up height (R). There are many formulae for evaluating these parameters. In this article, empirical equations of de Waal and van der Meer [9] and van der Meer and Jansen [10], and the formulae of Yamamoto and Horikawa [11] are used.

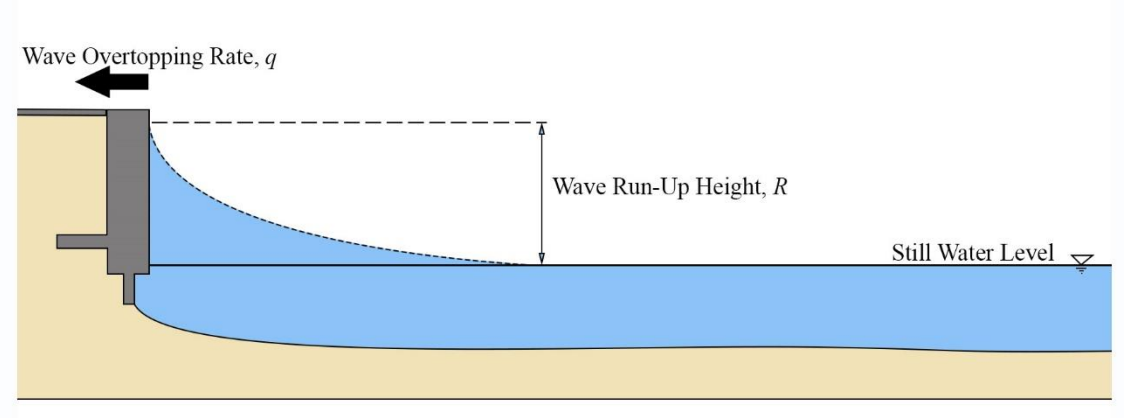

Figure 2.6. An illustration of wave overtopping. Where q is the wave overtopping rate; and R is the wave run-up height.

The empirical equations, Equations (2.15)–(2.17), of de Waal and van der Meer [9] and van der Meer and Jansen [10] evaluate the wave overtopping rate and the wave run-up height by using many empirical reduction parameters (γ) obtained from large-scale experiments. These are well-known equations, which can be used with the standard wave overtopping rates and the standard wave run-up heights in the Coastal Engineering Manual (CEM) [12], as shown in Figure 2.7, to evaluate the safety from the wave overtopping.

Table VI-5-6
Critical Values of Average Overtopping Discharges

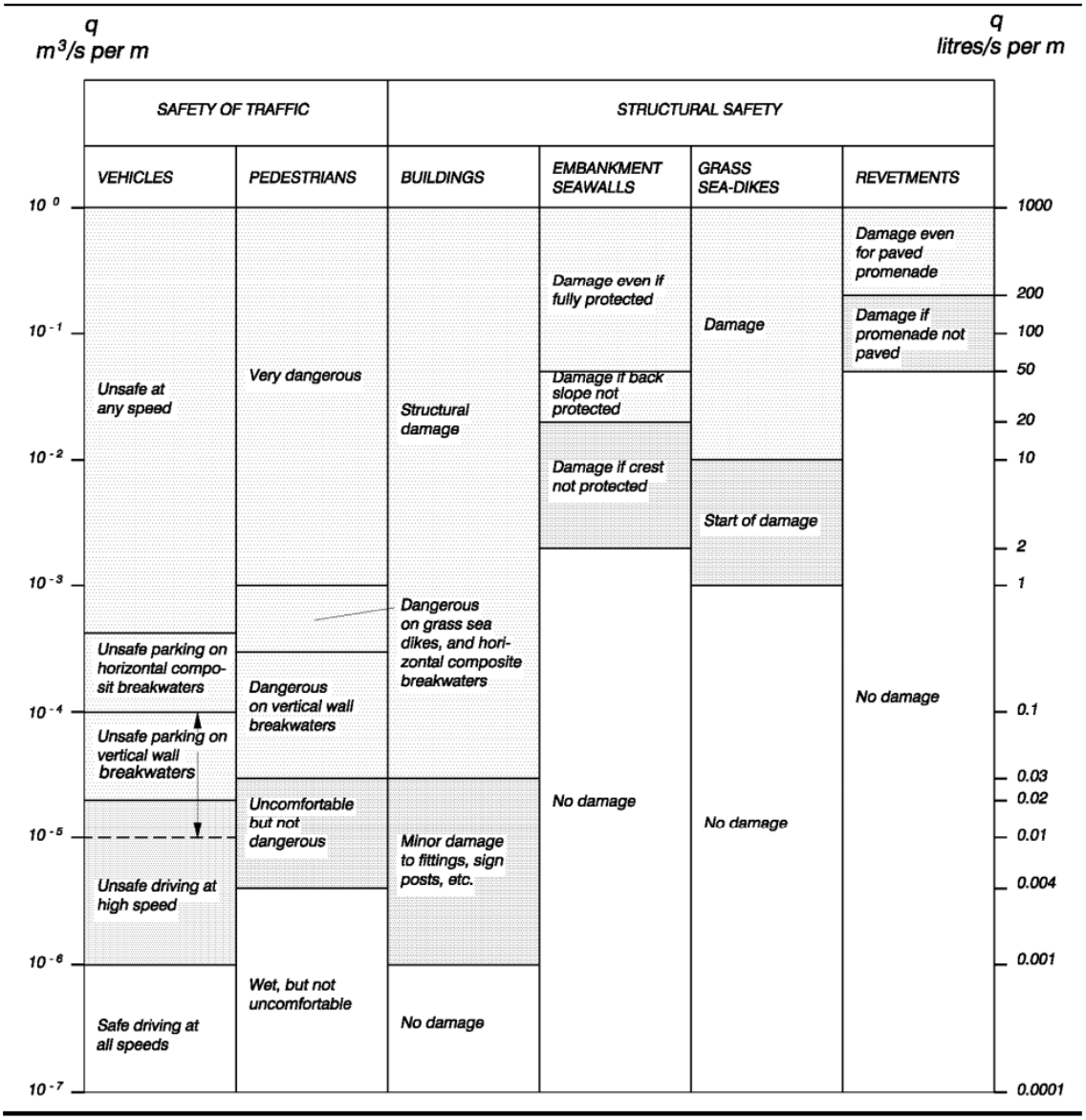

Figure 2.7. Standards for wave overtopping rate (extracted from Table VI-5-6 in Coastal Engineering Manual (US Corp of Engineering) [12]).

$$\frac{R_{u2\%}}{H_s} = 1.6\gamma_h\gamma_f\gamma_b\zeta_{op} \tag{2.15}$$

$$\zeta_{op} = \frac{\tan\alpha}{\sqrt{S_{op}}} = \frac{\tan\alpha}{\sqrt{H_s / L_0}} \tag{2.16}$$

$$\frac{q}{\sqrt{gH_s^3}}\sqrt{\frac{S_{op}}{\tan\alpha}} = 0.06\exp(-5.2\frac{R_c}{H_s}\frac{\sqrt{S_{op}}}{\tan\alpha}\frac{1}{\gamma_r\gamma_b\gamma_h\gamma_\beta}) \tag{2.17}$$

Where $R_{u2\%}$ is the 2% run-up level above the still water line; H_s is the significant wave height; γ_r is the reduction factor for the surface roughness; γ_f is the reduction factor for the slope roughness; γ_b is the reduction factor for the influence of a berm; ζ_{op} is the parameter calculated by Equation (2.16); α is the equivalent slope of a dike; S_{op} is the wave breaking parameter; L_0 is the wavelength in deep water; q is the irregular wave overtopping rate; R_c is the crown height of the dike; and γ_β is the reduction factor for oblique wave attack.

While the equations of de Waal and van der Meer [9] and van der Meer and Jansen [10] can consider the wave overtopping rate induced by irregular waves, the formulae of Yamamoto and Horikawa [11], Equations (2.18) and (2.21) can consider both irregular and regular waves.

$$R = 0.4(1-k)C^2(\cos\alpha)^2(\tan\alpha)^{0.8}(H_0 / L_0)^{-1/4}H_0 \tag{2.18}$$

$$(1-k)C^2 = 3.125\left(\tan\alpha\right)^{-0.2} \quad \text{when } 1/3 \le \tan\alpha \le 1/50 \tag{2.19}$$

$$\alpha = \tan^{-1}\left(\left(R + h_b\right)^2 / 2\beta\right) \tag{2.20}$$

Where R is the wave run-up height; H_0 is the offing wave height; $(1\text{-}k)C^2$ are the coefficients calculated by Equation (2.15); α is the hypothetical slope proposed by Nakamura et al. [13], as shown in Figure 2.8, which can be calculated by using Equation

(2.16); and β is the beach slope.

$$q = c[(X_0 / R) - \cot\alpha](R - H_c)^2 / 2 \tag{2.21}$$

Where q is the irregular or regular wave overtopping rate; and c is the overtopping coefficient; X_0 is the horizontal length of the shape of the wave run-up profile; R is the vertical length from the still water level to the wave run-up height; and α is the surface slope.

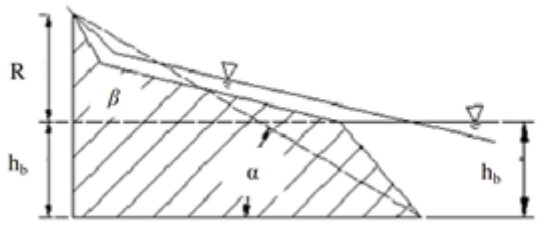

Figure 2.8. Hypothetical single slope proposed by Nakamura et al. [13].

By using either formulae for evaluating wave overtopping, the safety of a structure during a storm surge can be evaluated.

By using the following methods, the long-term and short-term changes can be simulated by using the one-line model and the topographical change model, respectively. Moreover, damage induced by the wave overtopping can be evaluated by using the wave overtopping rate and the wave run-up height formulae. These methods would be useful tools for planning a countermeasure for coastal erosion. By combining these methods, the procedure shown in Figure 2.9 is obtained.

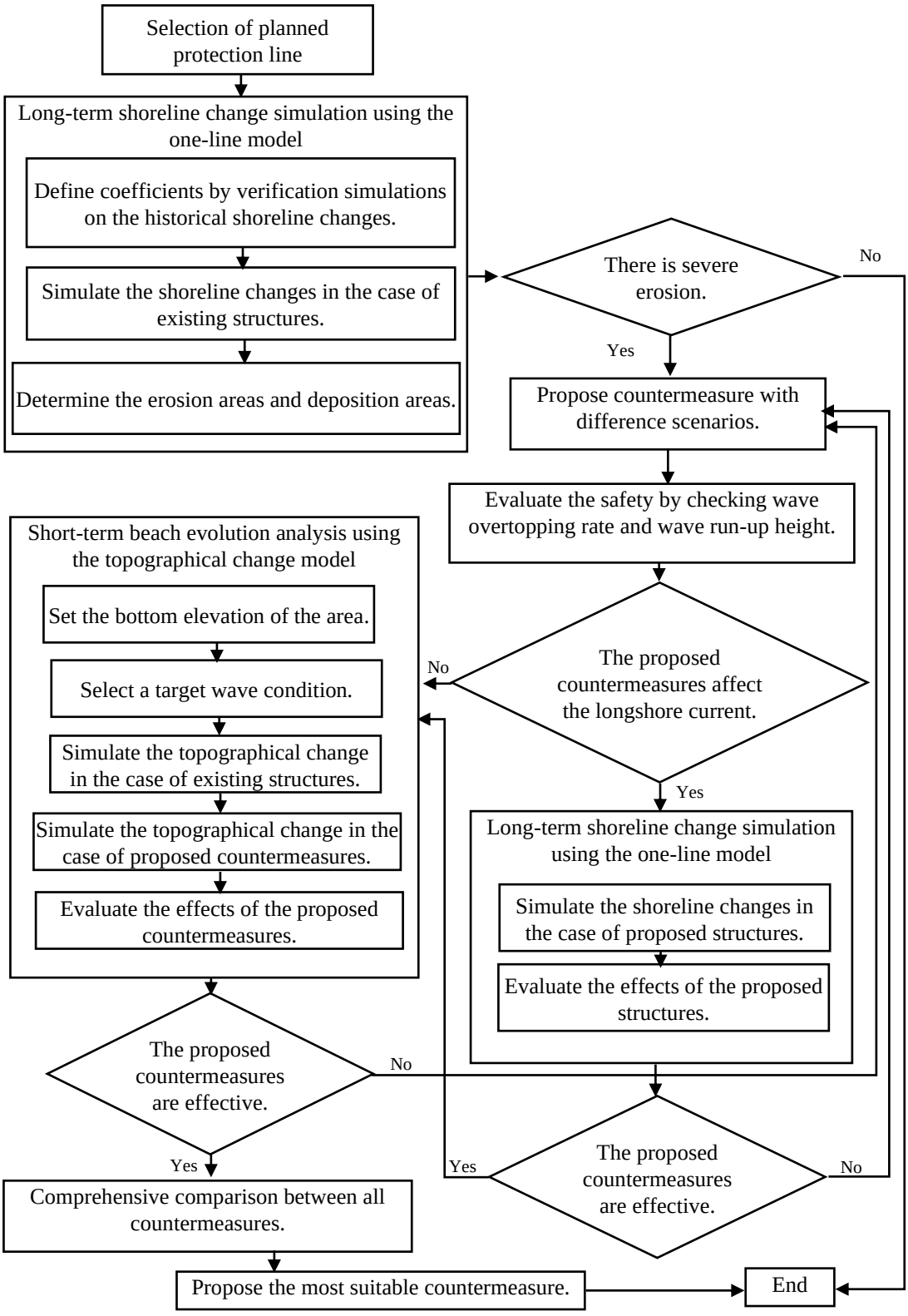

Figure 2.9. A design procedure for a suitable countermeasure using numerical models.

2.3 Applications of numerical models in Khlong Wan Coast

Silarom et al. [14] investigated coastal erosion in Khlong Wan Coast, then, they proposed a suitable countermeasure. First, field surveys and a long-term simulation using the one-line model were executed in order to elucidate the cause of coastal erosion and determine heavy erosion sections. Then, some countermeasures were examined by using the topographical change model of Ca et al. [6] and wave overtopping analysis. Finally, a suitable countermeasure was proposed.

Khlong Wan Coast is located in Ban Khlong Wan, Khlong Wan District, Prachuap Khiri Khan Province, West Coast of Thai Gulf, Thailand. The target area is north part of Klong Wan Coast (11°44'28.7"N, 99°47'07.1"E), as shown in Figures 2.10-2.11. Total shoreline length in the coast is about 13.4 km, while 1.8km of the length is classified as the medium eroded shoreline. The main industry of this area is fishery. Once, the villagers used the Klong Wan River as a fishery harbor. Then, according to population growth, the local government constructed a new fishery port, a huge breakwater, and detached breakwaters. These structures were designed to increase the service capacity of the coast by allowed vessels to dock behind the detached breakwaters. However, these structures have changed the circulation of currents and caused coastal erosion.

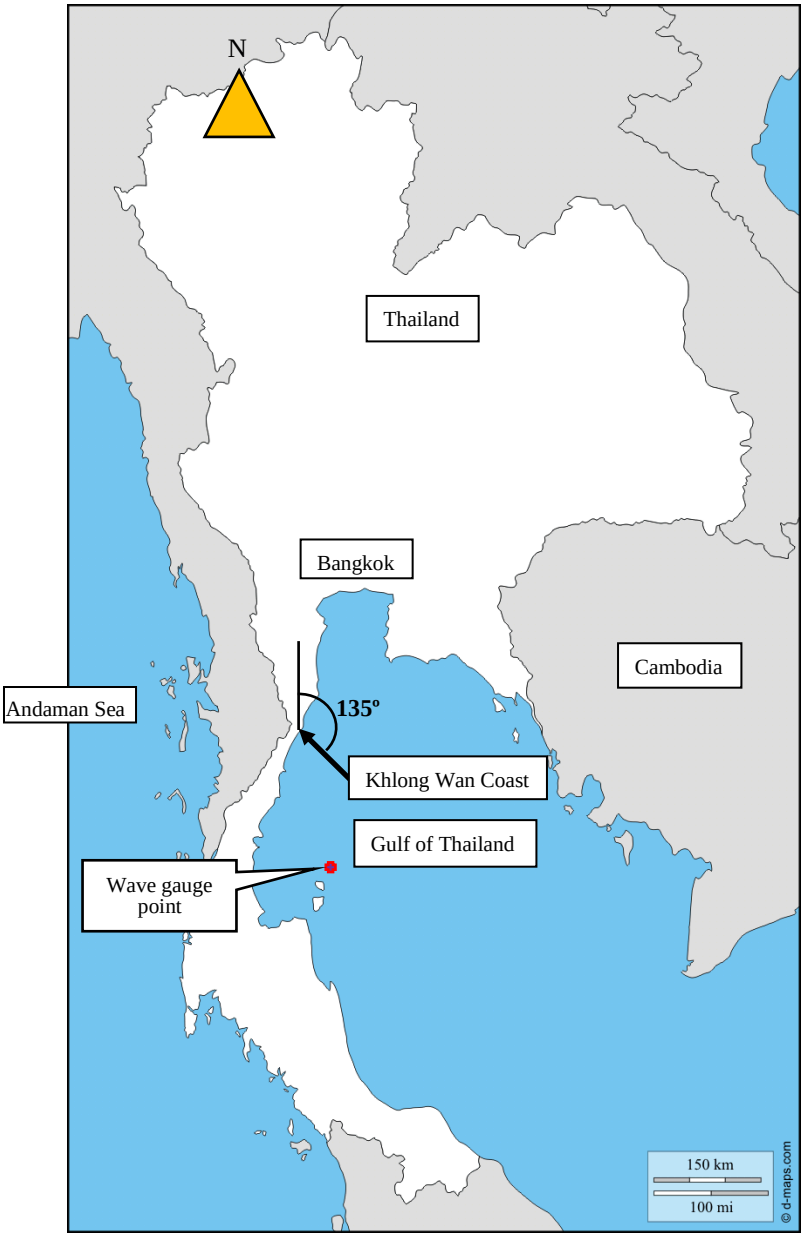

Figure 2.10. The location of the study area, Khlong Wan Coast, Prachup Khiri Khan Province, West Coast of Thai Gulf. (Thailand map image from d-map.com).

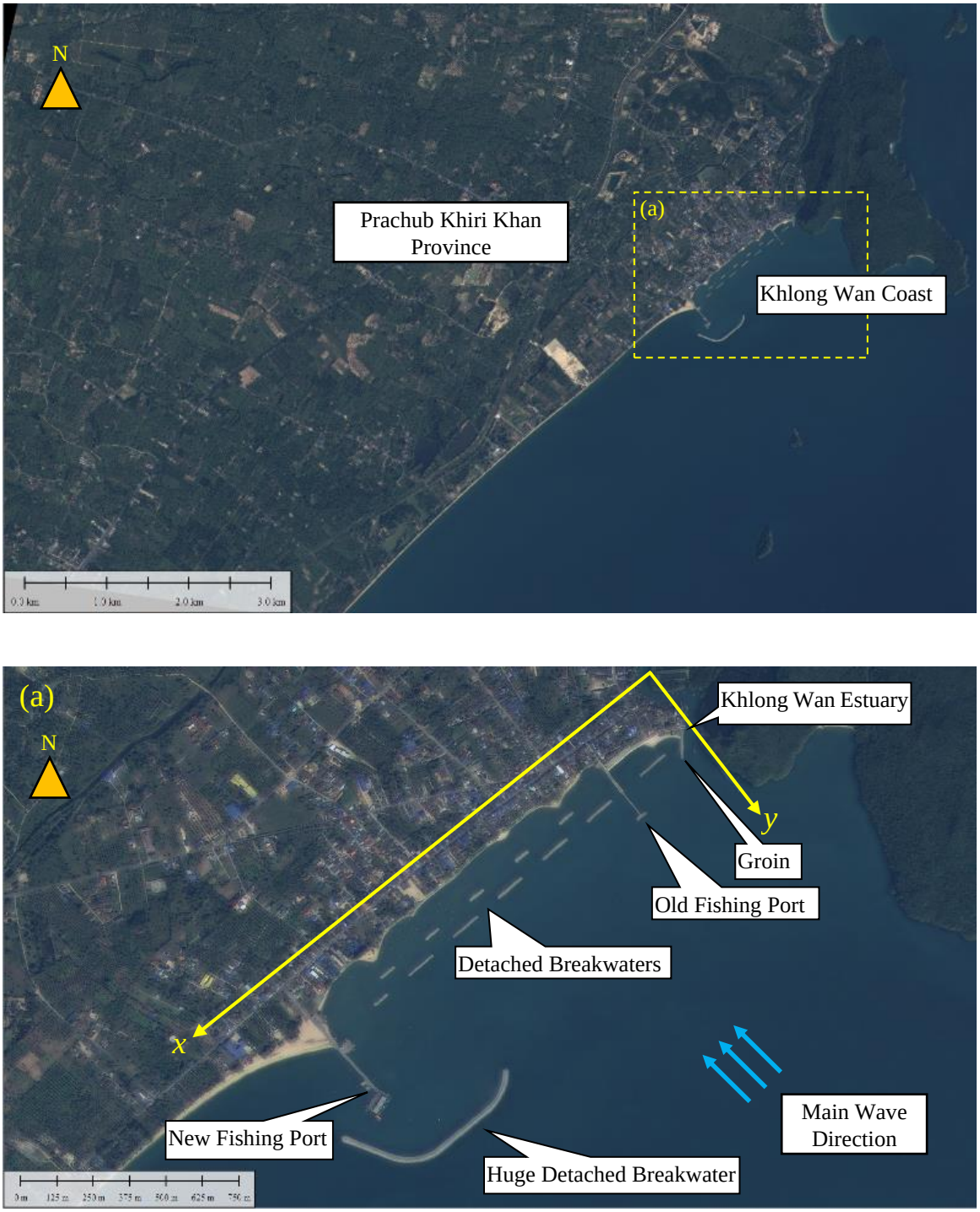

Figure 2.11. A satellite image of the study area. (From Geo-Informatics and Space Technology Development Agency). Where *x* and *y* are longshore and cross-shore axes in simulation model, respectively.

2.3.1 Field surveys

The authors and colleagues implemented field surveys in January 2015, March 2015, and August 2016. Data—which including photographs, topographical maps, beach profiles, sediment properties, and interviews—were collected. The results were used to identify and describe the situation of the study area.

From the surveys, the area behind the detached breakwaters is very narrow and is covered by a layer of mud. Thus, large vessels cannot get into the area, and it is dangerous for people to walk or swim in the area. The ports in the study area cannot service large vessels because the coast is shallow. Many villagers complained that the detached breakwaters had destroyed the beach scenery. Moreover, many fragments fallen during the construction have caused danger at the time of walking or cruising, which caused damage to fishery and tourist businesses.

The countermeasures of the study area consist of seven long detached breakwaters (the length=80m), five short detached breakwaters (the length=40m), a groin at Khlong Wan Estuary, a huge detached breakwater (the length=500m) near the new fishery port, and seawalls along the shoreline, as shown in Figure 2.11. Several pocket beaches formed behind the short-detached breakwaters.

Foundations of the new fishery port are pier type, which allows silt-and-sand supply to pass through them; however, a huge tombolo formed on the upstream of the port. The formation of the tombolo shows that the effects of the port and the huge detached breakwater are high. In addition, we found that a part of the seawalls was damaged by scour and outflow.

2.3.2 Materials

Shorelines obtained from aerial photographs taken in the year of 2000 and 2002 were used as verification data for simulations using the one-line model in case of before the construction of the coastal facilities. Shoreline obtained from a satellite image taken in 2012 was used to verify the model in case of after the construction.

Wave data—including significant wave heights, significant wave periods, and wind directions from 1993 to 2000 at Ko Tao observation station—was extracted from

reports of Geo-Informatics and Space Technology Development Agency, Thailand – GISTDA. The wave gauge point is shown as a red circle in Figure 2.10. The distance between the coast and the wave observation station is about 150km southward at an angle of 135º to the main wave direction, as shown in Figure 2.10. This wave data was used to investigate the shoreline change in the long-term by using the one-line model. Furthermore, wave data of Typhoon Linda was used to investigate the storm surge safety in the study area by using the topographical change model of Ca et al. [6].

2.3.3 Shoreline change simulations

The one-line numerical model based on the continuity equation, Equation (2.1), and Ozasa & Brampton's equation [5] were used to reproduce a long-term shoreline change. Since $a_2 \approx 1.5 a_1 \tan\beta$, and the average value of $\tan\beta$ in the study area is 1/20, $a_2 \approx 30 a_1$. However, a report by Hanson et al. [4] recommends that the value of a_2 should not be large. Thus, we defined that $a_2 = 3.24 a_1$. By using some trial simulations, the suitable value of a_1 was obtained (=0.1). Finally, a final equation was obtained, as expressed in Equation (2.22).

$$Q = (H^2 C_g)_b (a_1 \sin 2\alpha_b + 3.24 a_1 \cos\alpha_b \frac{\partial H}{\partial x}) \tag{2.22}$$

The longshore and offshore axes in the one-line simulations were set as shown in Figure 2.11. Verification simulation using the shoreline change from January of 2000 to December of 2002 was implemented. The comparison between the simulated- and measured-shorelines is shown in Figure 2.12. The comparison result shows that before the construction of the huge detached breakwater and the new fishery port, the sediment from the southwest side at the longshore distance of 1800m was transported to the northeast side. Moreover, the results show that the sand supply from the river was intercepted by the jetty and the groin.

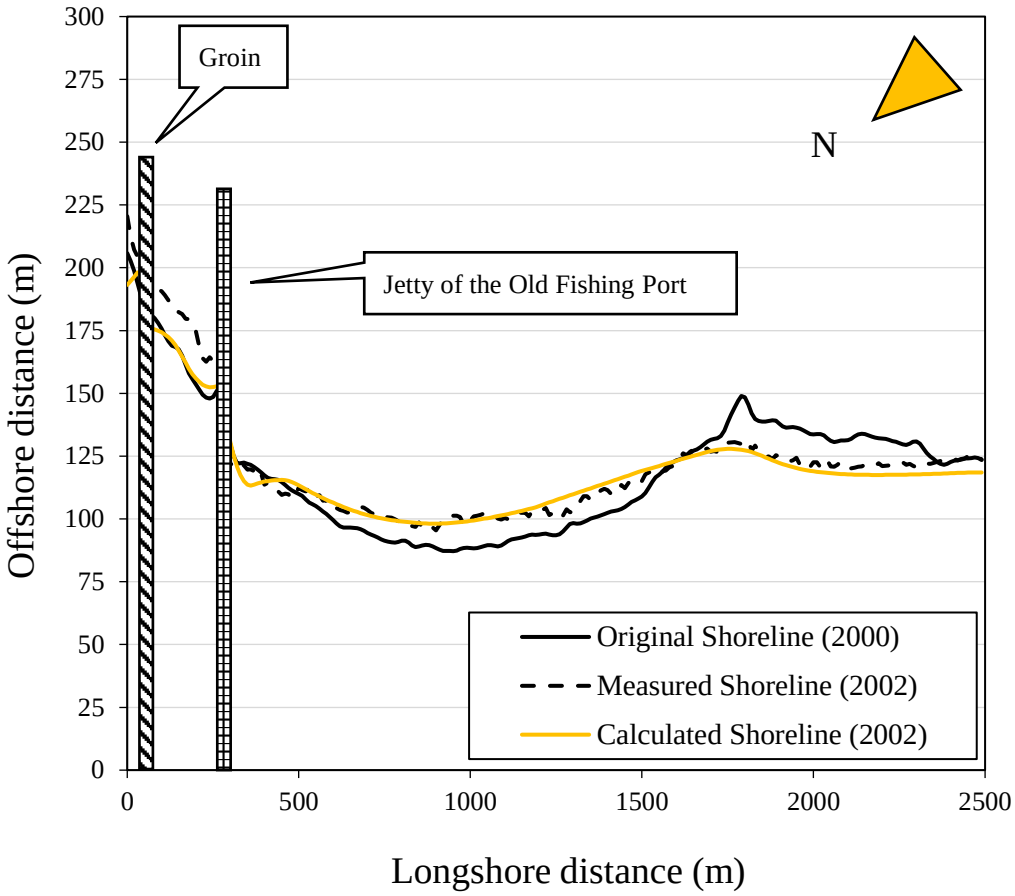

Figure 2.12. The comparison between the simulated- and the measured-shorelines from January of 2000 to December of 2002.

Figure 2.13 shows the comparison between the simulated- and the measured-shorelines from January of 2000 to March of 2012. The results show that after the construction of the huge detached breakwater in 2007, a lot of silt-and-sand from the southwest side of the new fishery port was blocked, and a tombolo formed at the southwest side. This result shows that even if the detached breakwaters were set up in the same term, these could not prevent the retreat of the shoreline in the central coast area because there is not enough sand supply to fulfill the area.

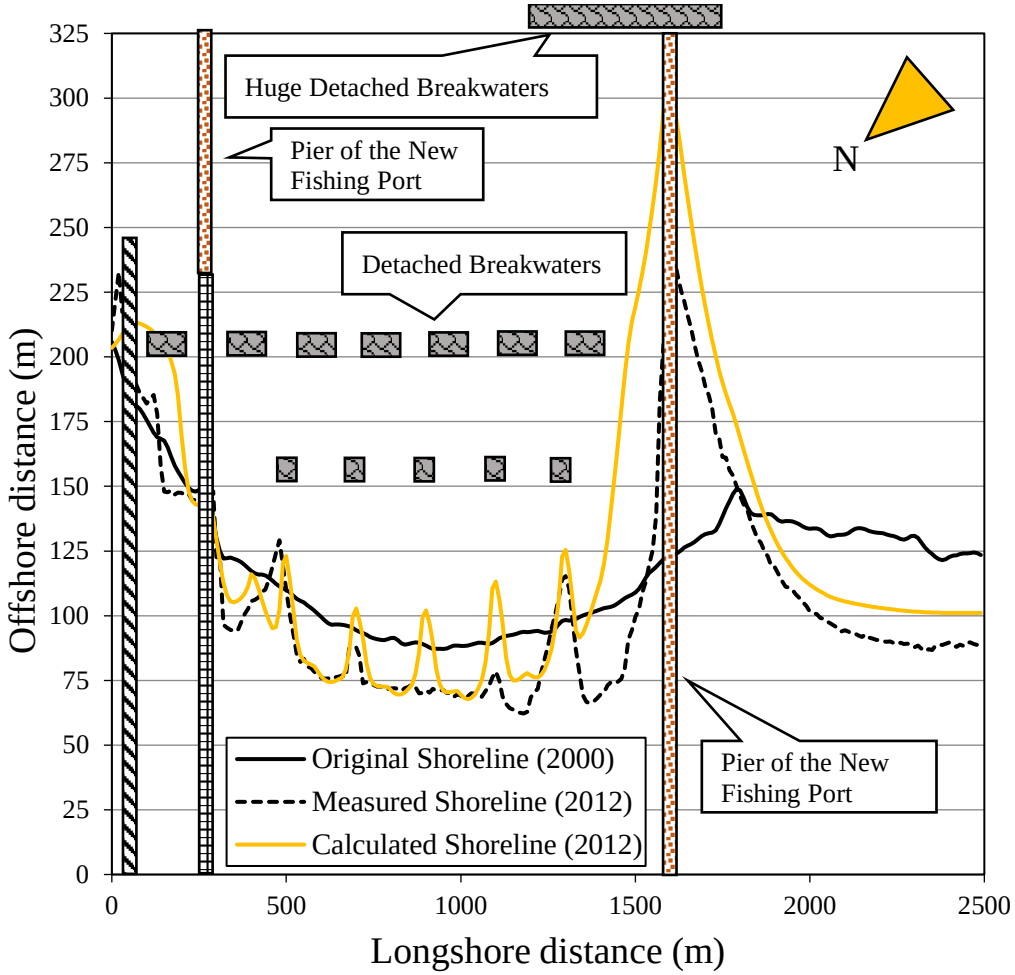

Figure 2.13. The comparison between the simulated- and the measured-shorelines from January of 2000 to March of 2012.

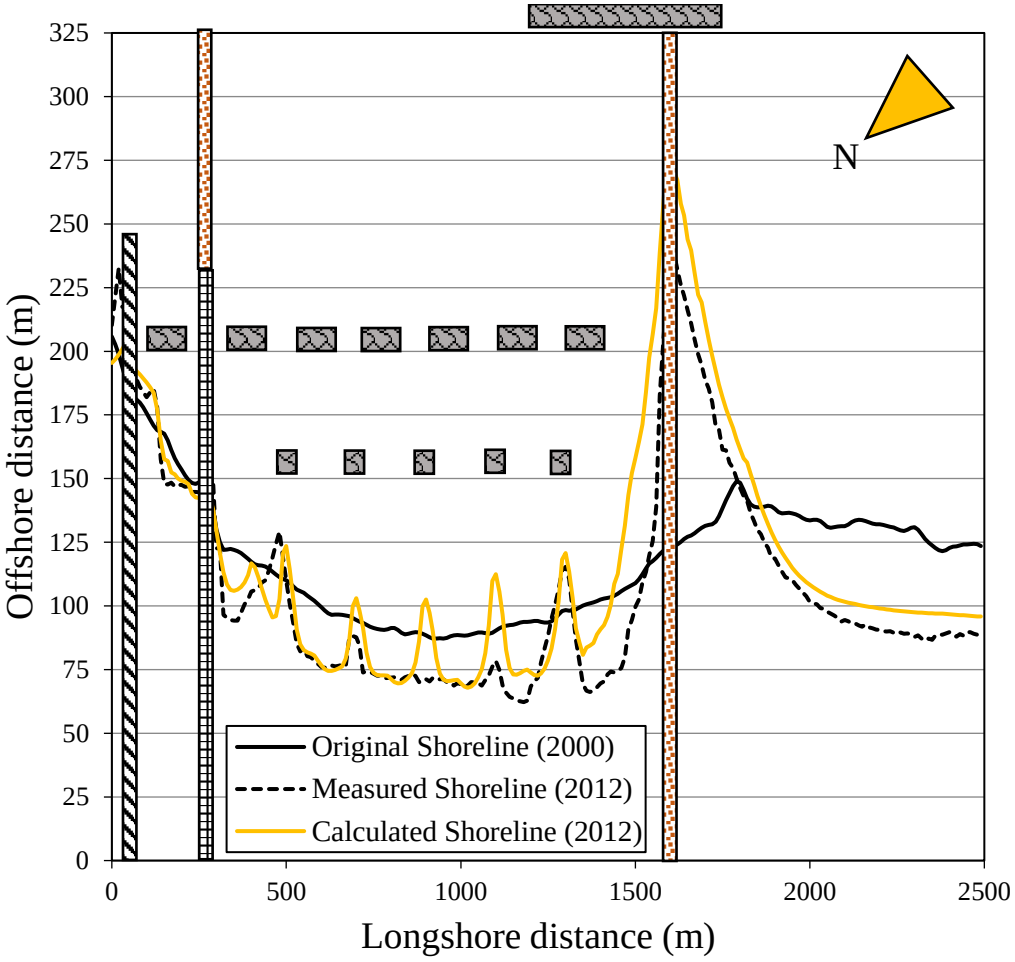

Figure 2.14. The comparison between the simulated- and the measured-shorelines from January of 2000 to March of 2012, when supply from the boundaries is zero.

To improve the accuracy of the simulation, the condition that the silt-and-sand supply from both boundaries are zero was used. The simulation result is shown in Figure 2.14. Although the degree of overestimation became smaller, since a wide beach extends on the outside of the right boundary and there is the river on the outside of the left boundary, this assumption is wrong. Moreover, the tendency of overestimation remains. However, the comparison between Figures 2.13 and 2.14 indicates that the silt-and-sand supply from the left- and right- boundaries can be disregarded to predict the shoreline change of the central coast area because the simulation result at the central coast area of those Figures is the same. Therefore, only the shoreline changes between the longshore distances of 300 – 1200m were considered. The shoreline change in ten years was simulated. The result is shown in Figure 2.15. The result shows that the most severe erosion section is the section between the longshore distances of 320 – 400m.

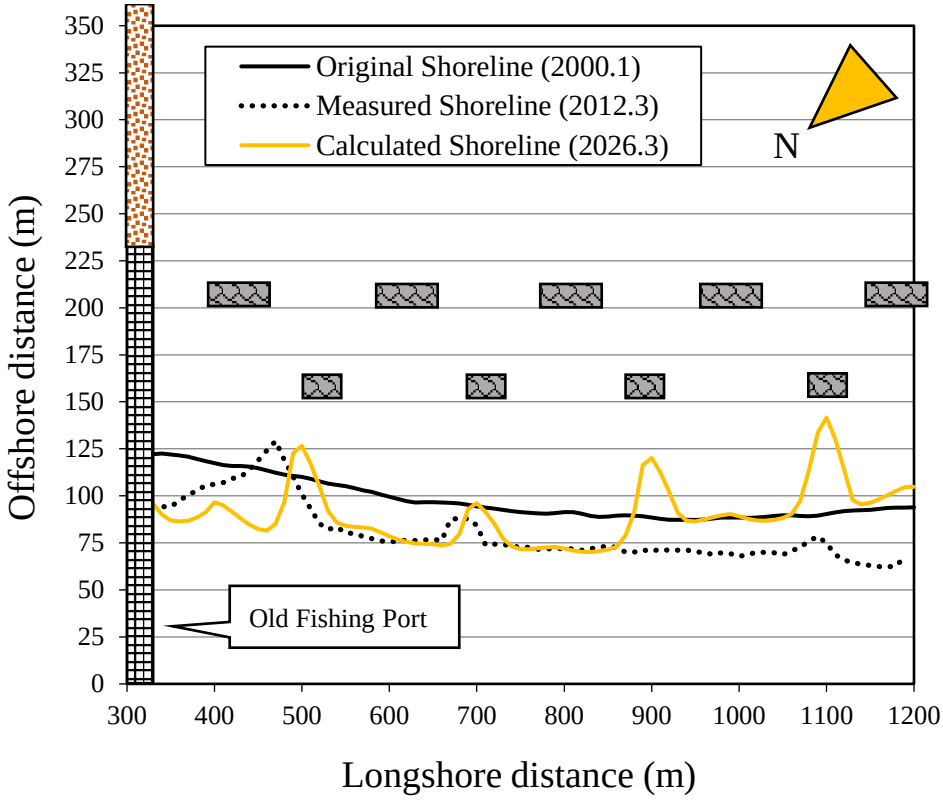

Figure 2.15. The comparison between the simulated- and the measured-shorelines from January of 2000 to March of 2026.

2.3.4 Evaluation of coastal protection capability

The prediction result using the one-line model, as shown in Figure 2.15, indicated that erosion of the section between the longshore distances of 320 – 400 m is the most serious. According to the field survey in March of 2015, we found that the beach width of the same area was very narrow, and the seawall of the same area suffered damage at the end of 2011. Therefore, in order to find the most suitable solution for this particular area, the examination of coastal protection was executed by using the evaluations on scour, wave overtopping, coastal environment conservation, and construction costs.

2.3.4.1 Examination of short-term beach change

The topographical change model of Ca et al. [6] was used to evaluate the topographical change in the critical section. We used the wave condition of Typhoon Linda (return period=10yrs), which has 3.0m of the significant wave height and 6.2s of

the wave period, and the duration is 10hrs. The simulated result is shown in Figure 2.16. From the result, the area at the right side of the old fishery port is the most serious part, in which the maximum scour depth at the center of the opening section was about 1m, as shown in Figures 2.16–2.17.

2.3.4.2 Examination of wave overtopping rate

In this part, empirical equations of de Waal and van der Meer [9] and van der Meer and Jansen [10], as expressed in Equations (2.15)–(2.17), were used to calculate wave overtopping induced by Typhoon Linda at the detached breakwater and the seawall. Moreover, the wave overtopping rate induced by regular waves were evaluated by using formulas, equations (2.18) and (2.21), of Yamamoto and Horikawa [11].

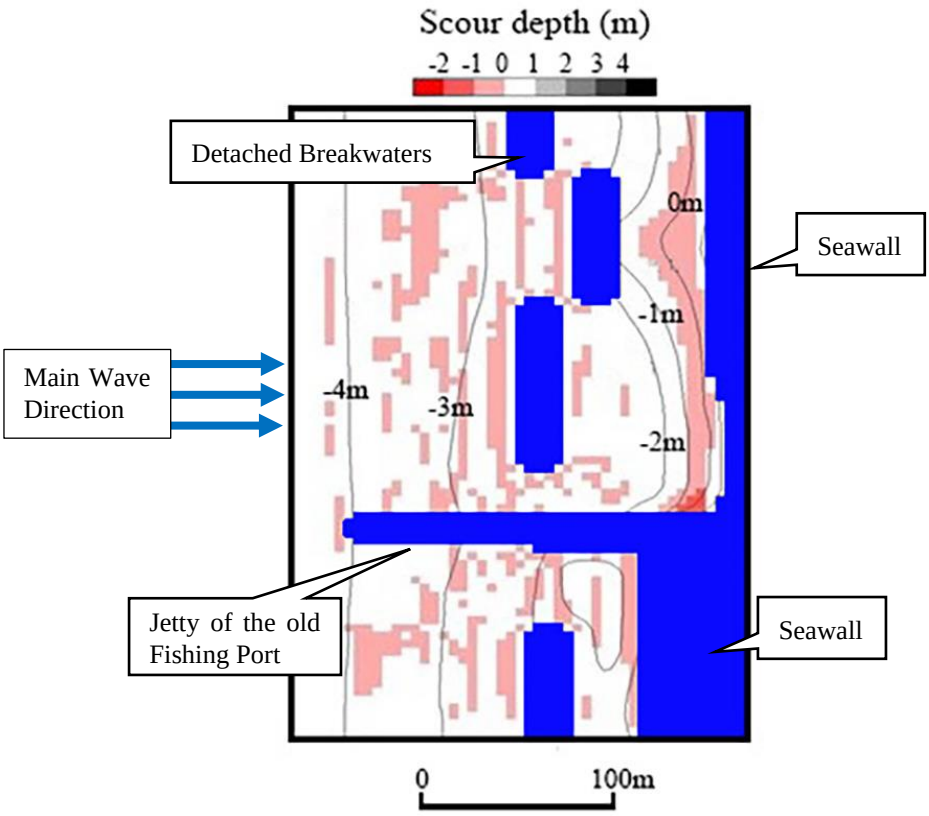

Figure 2.16. Result of scour situation when typhoon Linda acted for 10 hours by exist coastal facilities.

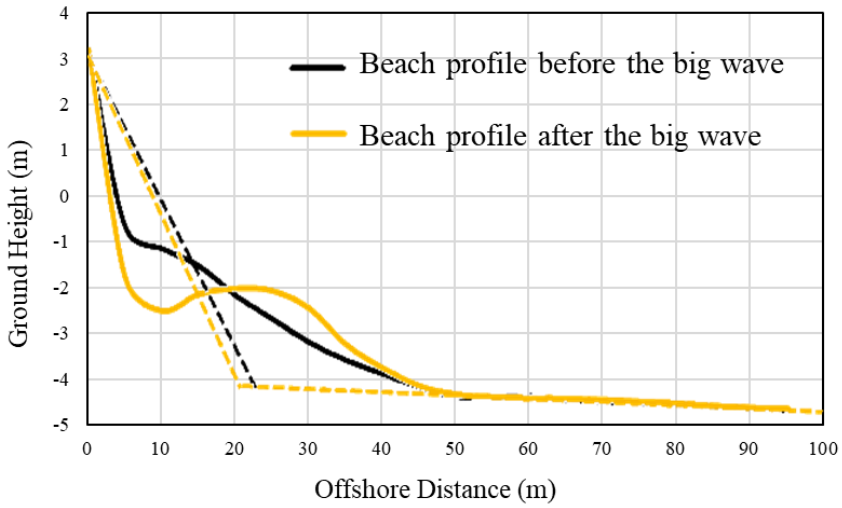

Figure 2.17. Beach profiles before and after big waves acted for 10 hours. Where dash lines are the hypothetical slopes calculated by a formula of Nakamura et al. [13].

The calculation condition was 3.0m of the significant wave height, 6.2s of the wave period, +1.3m of tidal level, and 0.7 of the diffraction coefficient of the structure. The wave overtopping rates in case of before- and after-scour of the existing coastal facilities were calculated. The calculated results are shown in Tables 2.1-2.2.

Coastal Engineering Manual (US Army Corps of Engineers [12]) purposed standard values of the wave overtopping rate for safety evaluation. The calculated results were compared to the standards. The calculated wave overtopping rates in original case using Yamamoto & Horikawa formulae are 1.0273m^3/m/s in case of before scour, and 1.0906m^3/m/s in case of after scour; while the results using Van der Meer et al. formulae are 0.0927m^3/m/s in case of before scour, and 0.1275m^3/m/s in case of after scour. These values indicate that the probability of destruction of the seawall is high (Refer to Table VI-5-6 in "Coastal Engineering Manual" in case of wave overtopping rate is more than 0.1m3/m/s, the possibility that the paved seawall is broken is very high). Therefore, the prevention capability of the existing facilities is not enough. Thus, an improvement is needed. By considering the wave overtopping rate reduction, the construction cost and the effect to the environment, the authors purposed three proposals of countermeasure improvement as follows:

1) Increase the crown height of the seawall by raising the crown height from 3.10 m (current) to 5.10m (+2.0 m of existing) on the mean tidal level: by using this

method, the wave overtopping rate responds to the typhoon of ten years in return period will be reduced. However, although seawalls can stop the shoreline retreatment, scour can occur at their fronts. In other words, seawalls have no ability to prevent coastal erosion. Moreover, increasing the seawall height will overlay the scenery of the beach.

2) Extend the detached breakwater: since waves can pass through the opening section between the jetty of the old fishing port and the detached breakwater, gap shut by extending the north side of the detached breakwater by 30m were proposed. Detached breakwaters can reduce the incident wave height by reflection and diffraction effects: that can cause shadow areas behind them, then salient or tombolo can form, these phenomena can trap sediment supplies behind the structures. This method can reduce the wave overtopping rate to zero and has sufficient effects on coastal erosion prevention. By the way, increasing the length of detached breakwater can worsen the scenery and construction cost is high.

3) Sand nourishment: a rich beach of 3.0 m on the mean tidal level in crown height and 0.056 in beach slope is proposed from the examination using formulae of Yamamoto et al. [12]. By using this proposal, seaward sand drift does not occur. Moreover, sand nourishments are friendly to the environment.

The wave overtopping rates of regular waves in each proposal were calculated by using formulae of Yamamoto & Horikawa [11] (the diffraction coefficient and the dissipation coefficient of the structure are 0.7 and 0.215, respectively). The calculated results are shown in Table 2.3. Moreover, the wave overtopping rates in irregular waves were calculated by using formulae of Van der Meer et al. [9,10] are shown in Table 2.4. Following the results from Tables 2.3 and 2.4, extending the detached breakwater length is clearly seen that the effect of wave overtopping reduction is very effective. Sand nourishment is also very good. By using these proposals, the destruction of seawall will not occur. In the case of raising the crown of the seawall, the wave overtopping rate is highest compared to other proposals.

Table 2.1. Calculated wave overtopping rates in regular waves using formulae of Yamamoto & Horikawa [11].

Examination Case	Kind of wave	Incident wave height (m)	Wave run-up height (m)	Wave overtopping rate (m^2/s)
Original case before scour	Significant	3.0x0.7=2.10	3.96	0.0000
	Maximum	3.0x1.9x0.7=3.99	5.61	1.0273 (failure)
Original case after scour	Significant	3.0x0.7=2.10	4.08	0.0000
	Maximum	3.0x1.9x0.7=3.99	5.80	1.0906 (failure)

Table 2.2. Calculated wave overtopping rates in irregular waves using formulae of Van der Meer et al. [10].

Examination Case	Incident wave height (m)	Run-up height exceeded 2% by irregular waves (m)	Wave overtopping rate (m^2/s)
Original case before scour	3.0x0.7=2.10	6.51	0.0927 (failure)
Original case after scour	3.0x0.7=2.10	7.05	0.1275 (failure)

Table 2.3. Calculated wave overtopping rates in regular waves using formulae of Yamamoto & Horikawa [11].

Examination Case	Kind of wave	Incident wave height (m)	Wave run-up height (m)	Wave overtopping rate (m^2/s)
Seawall made highly (3.1m → 5.1m)	Significant	3.0x0.7=2.10	4.08	0.0000
	Maximum	3.0x1.9x0.7=3.99	5.80	0.0728
Detached breakwater extended (+30m)	Significant	3.0x0.215=0.65	2.42	0.0000
	Maximum	3.0x1.9x0.215=1.23	3.10	0.0000
Sand nourishment	Significant	3.0x0.7=2.10	2.52	0.0000
	Maximum	3.0x1.9x0.7=3.99	3.28	0.0218

Table 2.4. Calculated wave overtopping rates in irregular waves using formulae of Van der Meer et al. [9,10].

Examination Case	Incident wave height (m)	run-up height exceeded 2% by irregular waves (m)	Wave overtopping rate (m^2/s)
Seawall made highly (3.1m→5.1m)	3.0x0.7=2.10	7.05	0.0070
Detached breakwater extended (+30m)	3.0x0.215=0.65	4.33	0.0037
Sand nourishment	3.0x0.7=2.10	2.56	0.0000

2.3.4.3 Comprehensive evaluation results

By considering the wave overtopping rates, as shown in Tables 2.1-2.4, evaluation of the countermeasures was proposed, as shown in Table 2.5. The explanation for each countermeasure is given below:

1) Increase the crown height of the seawall (3.1m→5.1m): this method cannot prevent the coastal erosion in front sand of the seawall. So, the prevention effect of coastal erosion is zero. Moreover, since the raising crown height of seawall will destroy the scenery, the conservation effect of the environment is minus one. In the other hand, the wave overtopping prevention by this method is good; thus, the score of the prevention effect of wave overtopping is two. The construction cost of the seawall of the crown height of 5.1 m is 300,000 baht/m and the necessary length is 80m. So, the total cost is 300,000 baht/m x 80 m = 24,000,000 baht.

2) Extend the detached breakwater (+30m): since the extent of the detached breakwater has sufficient effects on the prevention of erosion and wave overtopping, both scores of prevention effect of coastal erosion and the prevention effect of wave overtopping are two. However, the extending length of the detached breakwater worsens the coastal environment; thus, the score of the conservation effect of the environment is minus one. The construction cost of the existing detached breakwater is 800,000 baht/m and the length for expanding is 30m. So, the total cost is 800,000 baht/m x 30 m = 24,000,000 baht.

3) Sand nourishment: expanding the beach area with sand nourishment gives

sufficient effects to prevent both coastal erosion and wave overtopping; therefore, the scores of those are two. Moreover, sand nourishments have a good effect on the conservation of coastal environment; so, the score is also two. Since the sand nourishment will be set between the jetty of the old fishery port and the adjacent detached breakwater, we could assume that the sand nourishment dose not move to both sides. Since the sand nourishment will be constructed with the stable slope 0.056, we could assume that the on-off sand drift does not occur. The construction cost of is method is 2200 baht/m^3 and the necessary volume 9600 m^3; thus, the total cost is 21,100,000 baht.

Since the construction costs of the three proposals are nearly the same, the score of construction cost in all proposals becomes zero.

Table 2.5. A comprehensive comparison between all countermeasures.

Examination case	Prevention effect of coastal erosion	Prevention effect of wave overtopping	Conservation effect of environment	Construction costs	Total point
Seawall made highly	No effect 0	Better effect 2	Bad effect -1	300,000baht/m x80m = 24,000,000bahts	1
Detached breakwater extended	Better effect 2	Better effect 2	Bad effect -1	800,000baht/m x 30m = 24,000,000baht	3
Sand nourishment	Better effect 2	Better effect 2	Good effect 1	2200baht/m^3 x 9600m^3 = 21,100,000baht	5

2.3.5 Conclusions for analysis of Khlong Wan Coast

1) According to field surveys and the one-line simulation results, the jetty and the groin of the northeast coast, and the big tombolo, which was formed by the huge detached breakwater, caused heavy coastal erosion in the central coastal area by

blocking the sand supply. Therefore, even if eleven detached breakwaters were constructed for the same term, these cannot stop erosion.

2) In the southwest side beach of the groin, the prediction results using the one-line model show that the shoreline will retreat about 5m after ten years. The topographical change induced by big waves was simulated by using Ca et al.'s numerical model. The maximum scouring depth will become about 100cm. Therefore, we can acknowledge that this part of the beach will become the most dangerous area, and the coastal protection facilities must be improved.

3) According to the comprehensive evaluation of the prevention effects of coastal erosion and wave overtopping, the conservation effect of the environment, and the construction costs, as shown in Table 2.5, the sand nourishment by using the sand supply from the big tombolo near the new fishing port is the most proper countermeasure in the Khlong Wan Coast.

2.4 Application of numerical models in Chumphon Coast

Yamamoto et al. [15] analyzed the effects of coastal structures in Chumphon Coast and proposed a suitable countermeasure. Chumphon Province is at the top of the southern region of Thailand (10°27'N, 99°11'E), as shown in Figure 2.18. The terrains are divided into three parts: plains, coastal plains, and highlands and mountains. This province has a total shoreline length of about 222 kilometers. Chumphon Province is influenced by the southwest monsoons and the northeast monsoons. As a result, this province has only two seasons: summer and rainy season. Most of the villagers are fishermen and farmers. The authors selected Pak Nam Chumphon (Chumphon Estuary), Muang District, as the study area. The long-term shoreline change simulation and the short-term topographical change simulation were implemented to examine the safety of the coast.

In the area, there are two huge jetties and seawalls as erosion countermeasures; the length of the north jetty is about 1,000 meters and 850 meters for the south jetty. From a field survey in August of 2015, these jetties were built in the year of 2000 to maintain the navigation channel of the Chumphon Estuary. The south of the estuary is

home of the Pak Nam Municipality community. During the survey, the beach was under the construction of a recreation park. The shoreline length of the study area is about 270 meters. The beach is sandy; however, some parts have a layer of river mud. The deposition of this mud made the beach shallower, which then affects the tourist industry in the area. There are two islands near the study area. One is a small island, Mattaphon Island, and the other is a large island, Koh Samet Island. These islands have a strong influence on the study area because tombolo was found behind the small island. The scope of the study was determined, as shown in Figure 2.19.

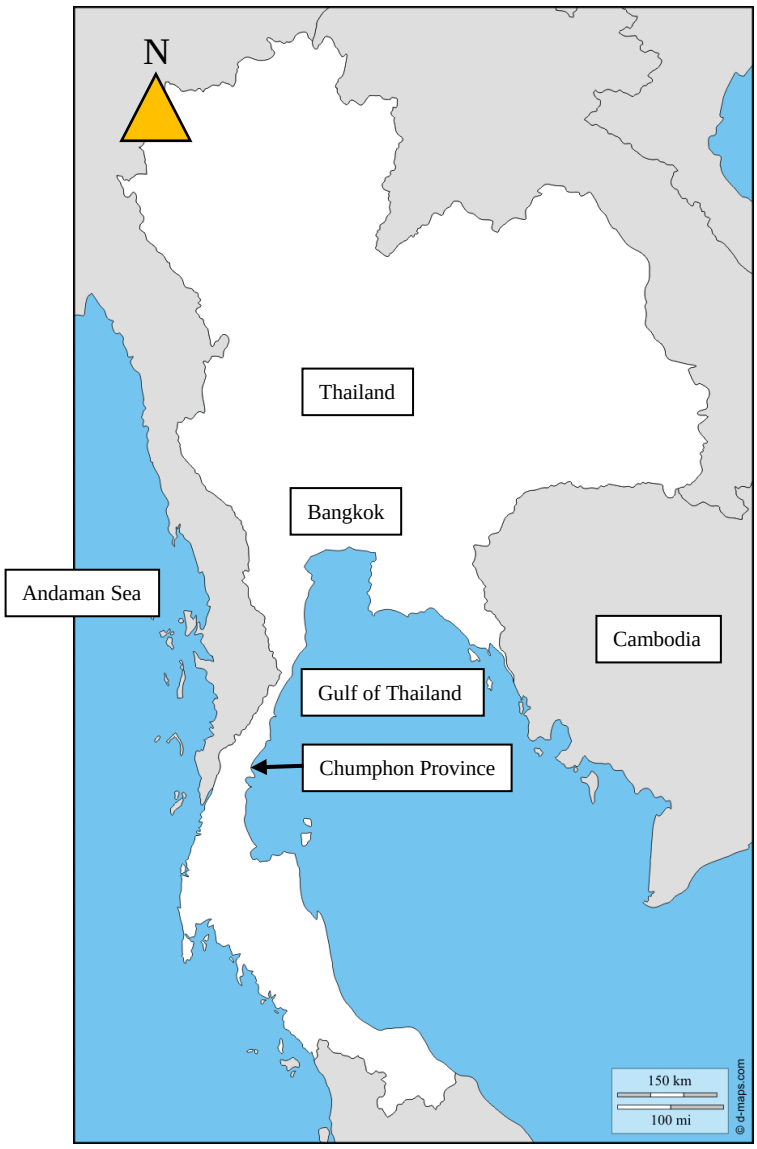

Figure 2.18. The location of study area, Chumphon City, Chumphon Province. (Thailand map from d-map.com).

Figure 2.19. A satellite image of the study area (from Google Maps).

2.4.1 Materials

Satellite images of the years of 1999 and 2011 were used as verification data for the one-line simulation. Wave data from 1993 to 2000 at Ko Tao observation station, which is about 65 km southeast from the coast, was extracted from reports of Geo-Informatics and Space Technology Development Agency, Thailand – GISTDA. Since there were some discontinuity in the wave data (due to maintenances of the buoy) the data at the time of the discontinuity was replaced by repeating the available data. A navigation chart form Marine Department of Thailand was used to determine the bathymetry of the area. The sediment discharge rate of the Chumphon Estuary used in the simulations was zero because the local government dredges the river every year (~90,000m^3/year) in order to maintain the navigation channel.

2.4.2 Shoreline change simulations

The shoreline changes from 1999 to 2011 was simulated by using the one-line model. This simulation was implemented in order to verify the inputs and the coefficients of the model. The coefficients in Ozasa & Brampton's equation [5] of 0.02-0.20 were used in the trial simulations. The coefficient of 0.10 yields an acceptable result, as shown in Figure 2.20. After the reliability of the model was confirmed, the shoreline changes in 2047 was examined. The simulation result is shown in Figure 2.21. From the result, the shoreline retreat of up to 26m occurred between the longshore distances of 3050m and 4450m (the northwestern side of the jetties), and the deposition of up to 75m occurred between the longshore distances of 4450m and 5150m. Additionally, a maximum of 230m of the deposition was predicted between 5470m and 5670m along the southeastern side of the jetties, and erosion was predicted between 5670m and 5870m and between 6070m and 6500m.

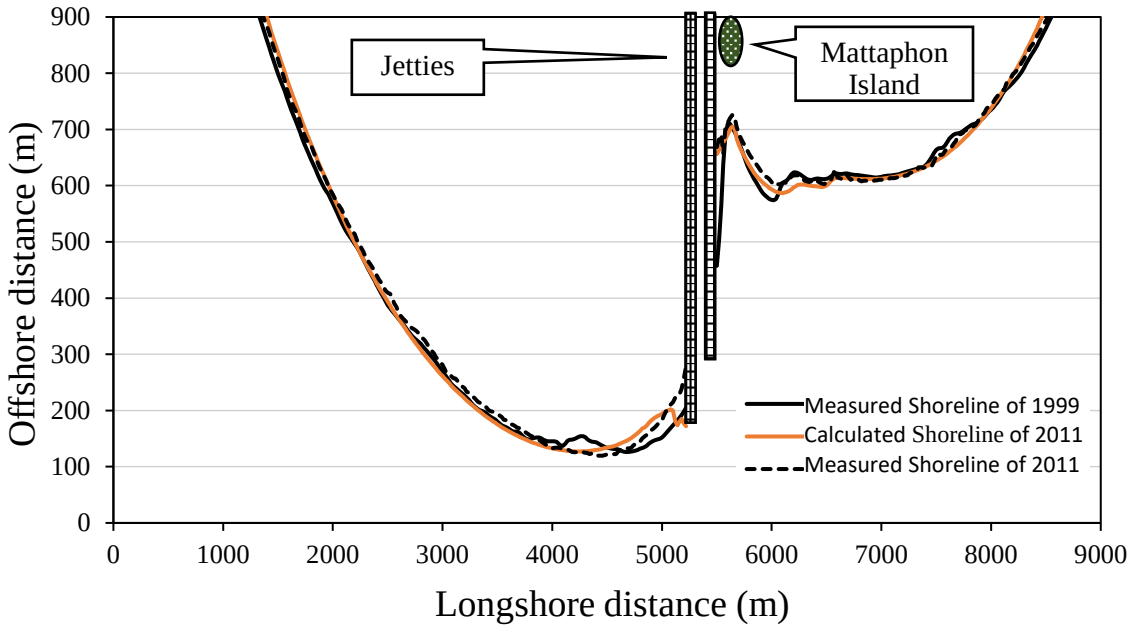

Figure 2.20. The comparison between the original-, the simulated-, and the measured-shorelines from 1999 to 2000.

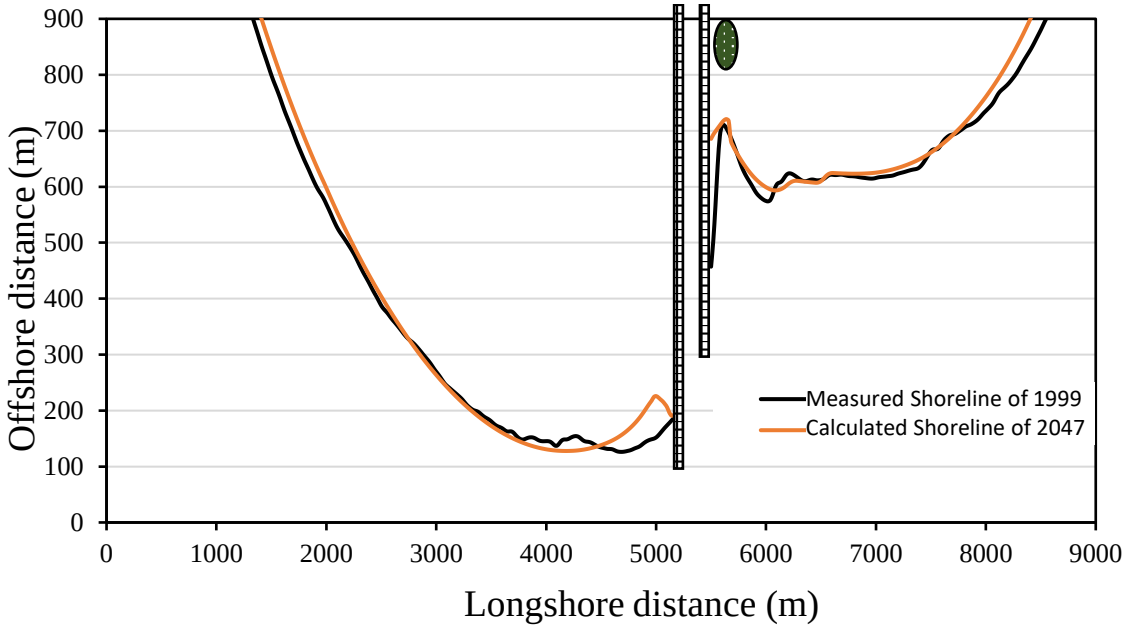

Figure 2.21. The comparison between the original shoreline in 1999 and the simulated shoreline in 2047.

2.4.3 Coastal protection measures in the eroded section

First, the eroded area between the coastal distances of 3050m to 4450m, as shown in Figure 2.21, was examined. There are some private houses and plantations in this particular area. The comparison between Figures 2.20 and 2.21 shows that the shoreline shape is stable; thus, it is difficult for the erosion rate to increases, even after 30 years. Thus, to purchase plantations and to move private houses (zoning) would be a good countermeasure. Assuming the worst situation, the cost of 18,000m^2 of the eroded plantation areas is about 60 million baht, and the relocation cost of houses is about 20 million baht (eight houses); thus, total cost is about 80 million baht. Therefore, this countermeasure is more economical than construction of structural countermeasures such as breakwaters or artificial reefs (250,000baht/m × 800m=200,000,000baht).

Next, the eroded area between the longshore distances of 6070m and 6500m is an uninhabited forest area, as shown in Figure 2.19. Since there is no extremely changes of shoreline (refer to the simulation result shown in Figure 2.21), countermeasures are not necessary.

Finally, although the long-term erosion between the longshore distances of 5670m and 5870m is very small, as shown in Figure 2.21, there are a seaside road and many houses in the area. Therefore, the safety analysis of this section must be implemented.

2.4.4 Examination of short-term beach change

Short-term topographical change analyses were implemented by using the topographical change model of Ca et al. [6]. The wave condition of Typhoon Linda ($H_{1/3}$=4.1m, and $T_{1/3}$=6.2s) acting for 10hrs was used. The calculation result is shown in Figure 2.22. As shown in Figure 2.22, heavy scour occurred, in which the maximum scour depth is 0.5m, on the A-A cross section. The cross section is shown in Figure 2.23.

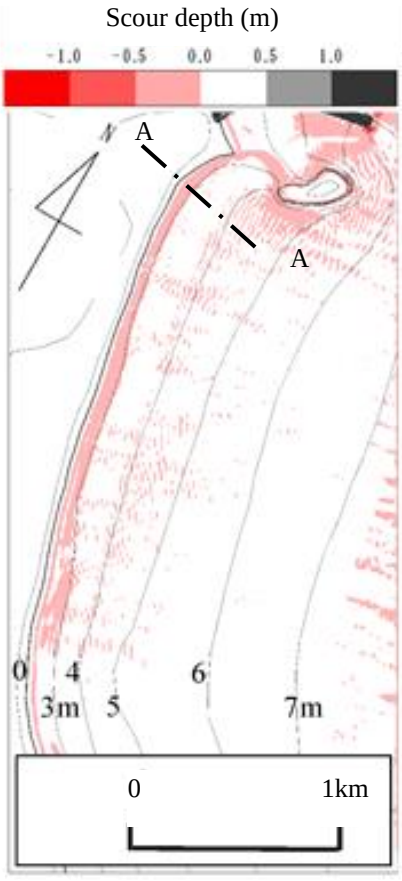

Figure 2.22. The result of scour situation when typhoon Linda acted for 10 hours in the case of the existing coastal facilities.

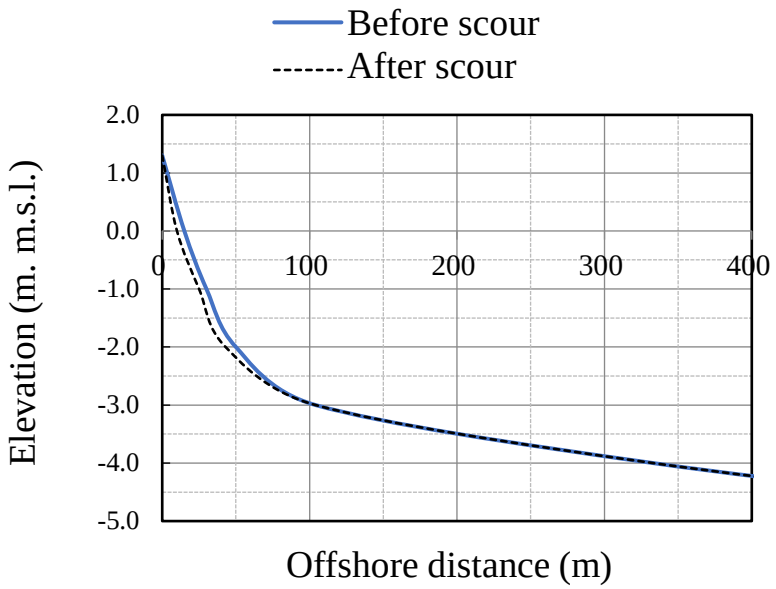

Figure 2.23. Cross sections of the section A-A in cases of before- and after-scour.

2.4.5 Examination of wave overtopping rate

The wave overtopping rates during the time of the typhoon at the section A-A was calculated by using the equations of Van der Meer et al. [9,10]. The results are shown in Table 2.6. Moreover, the overtopping rates induced by the maximum wave height and significant wave height were calculated; the results are shown in Table 2.7.

Table 2.6. Calculated wave overtopping rates using formulae of Van der Meer [9,10].

Case	Significant wave height (m)	Significant wave period (s)	Average bed slope	Tidal level (m)	Overtopping rate (induced by irregular wave) ($m^3/s/m$)
Original case before typhoon Linda	4.10	6.20	0.067	2.80	0.0024
Original case after Typhoon Linda	4.10	6.20	0.077	2.80	0.0061
Raising seawalls	4.10	6.20	0.077	4.80	0.0000
Breakwater (wave transmission rate = 0.4)	1.64	6.20	0.067	2.80	0.0000
Artificial reef (wave transmission rate = 0.4)	1.64	6.20	0.067	2.80	0.0000

Table 2.7. Calculated wave overtopping rates using formula of Yamamoto and Horikawa [11].

Case	Incident wave type	Wave height (m)	Wave period (s)	Beach slope	Tidal level (m)	Wave overtopping rate ($m^3/s/m$)
Original case before typhoon Linda	$H_{1/3}$	4.10	6.20	0.043	2.80	0.028
	H_{max}	7.38	6.20	0.043	2.80	0.558
Original case after Typhoon Linda	$H_{1/3}$	4.10	6.20	0.050	2.80	0.067
	H_{max}	7.38	6.20	0.050	2.80	0.699
Raising seawalls	$H_{1/3}$	4.10	6.20	0.050	4.80	0.000
	H_{max}	7.38	6.20	0.050	4.80	0.000
Breakwater (wave transmission rate = 0.4)	$H_{1/3}$	1.64	6.20	0.043	2.80	0.000
	H_{max}	2.95	6.20	0.043	2.80	0.000
Artificial reef (wave transmission rate = 0.4)	$H_{1/3}$	1.64	6.20	0.043	2.80	0.000
	H_{max}	2.95	6.20	0.043	2.80	0.000

Standard values from table-VI-5-6 of the Coastal Engineering Manual [12] and table-4.3 of the Guideline for Coastal Conservation Plan were used. In the original case, the irregular overtopping rate exceeds $0.001 m^3/s/m$. Thus, when compared this value to the table-4.3, the result shows that walking on this seawall is very dangerous. Furthermore, if the damage criteria in table-4.3 is applied, the regular wave overtopping rate of $0.05 m^3/s/m$ or more can be estimated that the road may be broken. Therefore, the following countermeasures were proposed in order to improve the safety of the area.

1) Raising the crown of the existing seawalls: raising the crown height by 2.0m (from MWL + 2.8m to MWL + 4.8m) to prevent overtopping induced by typhoon Linda.

2) A breakwater: for the same purpose, a breakwater with the wave dissipation coefficient of 0.4, and the crown height of MWL + 2.2m was proposed.

3) An artificial reef: an artificial reef with a wave transmission coefficient of 0.4, and the crown height of MWL – 0.5m was proposed.

Although beach nourishment can be used as a countermeasure, it is necessary to prevent the nourishment sand from flowing out in the northwest direction. Since additional structures are required for beach nourishment, which will cost additional construction cost, this method was not proposed.

2.4.6 Comprehensive evaluation comparison of the proposed countermeasures

To evaluate the proposed countermeasures, the effects of erosion prevention, wave overtopping prevention, environmental protection, construction costs were considered.

1) The effect of coastal erosion prevention. By using the formula of Yamamoto et al. [16], the offshore sediment transport rates shown in Table 2.8 were obtained. According to this result, raising the crown height of the seawall cannot be expected to prevent erosion, and was evaluated as zero point (no effect). On the other hand, the breakwater or the artificial reef can be expected to significantly reduce the amount of offshore sedimentation.

Table 2.8. Calculated results of cumulative amount of offshore drifting sand by the formula of Yamamoto et al. When Typhoon Linda acted for 10 hours.

Case	Incident wave height (m)	Wave period (s)	Beach slope	Median grain size of sediment (mm)	Offshore sand transport rate (m^3/10hr/m)
Raising seawalls	4.10	6.2	0.043	0.5	35.4
Breakwater	1.64	6.2	0.043	0.5	0.6

2) The effect of wave overtopping prevention: Since all the overtopping amounts of the three measures in Tables 2.6 and 2.7 are zero, it is deemed that all the measures have sufficient effects and a one-point evaluation is made.

3) The effect of the environment conservation. Since the raising of the crown of the seawall and the breakwater degrade the seaside view, these proposals were deemed to be -1 point. These proposals also affect the water quality of the land side sea area. However, since artificial reefs do not deteriorate the water quality and the landscape, it is evaluated as 0 point.

Since the construction cost of the seawall raising is considerably lower than the other two plans, the total score is calculated by setting the construction cost evaluation of the seawall raising plan to 1 point and the evaluation of the other two plans to 0 point. By this analysis, the artificial reef received the highest evaluation. Table 2.9 shows the summarize of the evaluations.

Table 2.9. Evaluation results and the construction costs of each plan.

Countermeasures	Coastal erosion prevention	Overtopping prevention	Environmental conservation	Construction costs	Total score
Raising seawalls	No effect 0	Effective 1	Bad effect to landscape -1	150,000baht/m ×200m = 30,000,000baht 1	1
Breakwater	Effective 1	Effective 1	Bad effects to landscape and water quality -1	250,000baht/m ×200m = 50,000,000baht 0	1
Artificial reef	Effective 1	Effective 1	Almost no effect 0	250,000baht/m ×200m = 50,000,000baht 0	2

2.4.7 Conclusions for analysis of Chumphon Coast

The result from the one-line model, as shown in Figure 2.21, indicates that erosion occurred at the longshore distances between 3050m and 4450m and between 5670m and 5870m. In the section of 3050m-4450m, the land reclamation (zoning) is the most suitable countermeasure. As for the section of 5670m-5870m, an artificial reef was the most effective based on the effects of erosion prevention, overtopping prevention, environmental conservation, and construction costs.

2.5 Conclusions

A design procedure for a suitable countermeasure using numerical models, as shown in Figure 2.9, was introduced. This procedure utilizes the prediction abilities of the line-model and the topographical change model to design coastal erosion countermeasures. First, the degree and the cause(s) of erosion are examined by using the one-line model. After that, if there is heavy erosion, various countermeasures are examined by using the wave overtopping formulae and the topographical change model. The author used the procedure to analyze two coasts in Thailand—Khlong Wan Coast and Chumphon Coast. Then, a suitable countermeasure for each coast was introduced.

As for Khlong Wan Coast, by analyzing the shoreline change using satellite images, aerial photographs, and the one-line model, the cause of erosion is a lack of sediment source by the blockage of structures. The big jetty in the south of the coast has been intercepted sand supplies from the south. Moreover, the riverine sediments from the Khlong Wan River in the north of the area are blocked by the small groin on the river mouth. Under this situation, coastal erosion occurred when big waves hit the coast; however, under the normal waves, which usually carry sand from deeper area to shallower area, sediment cannot flow inside the area due to the blockage of the structures, then resulted in heavy erosion. Various countermeasures were examined by using the wave overtopping formulae and the topographical change model. The most suitable countermeasure is sand nourishment.

As for Chumphon Coast, the same procedure was applied. The results from satellite images and aerial photograph analysis show that the cause of erosion is the blockage of

the riverine sediment from Chumphon Estuary by big jetties. However, the results from the one-line model show that this erosion is short-term erosion, which induced by the construction of the jetties. After some years, the beach can maintain the equilibrium shape. Sine the new equilibrium shoreline consists of some erosion parts, the safety of these parts was examined. Countermeasures were examined by using the wave overtopping formulae and the topographical change model. The most suitable countermeasure for erosion on the longshore distances between 3050m and 4450m is the land-reclamation because the population in that area is low. As for erosion on the longshore distances between 5670m and 5870m, an artificial reef was the most suitable countermeasure.

The results show that the design procedure, as shown in Figure 2.9, can be used to determine the most suitable countermeasure(s) for the Thai coasts. However, since there are some cases that the cause of the destruction was the outflow of backfilling materials, which cannot be simulated by existing models, further consideration of the outflow should be added in order to expand the consideration range of the procedure.

References

[1] Department of Marine and Coastal Resources. “Guidelines for Project Development and Coastal Erosion Prevention and Resolution Plans,” available online at https://www.dmcr.go.th/detailLib/3712 (in Thai)

[2] Japan Society of Civil Engineers (2000). “Design Manual for Coastal Facilities 2000,” 577p.

[3] Yoshimichi Yamamoto (2006). “Design Process of Coastal Facilities for Disaster Prevention,” Proceedings of the School of Engineering, Tokai University, Series E, Vol. 31, 2006, pp11-19.

[4] Hans Hanson (1989). “Genesis-A Generalized Shoreline Change Numerical Model,” Journal of Coastal Research, Vol.5 No.1, pp 1-27.

[5] Ozasa Brampton (1979). “Models for Predicting the Shoreline Evolution of Beaches Backed by Seawalls,” Report of the Port and Harbor Research Institute, Vol.18 No.4, pp. 77-104.

[6] Ca, VT, Yamamoto, Y, Tanimoto, K, and Arimura, J (2002). “Simulation on Wave Dynamics and Scouring near Coastal Structures by a Numerical Model,” Proceedings of the 28th International Conference on Coastal Engineering, American Society of Civil Engineers, pp. 1817-1829.

[7] Ribberink, J.S. (1998). “Bed-load transport for steady flows and unsteady oscillatory flows,” Coastal Engineering, Vol. 34, pp. 59-82.

[8] Van Rijn L.C. (1984). “Sediment Transport: Part II: Suspended Load Transport. Journal of Hydraulics. Div., Proc. American Society of Civil Engineers, 110 (HY11), pp. 1613-1641.

[9] De Waal, JP, and Van der Meer, JW (1992). “Wave run-up and Overtopping on Coastal Structures,” Proceedings of the 23rd International Conference on Coastal Engineering, American Society of Civil Engineers, II, pp. 1758-1771.

[10] Van der Meer, JW, and Janssen, W (1995). “Wave run-up and Wave overtopping at Dikes,” Wave Forces on Inclined and Vertical Wall Structures, Kobayashi and Demirbilek, eds., American Society of Civil Engineers, pp. 1-27.

[11] Yamamoto, Y., and Horikawa, K. (1992). “New Methods to Evaluate Wave Run-up Height and Wave Overtopping Rate,” Proceedings of the 23rd International Conference on Coastal Engineering, American Society of Civil Engineers, II, pp. 1734-1747.

[12] US Army Corps of Engineers (2002). “Coastal Engineering Manual,” available online at http://www.publications.usace.army.mil/USACEPublications/

[13] Nakamura, M., Sasaki, Y., and Yamada, J. (1972). “A study on wave runup on compound profile,” Proceedings of the 19th Conference on Coastal Engineering, Japan, Journal of Japan Society of Civil Engineers, pp. 309-312.

[14] Silarom, K., Yamamoto, Y., and Charusrojthanadech, N. (2017). “Analysis of Coastal Erosion in Khlong Wan Coast,” Proceedings of the 27th International Ocean and Polar Engineering Conference, 25-30 June 2017, San Francisco, California, USA, pp. 1519-1526.

[15] Yamamoto, Y., Silarom, K., and Yoshizawa, Y. (2017). “Investigation on Coastal Erosion and Examination of Coastal Protection Facilities at Chumphon Coast in Thailand,” Journal of Japan Society of Civil Engineers, Ser. B2 (Coastal Engineering) 2017, Vol 73(2), pp. I_1585-I_1590. doi:10.2208/kaigan.73.I_1585.

[16] Yamamoto, Y.; Horikawa, K.; and Tanimoto, K. (1996). “Prediction of Shoreline Change Considering Cross-shore Sediment Transport,” Proceedings of the 25th International Conference on Coastal Engineering (organized by American Society of Civil Engineers), Orlando, FL, USA, 2–6 September 1996; pp. 3405–3418, doi:10.1061/9780784402429.263.

III. Development of a numerical simulation model for simulating the outflow rate

3.1 Introduction

3.2 The concept of the model

3.3 A verification simulation using original CADMAS-SURF

3.4 Improvement of the calculated pressure from CADMAS-SURF

3.5 Applications of the model to field cases

3.6 Improvement of the design procedure

3.7 Conclusions

3.1 Introduction

In this chapter development of numerical model for simulating the outflow rate of backfilling materials from a coastal structure with an arbitrary shape is described. This chapter is based on synthesis on the following publications: Silarom et al. ([1], [2]), and Silarom and Yamamoto ([3], [4]). The chapter consists of four sections: introduction; the concept of the model; improvement of the calculated pressure from CADMAS-SURF; and applications of the model to field cases.

To visualize outflow, an example hydraulic model experiment is introduced. In this experiment, a 1/30 dike model filled with sand (median grain size = 0.2mm) was continuously hit by irregular waves, during which the significant wave height was 0.223m, and the significant wave period was 2.65s. This experiment uses a dike in the Hirono Coast in Shizuoka Prefecture, Japan and the wave conditions of Typhoon No. 9 from 1997 ($H_{1/3}$ = 6.69m, $T_{1/3}$ = 14.5s) as a prototype. The direction of the outflow is the offshore direction. When the effects of wave diffraction or shaded areas are not considered (e.g., the effects of detached breakwaters or breakwaters), the mechanism of outflow phenomena can be analyzed in two dimensions. Since the generated waves were uniform in the alongshore direction, the alongshore transportation in the experiment can be neglected. The experimental result is shown in Figure 3.1. In a coastal dike or a seawall filled by granular materials (e.g., Figure 3.1a), when the scour depth in front of the structure reaches the lowest edge of the structure (e.g., a sheet pile) (Figure 3.1b), incident waves can penetrate under the body of the structure. Thereafter, when the shear resistance at the lowest edge of the structure becomes smaller than the shear force generated by the return flow, the backfilling materials flow out via the return flow through the edge of the structure. When the materials at the lowest edges flow out, the remaining materials are moved to fill the void by the gravity until the slope becomes stable. In this way, the formation of a cave occurs (Figure 3.1c–f). This motion of backfilling materials is called the outflow (or suction). When the structure loses its backfilling materials, the stability and the protective ability of the structure become weaker than their designated values. Then, when middle-scale waves hit the structure, the possibility that the structure will be destroyed is high.

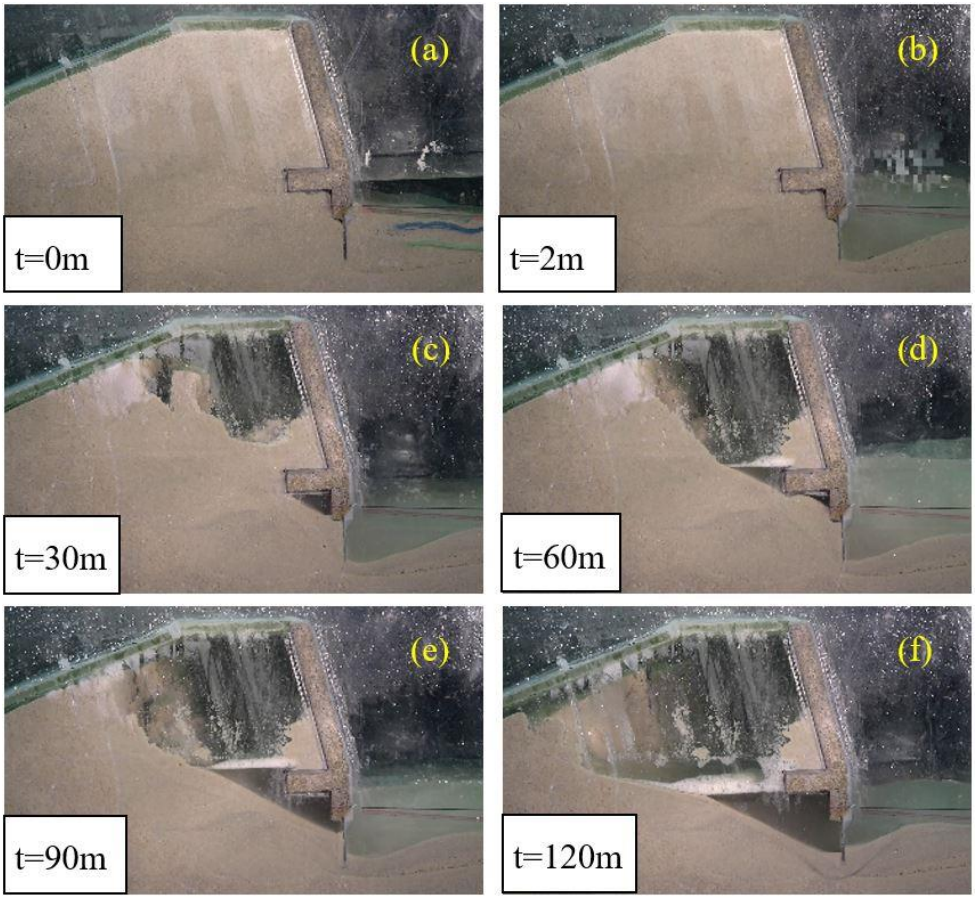

Figure 3.1. Scour and the outflow in a dike model.

As mentioned in chapter 1, the outflow of backfilling materials is one of the main reasons for the destruction of coastal structures constructed in very shallow areas and needs to be considered in the designing of such structures. There are few existing methods that can evaluate the outflow rate. For empirical approaches, Yamamoto and Minami [5] studied the mechanism of outflow phenomena by using experiments with a wave flume and a dike model. They were able to reproduce the outflow from a concrete-covered dike in Hirono Coast, Japan, which was damaged by Typhoon No. 9 in 1997. After they confirmed the reliability of their experimental methodology, they used their method to examine the effects of various parameters on the outflow rate. The results show that shear resistance decreases when the sand layer thickness in front of the structure becomes thinner and the outflow rate increases when the median grain size becomes finer. Due to these results, the authors proposed an empirical method for predicting the failure of a dike or a seawall induced by outflow. Ioroi and Yamamoto [6] performed many experiments in order to determine the relationship between the

outflow rate and the pore water pressure, the return flow velocity, and the median grain size of backfilling materials. They proposed an empirical outflow formula that could consider the effects of the median grain size, the sand layer thickness at the front of the structure, the maximum pore water pressure, and the maximum return flow velocity. Kuisorn et al. [7] performed field surveys on many coasts in Thailand and reported outflow damage on these coasts. They calculated the outflow rates by using Ioroi and Yamamoto's formula; the results show that the formula could be applied to field cases with acceptable accuracy.

For numerical approaches, Maeno et al. [8] and Kotani et al. [9] reported that the cyclic action of water pressure on the sand layer precipitated the formation of a cave inside a structure and caused the failure of the structure. The authors proposed a numerical model for simulating cyclic water pressure, based on the poro-elastic theory, which could simulate the cyclic pressure under a simple seawall. Nakamura et al. [10] proposed a simulation model based on the Volume of Fluid technique and the Biot model. Their model could simulate the outflow rate from the lowest edge of a rubble revetment. Since these models are limited by the shapes of structures, the author developed a numerical model that can simulate the outflow of backfilling from the lowest edge of a structure with an arbitrary shape.

3.2 The concept of the model

The model consists of two main parts: the sediment transport model and the hydrodynamics model. Many software can calculate water motions in a wave flume. In this research, CADMAS-SURF (SUper Roller Flume Computer-Aided Design of MAritime Structure) [11], a wave flume simulation model developed by Coastal Development Institute of Technology, Japan, was used to calculate wave motions, wave-structure-interactions, and water motions in porous media. The reasons that the author selected this model are (1) this model can calculate water motions in porous media and (2) the developer provides the source code of the model; thus, it is easy for the author to modify the model. The calculated results from CADMAS-SURF can be used to determine shear force induced by the return flow. Thereafter, the movement of the backfilling materials is determined by using the shear force acting on the outflow

layer and the shear strength of the layer. In this section, the detail of the model is explained.

3.2.1 The sediment transport model

The outflow of backfilling materials can be understood as a sheet flow of a layer of materials. Sheet flow is the process that water flows across the layer of soil and moves materials of the layer. In the outflow case, the sheet flow is generated by incident waves. Considering that the direction of the outflow is outward from the structures, the return flow of incident waves should be the main cause of the sheet flow. For the movement of the bed induced by wave force, it is believed that bedload particles are moved by the shear force acting on the surface layer of the bed, and this movement is resisted by the shear strength of the bed, as shown in Figure 3.2. If the shear force is greater than the shear resistance, the bed particles are moved. Typically, a formula, Equation (3.1), for calculating the bedload transport rate, has a form proportional to the 1.5th power of the difference between the shear force and the critical shear force according to the assumption that this rate is proportional to the power generated by the shear force:

$$\frac{q}{w_s D_{50}} = m(|\theta| - \theta_c)^{1.5} \frac{\theta}{|\theta|}, \tag{3.1}$$

Where q is the bed load transportation rate; w_s is the settling velocity; D_{50} is the median grain size of the bed; m is a coefficient; θ is the Shield parameter (dimensionless shear stress acting on the bed); and θ_c is the critical Shield parameter (dimensionless shear strength of the bed).

However, when the region of the outflow is the inner side of a structure, which is semi-enclosed or enclosed by the structure, the movement of the sediment is mainly controlled by excess pore water pressure (="the total pore water pressure" – "the static pore water pressure"). Thus, the outflow rate should be considered as a function of this pressure. The critical shear stress on the outflow layer is the shear strength of the outflow layer, which can be calculated by using the Coulomb–Terzaghi shear strength equation, shown in Equation (3.2). The shear stress acting on the outflow layer can be

evaluated by using the typical fluid force equation shown in Equation (3.3). Since the outflow occurs when a soil layer in front of the structure is entirely scoured (d_t in Equation (3.2) ≈ 0), the critical shear stress in front of the structure must be a function of the excess pore water pressure. Moreover, since the fluid pressure is proportional to the square of the flow velocity, as shown in Equation (3.4), the shear stress must be a function of this pressure as well. Therefore, the outflow rate should be proportional to the difference between the Shields parameter (dimensionless shear stress) and the critical Shields parameter (dimensionless critical shear strength), which can be calculated using Equations (3.5) and (3.6), respectively, by considering that the rate is a function of the excess pore water pressure. In summary, when the inflow rate is very small compared to the outflow rate, the flow velocity of Equation (3.3) can be specified as the return flow velocity, and thus the outflow rate formula can be expressed as shown in Equation (3.7).

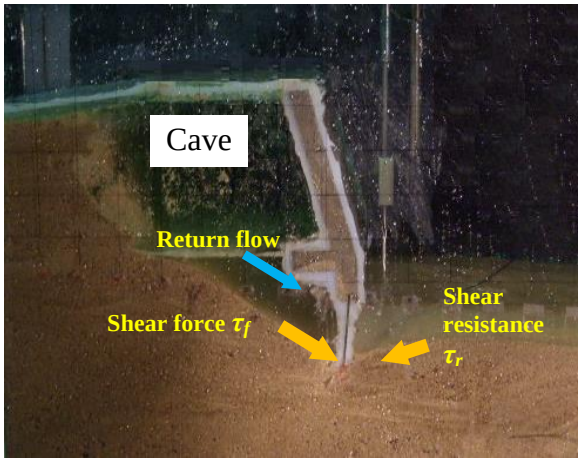

Figure 3.2. An illustration of sand outflow phenomenon.

$$\tau_r = ((\rho_s - \rho_w) g d_t - p) \tan\phi \,, \tag{3.2}$$

$$\tau_f = \frac{f}{2} \rho_w u^2 \,, \tag{3.3}$$

$$p^* = \frac{1}{2}\rho_w c v^2 \tag{3.4}$$

$$\theta = \frac{\tau_f}{(\rho_s - \rho_w) g D_{50}}, \tag{3.5}$$

$$\theta_c = \frac{\tau_r}{(\rho_s - \rho_w) g D_{50}}, \tag{3.6}$$

$$\frac{q}{w_s D_{50}} = \beta(\theta - \theta_c), \tag{3.7}$$

Where τ_r is the shear strength of the backfilling materials; ρ_s is the density of the backfilling materials; ρ_w is the density of water; g is the gravitational acceleration; d_t is the thickness of the backfilling materials; p is the excess pore water pressure; ϕ is the friction angle of the backfilling materials; τ_f is the shear stress acting on the backfilling materials generated by the return flow; f is the outflow coefficient (=1); u is the return flow velocity; p^* is the water pressure; c is the fluid force coefficient; v is the flow velocity; θ is the Shield parameter (dimensionless shear stress acting on the backfilling materials); θ_c is the critical Shield parameter (dimensionless shear strength of the backfilling materials); D_{50} is the median grain size of the backfilling materials; q is the outflow rate of the backfilling materials (included porosity); and β is the proportional coefficient.

Ioroi and Yamamoto [6] performed many experiments on the outflow phenomena (refer to Table 1) by using the same method of Yamamoto and Minami [5] in order to get an outflow rate formula and an empirical coefficient, β. They proposed an outflow rate formula, Equations (3.8)–(3.9), and empirical equation, Equation (3.10), for getting the coefficient, which can calculate the outflow rate using maximum pore water pressure and the maximum return flow velocity. However, since this formula was designed to use with the maximum pore water pressure and the maximum return flow velocity at the lowest edge of the structure, the accuracy when calculating the outflow rate in sections inside the structure may not good.

$$\frac{q}{w_s D_{50}} = \beta(\theta - \theta_c)\frac{1}{2}\left(1 + \cos\left(\frac{\alpha t}{T}\right)\right) \tag{3.8}$$

$$\left.\begin{aligned} \alpha &= -9.0\times10^{-5}(D_{50}/0.2) + 0.0031 \quad [1 \le D_{50}/0.2 \le 25] \\ \alpha &= -3.39\times10^{-5}(D_{50}/0.2) + 0.0017 \quad [25 \le D_{50}/0.2 \le 50] \end{aligned}\right\} \tag{3.9}$$

$$\beta = 0.028e^{-0.35\left(\frac{D_{50}}{0.2}\right)} \tag{3.10}$$

Where α is the time rearrangement coefficient calculated by Equation (3.9); t is the elapsed time; T is the incident wave period; the unit of D_{50} in Equations (3.9)–(3.10) is mm.

After getting the outflow rate, the cave of the backfilling materials is calculated by using the continuity equation for sediment transport, Equation (3.11). In addition, the slope stability of the backfilling materials is considered by using an argument that the slope of the cave must not exceed than the repose angle of the materials, Equation (3.12). By using these equations, a formation and a shape of a cave inside a structure can be calculated.

$$\frac{\Delta q_i}{\Delta x} = \frac{\Delta d_i}{\Delta t} \tag{3.11}$$

$$\frac{d_{i+1}^t - d_i^t}{\Delta x} \le \tan\theta_{\text{repose}} \tag{3.12}$$

Where x is the horizontal coordinate; the subscription i denotes the mesh number in x-direction; d is the thickness of the backfilling materials; Δx is the mesh size in x-direction; Δt is the time step; superscript t donates time; and θ_{repose} is the repose angle of the backfilling materials.

In summary, the outflow rate can be calculated by using Equation (3.7). The

Shields parameter and the critical shields parameter in Equation (3.7) can be calculated by using Equations (3.5) and (3.6), respectively. The calculated outflow rate is used to calculate the evolution of a cave by using the continuity equation, Equation (3.11), and the slope stability argument, Equation (3.12).

Table 3.1. The experimental setup of Ioroi and Yamamoto [6].

Case no.	Actual value			Scaled value		
	Significant wave height $H_{1/3}$ (m)	Wave period T (s)	Median grain size D_{50} (mm)	Significant wave height $H_{1/3}$ (m)	Wave period T (s)	Median grain size D_{50} (mm)
1	6.69	14.5	-	0.223	2.65	0.20
2						0.66
3						5.00
4						10.0

3.2.2 CADMAS-SURF

CADMAS-SURF (SUper Roller Flume Computer-Aided Design of MAritime Structure) is a numerical wave flume for maritime structural design, which was developed by the Coastal Development Institute of Technology, Japan. This model can simulate wave dynamics, wave-structure interactions, and, especially, fluid motion in a porous medium, which can be used for outflow calculation. In the 2D version, hydrodynamics is simulated mainly by the continuity equation, Equation (3.13), Navier–Stokes motion equations, Equations (3.14)–(3.18), and the surface motion is captured by the Volume of Fluid technique, Equation (3.19). The flow in a porous medium that can be treated by using two methods—one is the drag force coefficient method, Equations (3.20)–(3.21), and the other is the Dupuit–Forchheimer (D–F) method, Equations (3.22)–(3.25). The D–F method can adequately consider the effects of pressure attenuation due to either precast concrete armor units (e.g., hollow tetrahedrons, tetrapods, and hexapods), spherical or cubic concrete blocks, stones, or pebbles. The recommended values of the parameters α_0 and β_0 for these wave dissipation materials are given in the manual of CADMAS-SURF.

$$\frac{\partial \gamma_x u}{\partial x} + \frac{\partial \gamma_z w}{\partial z} = 0 \tag{3.13}$$

$$\lambda_v \frac{\partial u}{\partial t} + \frac{\partial \lambda_x uu}{\partial x} + \frac{\partial \lambda_z wu}{\partial z} = -\frac{\gamma_v}{\rho}\frac{\partial p}{\partial x} + \frac{\partial}{\partial x}\left\{\gamma_x \nu_e \left(2\frac{\partial u}{\partial x}\right)\right\} + \frac{\partial}{\partial z}\left\{\gamma_z \nu_e \left(\frac{\partial u}{\partial z} + \frac{\partial w}{\partial x}\right)\right\} - R_x, \tag{3.14}$$

$$\lambda_v \frac{\partial w}{\partial t} + \frac{\partial \lambda_x uw}{\partial x} + \frac{\partial \lambda_z ww}{\partial z} = -\frac{\gamma_v}{\rho}\frac{\partial p}{\partial z} + \frac{\partial}{\partial x}\left\{\gamma_x \nu_e \left(\frac{\partial w}{\partial x} + \frac{\partial u}{\partial z}\right)\right\} + \frac{\partial}{\partial z}\left\{\gamma_z \nu_e \left(2\frac{\partial w}{\partial z}\right)\right\} - R_z - \gamma_v g, \tag{3.15}$$

$$\lambda_v = \gamma_v + (1-\gamma_v) C_M \tag{3.16}$$

$$\lambda_x = \gamma_x + (1-\gamma_x) C_M \tag{3.17}$$

$$\lambda_z = \gamma_z + (1-\gamma_z) C_M \tag{3.18}$$

$$\gamma_v \frac{\partial F}{\partial t} + \frac{\partial \gamma_x uF}{\partial x} + \frac{\partial \gamma_z wF}{\partial z} = 0 \tag{3.19}$$

$$R_x = \frac{1}{2}\frac{C_D}{\Delta x}(1-\gamma_x) u\sqrt{u^2 + w^2} \tag{3.20}$$

$$R_z = \frac{1}{2}\frac{C_D}{\Delta z}(1-\gamma_z) w\sqrt{u^2 + w^2} \tag{3.21}$$

$$R_x = \gamma_v(\gamma_x u)\left(\alpha + \beta\sqrt{(\gamma_x u)^2 + (\gamma_z w)^2}\right) \tag{3.22}$$

$$R_z = \gamma_v(\gamma_z w)\left(\alpha + \beta\sqrt{(\gamma_x u)^2 + (\gamma_z w)^2}\right) \tag{3.23}$$

$$\alpha = \alpha_0 \frac{(1-\gamma_v)^3}{\gamma_v^2}\frac{\nu}{d^2} \tag{3.24}$$

$$\beta = \beta_0 \frac{(1-\gamma_v)}{\gamma_v^3}\frac{1}{d} \tag{3.25}$$

Where, x and z are the horizontal and vertical coordinates; γ_x and γ_z are the sectional permeability in horizontal- and vertical-directions, respectively; γ_v is the porosity; u and w are the velocities in horizontal- and vertical-directions, respectively; v_e is the kinematic viscosity; p is the water pressure; ρ is the water density, λ_v, λ_x, λ_z are coefficients expressed in Equations) 3.16(–)3.18(; C_M is the coefficient of inertia; R_x and R_z are the drag force in the horizontal- and vertical-directions, respectively; C_D is the drag force coefficient; Δx and Δz are the mesh size in horizontal- and vertical-directions, respectively; F is the VOF function; α and β are coefficients calculated by Equations (3.24) and (3.25), respectively; α_0 and β_0 are the coefficients for D–F method; d is the representative size of the wave dissipation unit.

By using CADMAS-SURF, the time history of the pressure and velocity inside the backfilling materials of a structure can be calculated. The calculated pressure and the calculated velocity will be used for critical shear stress and shear stress calculations, as expressed in Equations (3.26) and (3.27), respectively. Therefore, the outflow rate on any given point at any time step can be simulated.

$$\tau_r = \left(\left(\rho_s - \rho_w\right) g d_t - \left(P_{\mathrm{CAD}} - \rho_w g h\right)\right) \tan\phi \tag{3.26}$$

$$\tau_f = \frac{f}{2} \rho U_{\mathrm{CAD}}^2 \tag{3.27}$$

Where P_{CAD} is the calculated pressure from CADMAS-SURF (p in Equations (3.14)–(3.15); h is the still water depth; and U_{CAD} is the calculated velocity in the horizontal direction from CADMAS-SURF (u in Equations (3.14)–(3.15)).

3.3 A verification simulation using original CADMAS-SURF

A simulation using the original CADMAS-SURF and the empirical formula for getting the proportional coefficient of Ioroi and Yamamoto [6] was implemented to investigate the efficiency of the model by comparing the simulated result to the results of a hydraulic model experiment. In this section, the simulation procedure, the

simulation results, the experimental setup, and the experimental results are pointed out.

3.3.1 The simulation procedure

The outflow rate and the accumulated outflow rate (the time integral of the outflow rate) are calculated using the shear force and the critical shear force calculated from the calculated pressure and velocity in each time step by using CADMAS-SURF. The following steps are the procedure of the simulation:

1) Set the dimension of the obstacles (impermeable structures), porous media, and wave conditions in CADMAS-SURF.

2) Determine the measuring line at the lowest edge of the structure. This line was set 1 mesh below the lowest edge of the structure. The vertical length from this line to the elevation of the backfilling surface in each mesh is defined as $d_{\max,i}$ for the initial time and d_i for the other, where i is the mesh number in the horizontal direction. This line is also used as the datum line to calculate the static water pressure in Equation (3.26).

3) Calculate the proportional coefficient, β, using Equation (3.10).

4) Calculate the pressure and velocity in each mesh on the measuring line using CADMAS-SURF.

5) If the direction of the flow velocity is out of the structure, calculate the shear resistance and the shear force on each mesh using Equations (3.26) and (3.27). Then calculate the Shields parameter, the critical Shield parameter, and the outflow rate using Equations (3.5)–(3.7).

6) Calculate the thinned height of the backfilling materials in each mesh by using the continuity equation for sediment transport, Equation (3.11).

7) Subtract the backfilling layer thickness by the thinned height, calculated using Equation (3.28), in each mesh. Where d_i is the backfilling layer thickness of mesh number i; the superscripts t and Δt are the elapsed time and the time step, respectively.

$$d_i^{t+\Delta t} = d_i^t - \Delta d_i^t \,. \tag{3.28}$$

8) Check the slope stability by using the assumption that the slope of the backfilling materials must not exceed the repose angle of the materials. This argument is shown in Equation (3.12). If the calculated slope does not agree with Equation (3.12), the thickness of the calculated mesh and the next mesh are adjusted until they satisfy the argument.

9) Compute the next time step.

3.3.2 Simulation condition for the verification

Outflow damage to a dike in the Hirono coast, Ishikawa Prefecture, Japan, which was induced by Typhoon no. 9 of 1997, was used as verification data. The author scaled the dimension of the dike by 1/30 to make the size of the model suitable for a hydraulic wave flume. During the impact of Typhoon no.9 from 1997, significant wave heights, significant wave periods, and the duration time were mentioned in a publication of Yamamoto and Minami [5], as shown in Table 3.2. Since it was difficult to reproduce various input wave data in both simulation and experiment, the author used the average significant wave height and the average significant wave period of 6.69m and 14.5s, respectively. The significant wave height and the significant wave period were scaled to 0.223m and 2.65s, respectively, by using Froude law. In consideration of the grain size, according to a report of Ioroi and Yamamoto [6] the backfilling materials of the prototype dike consisted of grain sizes of 0.4mm. Ito and Tsuchiya [12] studied the grain size ratio of the model as a prototype by using small- and large-scale model experiments and proposed a diagram, Figure 3.3, for obtaining the grain size ratio. By using this diagram, an accurate scale of the grain size can be obtained. Thus, the median grain size of the backfilling materials was scaled by using the similarities of the beach profiles by Ito and Tsuchiya. In this study, the scale of the grain size was about 1/3, and therefore the grain size in the experiment and the simulations was scaled from 0.4mm to 0.13mm. However, since it was difficult to prepare the sand of 0.13mm in median diameter, sand of 0.2mm in median diameter was used. The experimental and the simulation conditions were shown in Table 3.3. The shape of the dike is shown in Figure 3.4.

Table 3.2. Wave conditions of Typhoon no. 9 from 1997 [5].

Elapsed time (hr)	Significant wave height $H_{1/3}$ (m)	Significant wave period $T_{1/3}$ (s)
0-5.47	6.40	15.23
5.47-9.42	6.70	14.51
9.42-11.39	6.20	13.58

Table 3.3. Experimental and simulation setups for verification simulations.

Actual value			Scaled value		
Significant wave height $H_{1/3}$ (m)	Significant wave period $T_{1/3}$ (s)	Median grain size D_{50} (mm)	Significant wave height $H_{1/3}$ (m)	Significant wave period $T_{1/3}$ (s)	Median grain size D_{50} (mm)
6.69	14.5	0.4	0.223	2.65	0.20

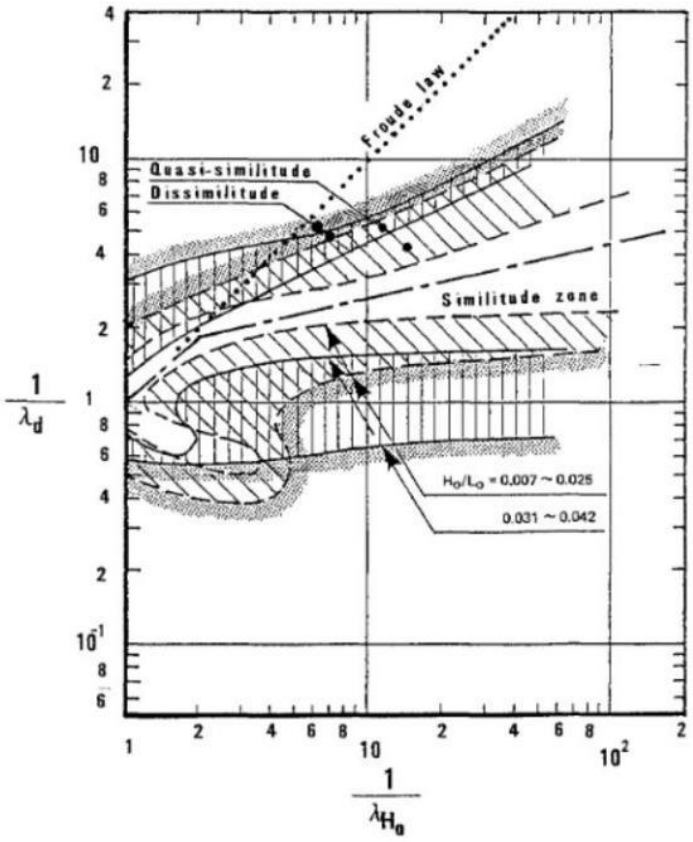

Figure 3.3. A similitude of beach profile proposed by Ito and Tsuchiya [12]. Where λ_d is the scale of median grain size.

Figure 3.4. A simulated dike in CADMAS-SURF. The white color represents obstacles (impermeable structures); the gray color represents porous media; the white line represents the water level.

3.3.3 Simulation result

Outflow rates on each mesh were calculated using calculated pressures and calculated velocities from CADMAS-SURF. The outflow rates and the accumulated outflow rates in the time domain of the verification simulation are shown in Figures. 3.5 and 3.6, respectively.

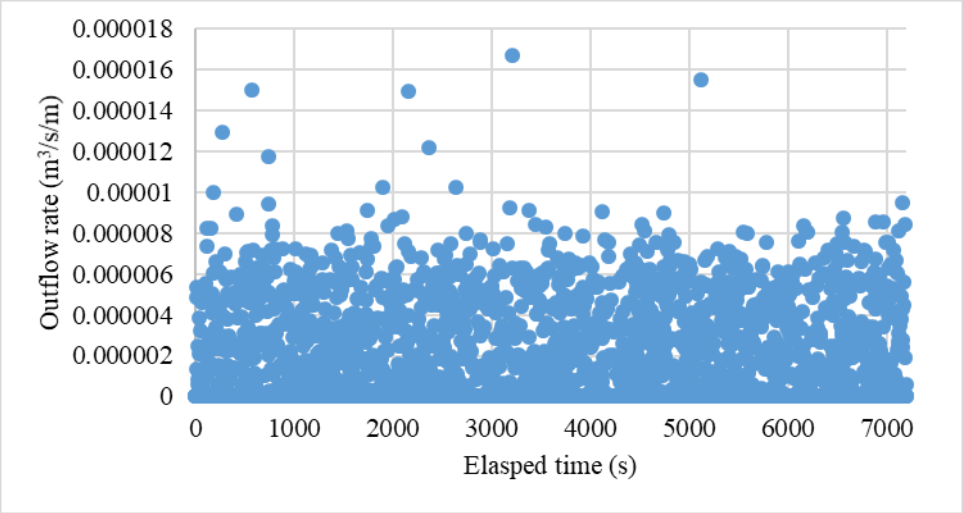

Figure 3.5. The outflow rates in the time domain of the verification simulation.

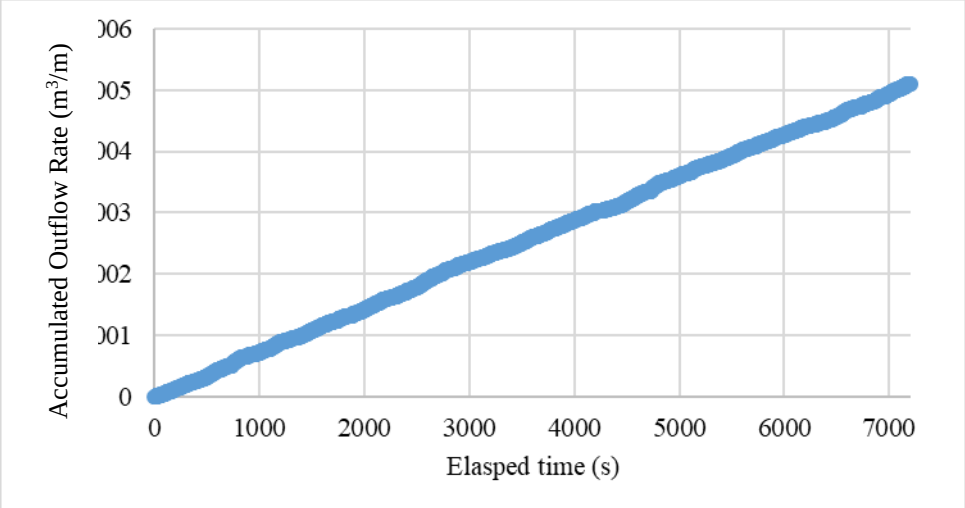

Figure 3.6. The accumulated outflow rates in the time domain of the verification simulation and the verification experiment.

3.3.4 A hydraulic model experiment for verification data

To verify the accuracy of the model, a hydraulic model experiment was implemented. A dike model with a scale of 1/30 was produced by using the dike in the Hirono coast as a prototype. The model was set in a wave flume, with a width of 0.5 m, a height of 0.8 m, and a length of 22 m, as shown in Figure 3.7. The seaward slope of the dike was made of concrete, the crown part and the leeward slope were made of acrylic plates, and all joints were sealed with silicone. Irregular waves were generated by a ball-screw-driven wave generator and measured with wave gauges. The Bret–Schneider wave spectrum was used. The wave reflection was controlled by software of the wave generator. Testing experiments were performed in order to verify the accuracy of the input signals for the wave generator. A pore pressure meter was set under the sheet pile of the dike. As mentioned in section 3.2.2, the geometry, significant wave height, and significant wave periods of Typhoon no. 9 from 1997 were scaled using Froude's law of similitude, and the median grain size was scaled by using Ito and Tsuchiya's diagram [12], as shown in Table 3.3. The formation of a cave is captured by a digital video camera. Then, the accumulated outflow rate and the outflow rate are obtained by analyzing the video in imposed elapsed times. The time domain of the accumulated outflow rate in the experiment is shown in Figure 3.8. The comparison between the calculated result using the original CADMAS-SURF and the experimental result shows that the accuracy of the model is not good—the calculated result is lower estimated. Therefore, an improvement of the model is needed.

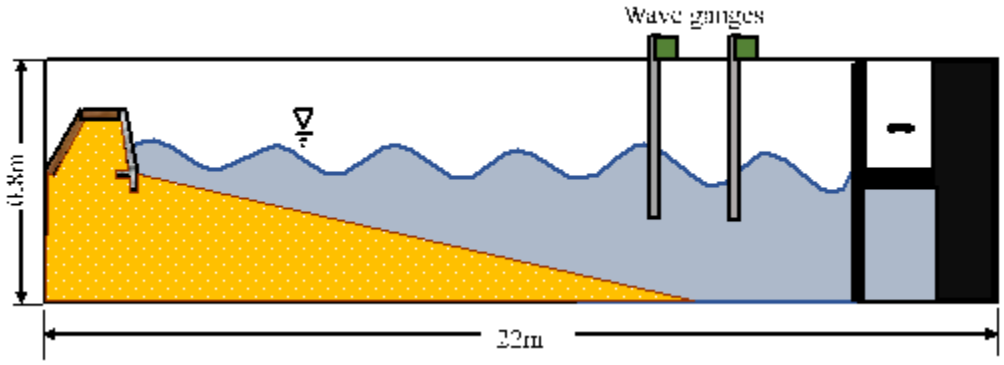

Figure 3.7. The setup of the wave flume in the verification experiment.

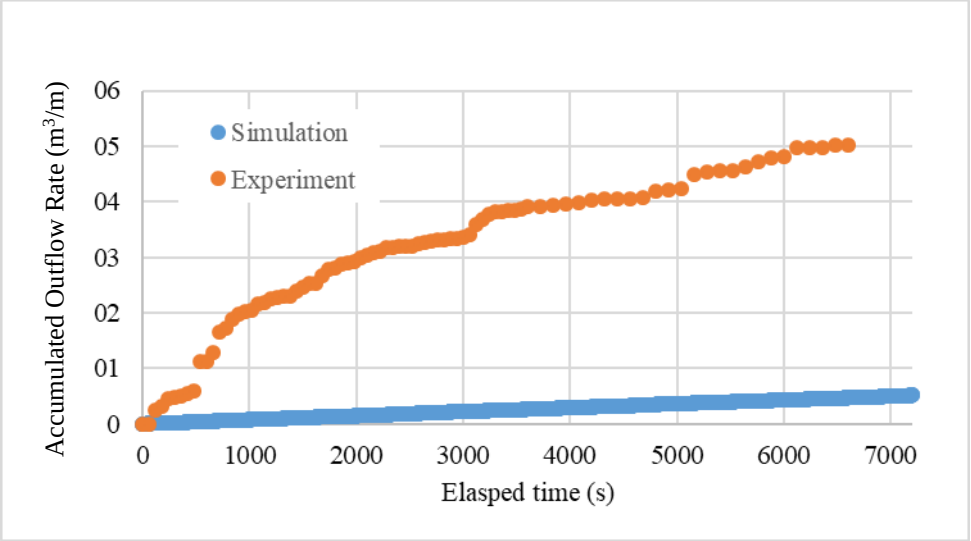

Figure 3.8. The comparison between the simulated result and the experimental result.

3.4 Improvement of the calculated pressure from CADMAS-SURF

As mentioned in section 3.2.2, CADMAS-SURF can consider the different of grain size of backfilling materials to pressure attenuation by using the drag force coefficient or Dupit-Forchiheimer method. However, the calculated pressure distribution inside a covered coastal dike (the front slope and a crown part are covered by concrete, and a leeward slope is covered by asphalt or concrete) and a covered seawall (the front slope and the crown part are covered by concrete) filled by very fine materials seems to be overestimated because this model cannot sufficiently consider the effects of fine grains (D_{50} < 1 mm) ([13]). The reasons for this limitation are as follows:

1) Since the suitable value for the drag force coefficient (C_D in equations (3.26)-(3.27)) for very fine materials is very large, and this value is a value depending on the Reynolds number, which is non-constant value, it is difficult to use the drag force coefficient method.

2) The Dupuit–Forchheimer method was derived from a steady flow stage and empirical coefficients are required for each material. Although there are recommended values of these coefficients for precast concrete blocks, stones, and pebbles, which can be used with reasonable accuracy, there is no such a value for very fine materials. Moreover, the smaller value of the median grain size affects the stability of the

calculation; thus, it is difficult to use this method for various cases with different material characteristics, especially in coastal areas, which consist of fine sand.

The calculated pressures distribution inside the dike was not matched to the experiment's results, as shown in Figure 3.9. To evaluate the outflow rate by using CADMAS-SURF, modification coefficients were introduced. These coefficients can be used to arrange the calculated pressure instead of the drag force coefficient method or the Dupit-Forchheimer method.

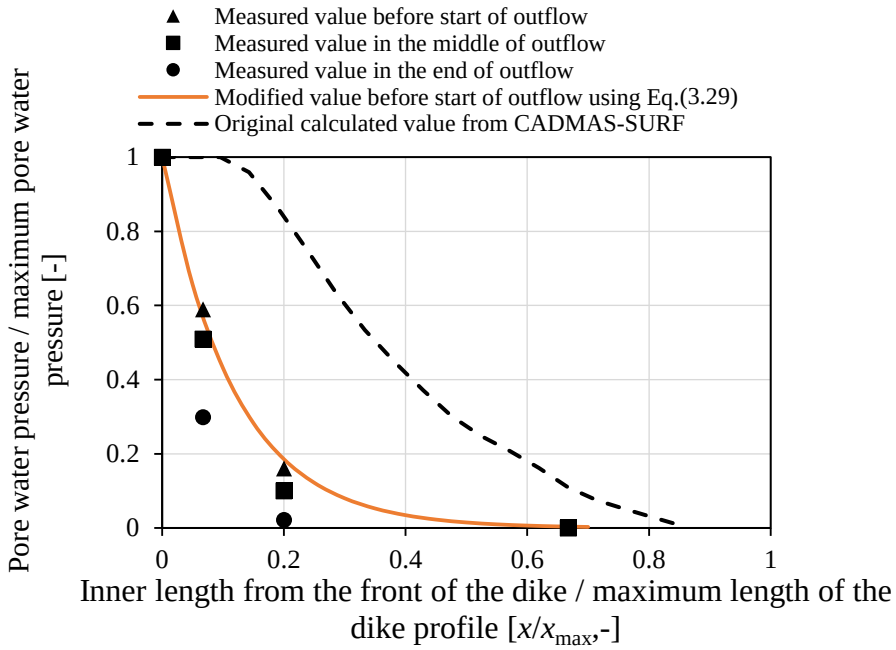

Figure 3.9. Pressure distribution inside the dike.

3.4.1 The modification coefficients

Experiments and trial simulations were performed in order to obtain the modification coefficients. These coefficients could take the effects of a grain size and a sand layer thickness into an account. In the experiments, pore water pressure meters were set at the dimensionless length inside the dike model (ratio between the inner length from the front of the dike and total length of the dike (x/x_{max})) of 0, 0.067, 0.200, and 0.677 indicated by the points 1, 2, 3, and 4 in Figure 3.10 in order to get the pressure distribution ratio inside the dike. Moreover, to consider the changing of sand layer thickness to pressure attenuation, the experiments were performed by varying the sand layer thickness to three situations; 1) before the start of outflow, 2) the middle of

outflow, and 3) the end of outflow as shown in Table 3.4. With these setups, the pressure distribution inside the dike and the pressure changing with the sand layer thickness could be obtained. The results are shown in Table 3.5.

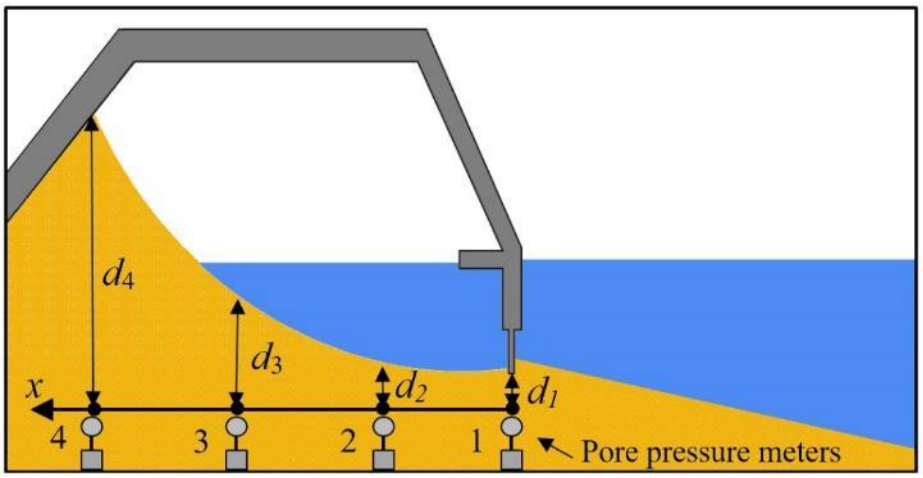

Figure 3.10. Positions of pore pressure meters.

Table 3.4. The sand layer thickness setup.

Situation	d_1 (cm)	d_2 (cm)	d_3 (cm)	d_4 (cm)
1) Before start of outflow	8	29	29	25
2) The middle of outflow	1	10	19	25
3) The end of outflow	0	5	9	25

Table 3.5. Pressure ratios from the experiments.

x/x_{max}	Pressure ratio (p/p_{max})		
	1) Before start of outflow	2) The middle of outflow	3) The end of outflow
0	1	1	1
0.067	0.590	0.510	0.299
0.200	0.161	0.100	0.022
0.677	0	0	0

From Tables 3.4 and 3.5, the relation between the ratio of maximum pore water pressure to pore water pressure and the dimensionless length inside the dike (x/x_{max}) in each situation was obtained, as shown in Figure 3.9. By considering the reduction of pressure from the case of before the start of the outflow (the maximum case) to the dimensionless layer thickness (the ratio of the maximum layer thickness and the layer thickness ($d_i/d_{max,\,i}$)), a reduction coefficient diagram could be determined, as shown in Figure 3.11. An illustration of the parameter x, x_{max}, d, and d_{max} is shown in Figure 3.12. Then, the author proposed empirical equations for obtaining reduction coefficients to improve the pressure calculated by CADMAS-SURF by using best matching functions for the diagrams shown in Figures 3.9 and 3.11. These empirical equations are as follows:

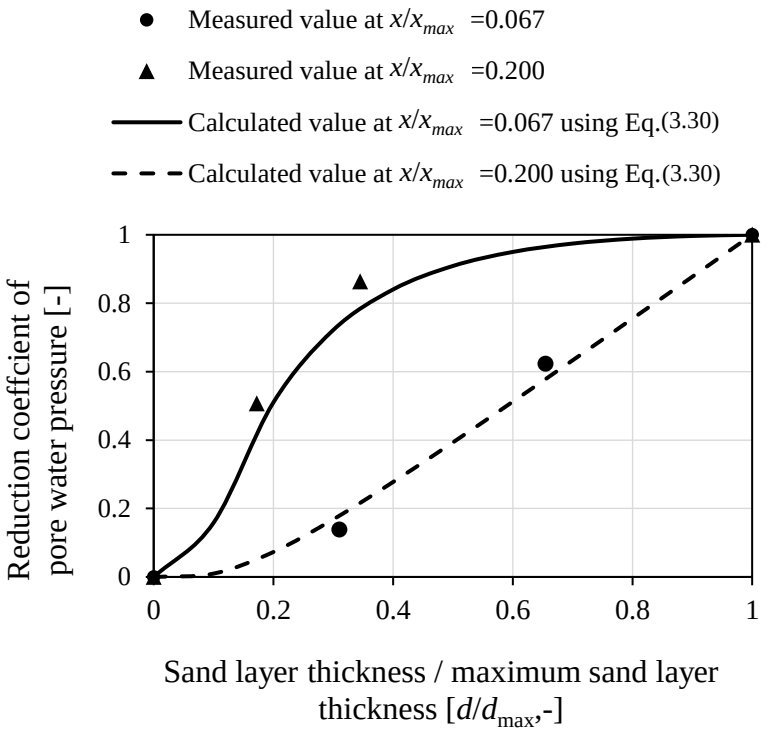

Figure 3.11. Relation between the reduction coefficient and sand layer thickness.

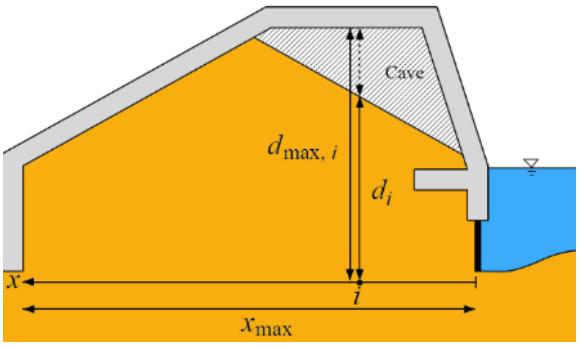

Figure 3.12. An illustration of the parameter x, $x_{\max}$, d, and $d_{\max}$.

1) The empirical equation, Equation (3.29), for determining the reduction coefficient of the inner length inside a structure: the experimental results show that the (dimensionless) pore water pressure decreases when the inner length inside the dike increases, and the layer thickness becomes thinner. This empirical equation was obtained by using the best matching function for the diagram, Figure 3.9, of the experimental results when there is no thinned layer (before start of outflow). Thus, the equation can be used to improve the horizontal pressure distribution inside the structure.

$$C_x = 0.00022^{x/x_{\max}}, \tag{3.29}$$

Where C_x is the reduction coefficient for the inner length inside a structure; x is the inner length inside a structure; and $x_{\max}$ is the total length of a structure.

2) The empirical equation, Equation (3.30), for obtaining a reduction coefficient by the backfilling layer becoming thin: since Equation (3.29) can consider pressure attenuation only when there is no cavity inside the structure, this empirical equation is proposed to consider cases where the pressure decreases when the backfilling layer is thinned by the outflow. The experimental results show that pressure attenuation due to the formation of a cave is not only a function of the thickness of the backfilling materials but also a function of the inner length inside the dike. Thus, by analyzing a diagram, Figure 3.11, of the pressure changes due to the thinned heights at some inner lengths inside the dike, Equations (3.30) and (3.31) were obtained.

$$C_d = \begin{cases} \exp\left(0.269 - \dfrac{0.263}{d/d_{\max}} + \chi \ln(d/d_{\max})\right) & \text{when } C_d \le 1 \\ 1 & \text{when } C_d > 1 \end{cases}, \tag{3.30}$$

$$\chi = 45.0 - 23.7 \exp\left(\frac{-(x/x_{\max}) - 3.265}{4.953}\right), \tag{3.31}$$

Where C_d is the reduction coefficient for the changing of the layer thickness; d is the thickness of the backfilling materials; $d_{\max}$ is the maximum thickness of the backfilling materials; and χ is a coefficient calculated by Equation (3.31).

3) The empirical equation, Equation (3.32), for obtaining a coefficient for the median grain size: the experimental results show that the pore water pressure decreases when the median grain size of the backfilling materials becomes larger. Since the actual size of the median diameter of the very fine backfilling materials cannot be set in CADMAS-SURF due to the reasons mentioned above, this equation was proposed to improve the calculated pressure. Yoshizawa et al. [14] proposed an empirical equation that can calculate the reduction coefficient for the grain size. However, this equation is designed for Ioroi's formulae (Equation (3.8)). Thus, the author modified the coefficients in Yoshizawa's formula as shown in Equation (3.32), by using some trial simulations. This equation can be used in the new outflow equation (Equation (3.7)).

$$C_{D_{50}} = 0.65\left(\frac{0.2}{D_{50}}\right)^{0.85} + 0.35, \tag{3.32}$$

Where C_{D50} is the modification coefficient for the median grain size; and the unit of D_{50} is mm.

Finally, the calculated pressure from CADMAS-SURF is modified by three coefficients: the non-dimensional maximum pore pressure distribution for horizontal length inside the dike, the reduction coefficient for the sand layer thickness, and the

reduction coefficient for the grain size, as expressed by Equation (3.33). This improved pressure is used to calculate the critical shear stress, as shown in Equation (3.34).

$$p_{\mathrm{MOD}} = C_x C_d C_{D50} \left(p_{\mathrm{CAD}} - \rho_w g h \right) \tag{3.33}$$

$$\tau_r = \left(\left(\rho_s - \rho_w \right) g d_t - p_{\mathrm{MOD}} \right) \tan \phi \tag{3.34}$$

Where p_{MOD} is the modified pressure.

3.4.2 The new empirical equation for getting the proportional coefficient

The proportional coefficient (β) is used for converting the difference between the shear stress and the critical shear stress to the sand outflow rate. According to the sand outflow rate formula of Ioroi and Yamamoto [6], the empirical equation, Equation (3.10), for getting this proportional coefficient was proposed by using results from hydraulics experiments. However, this equation was designed to calculate the outflow rate by using maximum pore water pressure at the lowest edge of the dike or the seawall only. So, to calculate the sand outflow rate on each grids and times using Equation (3.7), a new empirical equation for getting the proportional coefficient must be proposed. The proportional coefficient can be obtained by using the relationship between the sand outflow rate, the shear stress, the critical shear stress, and the median grain size, which can be measured from hydraulic experiments, and trial simulations. Therefore, the new empirical equation, Equation (3.35), for getting the proportional coefficient was obtained by using experimental data and simulation data mentioned above.

$$\beta = 0.321 \exp\left(-0.25 \left(\frac{D_{50}}{0.2} \right) \right), \tag{3.35}$$

Where the unit of D_{50} is mm.

3.4.3 The improved simulation procedure

The new simulation procedure was proposed by adding the modification coefficients calculation part, the improvement of the calculated pressure part, and the new critical shear stress calculation part. The new procedure is the following:

1) Set the dimension of the obstacles (impermeable structures), porous media, and wave conditions in CADMAS-SURF.

2) Determine the measuring line at the lowest edge of the structure. This line should be around 1 to 3 meshes below the lowest edge of the structure. The vertical length from this line to the elevation of the backfilling surface in each mesh is defined as $d_{\max,\, i}$ for the initial time and d_i for the other, where i is the mesh number in the horizontal direction. This line is also used as the datum line to calculate the static water pressure in Equation (3.33).

3) Calculate the proportional coefficient, β, using the new equation, Equation (3.35).

4) Calculate the reduction coefficients, C_x, C_d, and C_{D50}, using Equations (3.29)–(3.32).

5) Calculate the pressure and velocity in each mesh on the measuring line using CADMAS-SURF, then modify the calculated pressure using Equation (3.33).

6) If the direction of the flow velocity is out of the structure, calculate the critical shear stress and the shear stress using Equations (3.34) and (3.27). Then calculate the Shields parameter, the critical Shield parameter, and the outflow rate using Equations (3.5)–(3.7).

7) Calculate the thinned height of the backfilling materials in each mesh by using the continuity equation for sediment transport, Equation (3.11).

8) Subtract the backfilling layer thickness by the thinned height, calculated using Equation (3.28), in each mesh.

9) Check the slope stability by using the assumption that the slope of the backfilling materials must not exceed the repose angle of the materials. This argument is shown in Equation (3.12). If the calculated slope does not agree with Equation (3.12), the thickness of the calculated mesh and the next mesh are adjusted until they satisfy the argument.

10) Compute the next time step.

The calculated result using this methodology is show in Figure 3.13. The simulated result is in good agreement to the experimental result. A flow chart of the simulation is shown in Figure 3.14.

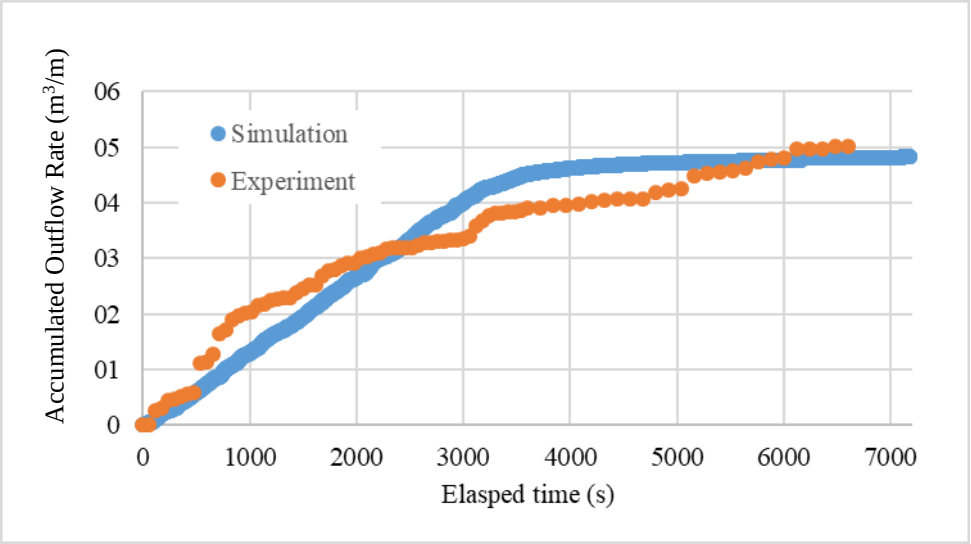

Figure 3.13. The comparison between the simulated result using empirical equations and the experimental result.

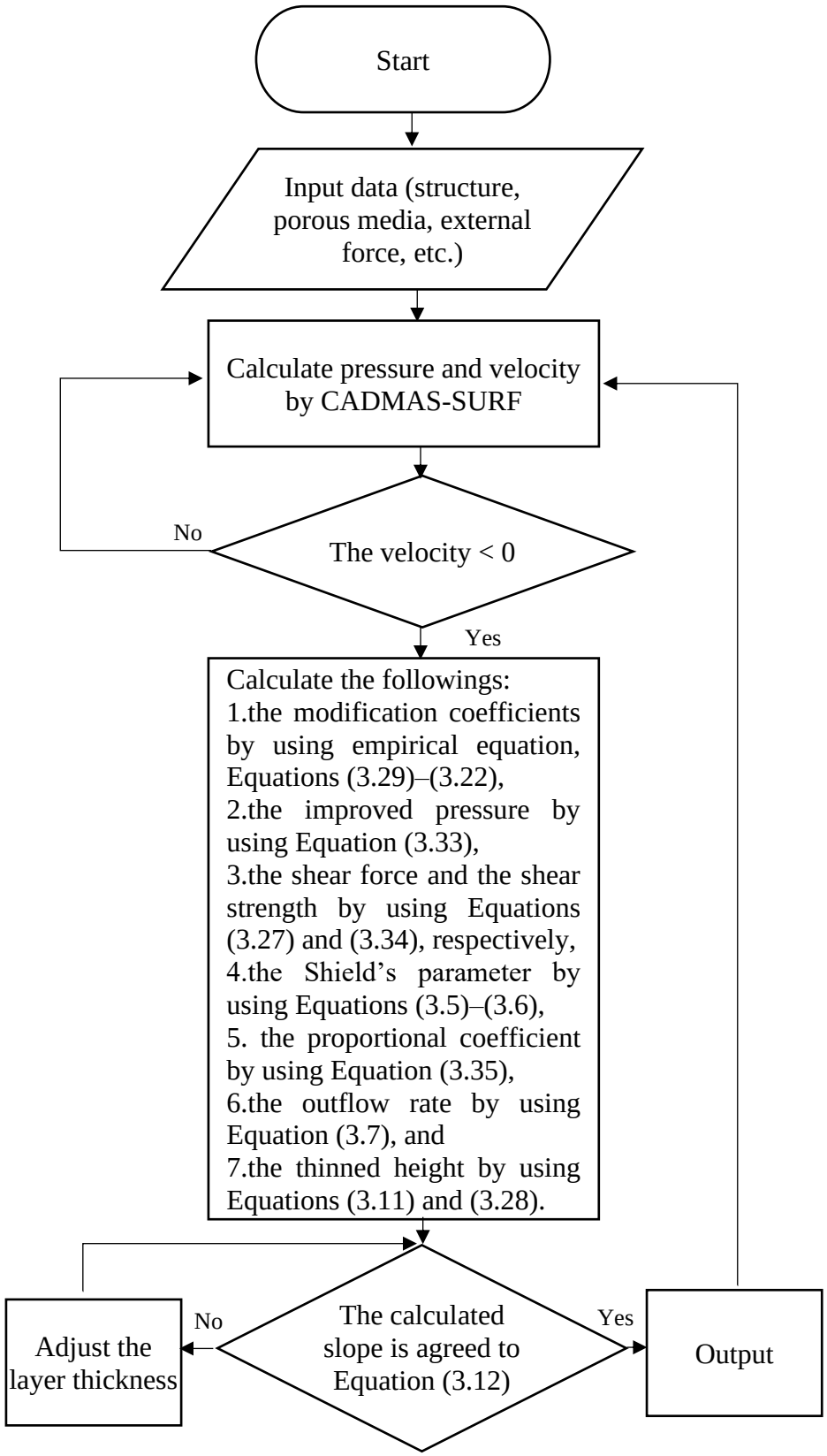

Figure 3.14. The flow chart of the simulation.

3.4.4 Examination of the effects of water depth and wave periods on the outflow

The effects of many parameters on the outflow rate have been elucidated by some researchers. For example, Ioroi and Yamamoto [6] and Ioroi et al. [13] performed many experiments and proposed an empirical outflow formula that can consider the effects of pore water pressure, return flow velocity, median grain size, the dry density, and the uniformity coefficient. However, there is no available information on the effects of water depth and wave periods. Since the wave period and water depth influence the flow velocity, the wave steepness, Iribarren number, and so on (which in turn affect the coastal sediment processes, and thus the outflow rate), it is important to examine these parameters to elucidate their effects on the outflow rate. In this section, hydraulic model experiments were performed to determine the relation between these parameters and the outflow. Moreover, examinations were conducted to check whether the empirical formula of Ioroi et al. or the proposed numerical model can consider the effects of wave periods or water depth.

The experiments were implemented by using the same methodology used in section 3.3.4. To reproduce the heavy scour and outflow rate, the front beach slope of 1/15 was used according to the stable beach slope, calculated by the stable beach slope formula of Yamamoto et al. [15], for the experiments is from 1/30 to 1/16. This slope is the average slope for eroded beaches in Japan. The significant wave height and median grain size of the backfilling materials were set to 0.12m and 0.2mm, respectively. The experimental conditions and external forces used in the experiments are shown in Table 3.6.

Table 3.6. Experimental conditions and external forces.

Case	Significant wave height, $H_{1/3}$ (m)	Significant wave period, $T_{1/3}$ (s)	Wave steepness in deep water	Water depth, h_0 (m)	Water depth at the toe of the dike, h_t (m)
E-1	0.12	2.00	0.0192	0.35	0.05
E-2	0.12	2.00	0.0192	0.40	0.10
E-3	0.12	2.00	0.0192	0.50	0.20
E-4	0.12	1.50	0.0342	0.50	0.20
E-5	0.12	2.50	0.0123	0.50	0.20

The experimental results are shown in Figures 3.15 and 3.16. The results indicate that the outflow volume (= the accumulated outflow rate) increases when the wave period increases and decreases when the water depth increases. These trends are similar to those of the maximum scour depth in front of a seawall (e.g., in [16], [17]). By considering the wave periods in terms of wavelengths in deep water, the results shown in Figure 3.16 were obtained. The results show that the outflow rate is proportional to the wavelength in deep water, which is a function of T^2 ($L_0 = gT^2/2\pi$).

To confirm that the same trends can be calculated by using the numerical model consisting of CADMAS-SURF and the empirical equations, simulations on the same wave conditions were implemented. The wave conditions in the front of the dike are the same as those of the experimental ones. However, water depth in the offing area was increased by 25cm because the wave-generation method cannot work when the water depth is insufficient. When the conditions in the adjacent area of the dike (e.g., the front beach slope and the water depth at the front of the dike) and the wave conditions in the offing area are the same, the wave breaking point and the wave breaking criteria must be the same, and thus, the incident wave conditions in front of the dike must be the same. Therefore, this technique can be used. The simulation conditions are shown in Table 3.7, and the calculated results are shown in Figures 3.15–3.18. A comparison between the results from the experiments and the simulations shows the same trend for the outflow volume. Even the absolute errors of cases S-3 and S-4 were not significantly different from those of other cases, but the relative errors of these cases were not good. It must be mentioned that the accuracy of the model is not

good when the total outflow volume is very small. However, the results could show that the accuracy of the simulated relationship between the concerned parameters and the outflow rates is better than that of the existing empirical formula. When the outflow damage is a ratio between the total outflow volume and the initial backfilling materials, the significance of the difference between the measured outflow volume (E-3 and E-4) and the calculated outflow volume (S-3 and S-4) is small because these values were very small compared to the initial backfilling materials. Therefore, the results can be useful to evaluate the effects of the parameters or even a degree of damage.

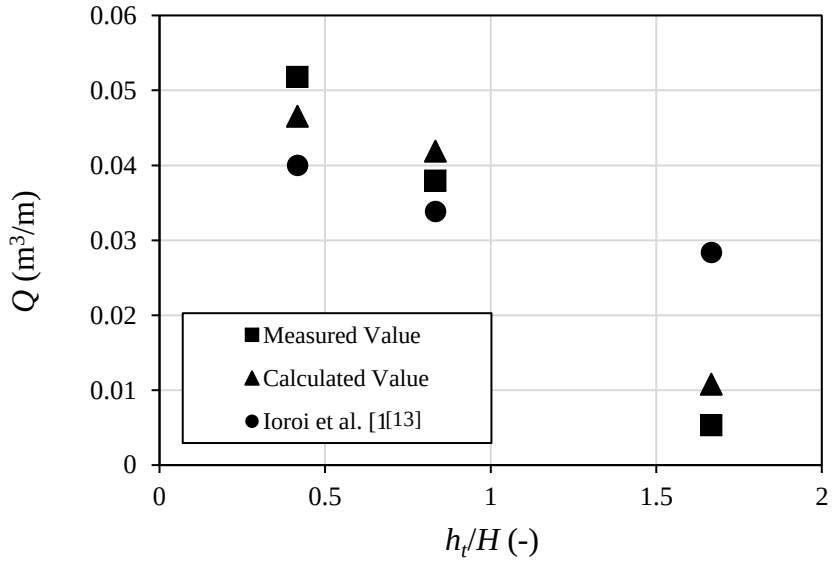

Figure 3.15. The trend of the dimensionless water depth for the outflow volume in the experiments, the simulations, and the calculations.

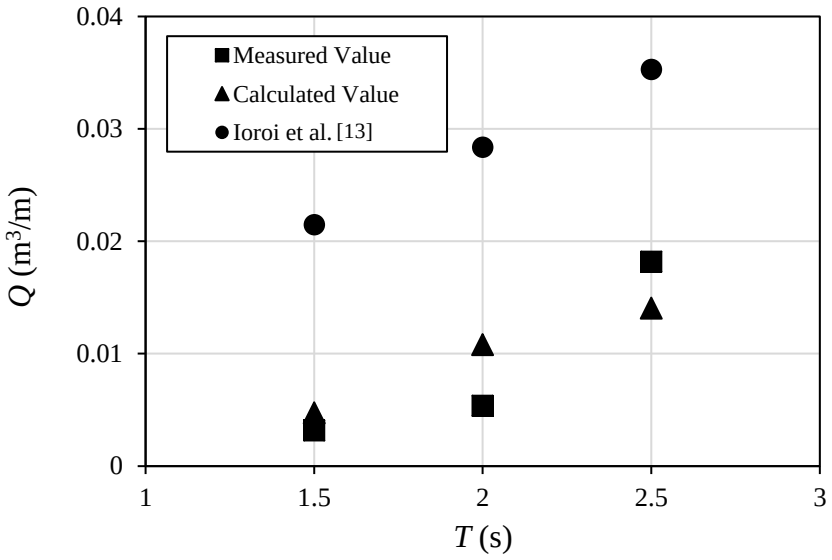

Figure 3.16. The trend of the wave period for the outflow volume in the experiments, the simulations, and the calculations.

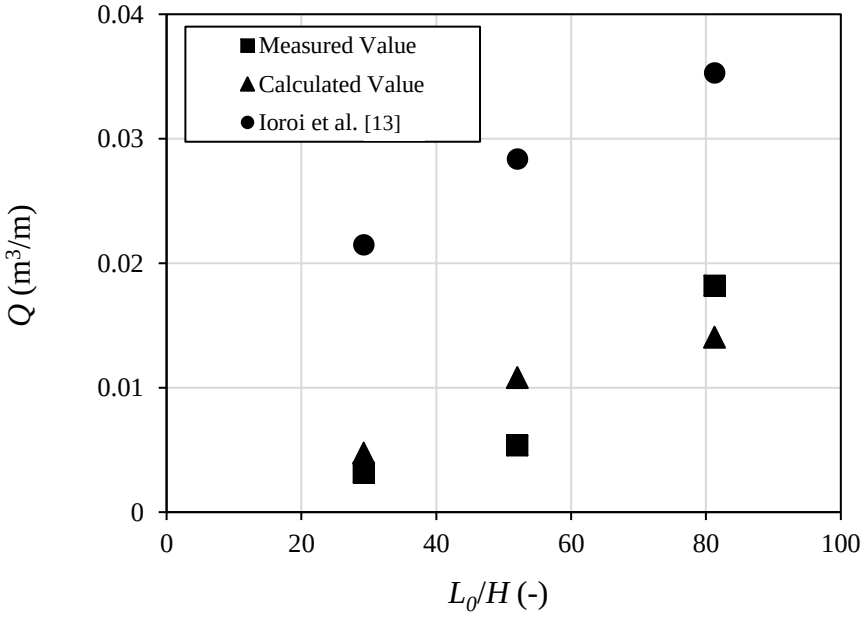

Figure 3.17. The trend of the nondimensional wavelength for the outflow volume in the experiments, the simulations, and the calculations.

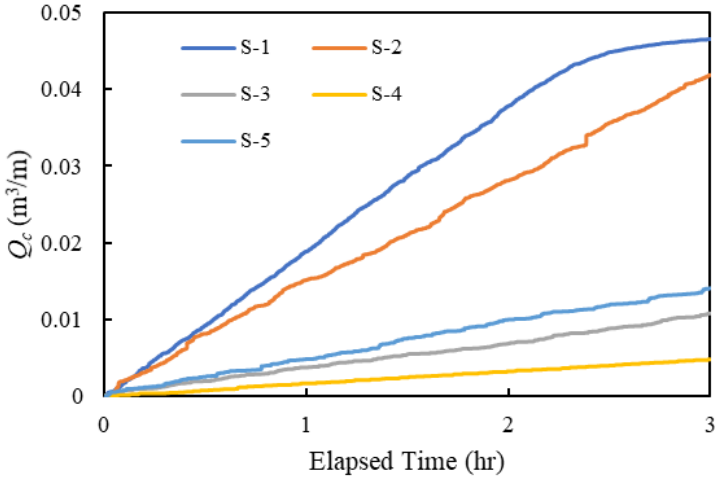

Figure 3.18. The time history of the outflow volume in the simulations.

Table 3.7. Simulation conditions and external forces.

Case	Significant wave height, $H_{1/3}$ (m)	Significant wave period, $T_{1/3}$ (s)	Wave steepness in deep water	Water depth, h_0 (m)	Water depth at the toe of the dike, h_t (m)	Calculated outflow volume Q_c (m^3/m)
S-1	0.12	2.00	0.0192	0.60	0.05	0.047
S-2	0.12	2.00	0.0192	0.66	0.10	0.042
S-3	0.12	2.00	0.0192	0.75	0.20	0.011
S-4	0.12	1.50	0.0342	0.75	0.20	0.005
S-5	0.12	2.50	0.0123	0.75	0.20	0.014

Ioroi and Yamamoto's formula [6], Equations (3.8)–(3.10), (3.36)–(3.41), introduced empirical equations, Equations (3.38)–(3.41), for calculating the maximum pore water pressure and the maximum return flow velocity, which can be used to calculate the shear force and the shear resistance at the lowest edge of a dike by using Equations (3.36) and (3.37). These shears are used to calculate the outflow rate subject to the time rearrangement part (=0.5(1 + cos($\alpha t/T$))) of Equation (3.8), which can take the incident wave period into account. In this particular section, the validity of the wave period and the maximum elapsed time depends on the rearrangement coefficient, α,

which can be expressed as t/T≤α/π. The time rearrangement coefficient depends on the median grain size. Thus, the validity of the maximum elapsed time is limited by the wave period and the median grain size. In other words, the accumulated sand outflow rate is directly affected by the wave during the maximum duration of the outflow. Moreover, since the wave period affects the shoaling coefficient, which affects the incident wave height, this formula can indirectly account for the effect of the wave period by considering the incident wave height in Equation (3.38) to be affected by the wave period. This formula can also consider the effects of water depth on the maximum return flow velocity by using Equation (3.41). When the water becomes deeper, the incident wave height becomes larger, and the pressure at the toe of a structure becomes smaller. However, the empirical equation for calculating the maximum pore water pressure, Equation (3.38), cannot consider the pressure attenuation due to water depth. Thus, the calculated maximum pore water pressure must be overestimated when applying this formula in deeper areas.

$$\tau_r = ((\rho_s - \rho_w) g d_t - P_{ob\max}) \tan\phi, \tag{3.36}$$

$$\tau_f = \frac{f}{2} \rho_w V_{\max}^2, \tag{3.37}$$

$$\frac{P_{ob\max}}{\rho_w g H} = a \tanh\left(\frac{0.03H}{d_t}\right)^b, \tag{3.38}$$

$$a = 0.37(0.2 / D_{50})^{0.85} + 0.30, \tag{3.39}$$

$$b = 0.55(0.2 / D_{50})^{0.78} + 0.05, \tag{3.40}$$

$$V_{\max} = \sqrt{\frac{2P_{ob\max}}{\rho_w\left(\frac{h_t}{H} + 1.0\right)^{1.11}}}, \tag{3.41}$$

Where $P_{ob\max}$ is the maximum excess pore water pressure during all return flows; d_t is

the layer thickness at the lowest edge of the structure; V_{max} is the maximum return flow velocity in the horizontal direction; H is the incident wave height; a and b are coefficients calculated by Equations (3.39)–(3.40); h_t is the water depth at the front of the structure; and the unit of D_{50} in Equations (3.39)–(3.40) is mm.

The examination of the formula was implemented using the maximum elapsed time for the imposed incident wave periods when the median grain size equals 0.2mm, and the offing wave height was set to a constant value of 0.12m. The parameters used in this examination are shown in Table 3.8. The calculated results are shown in Figures 3.14–3.16.

Table 3.8. Conditions used in the examination of Ioroi et al.'s formula.

Case	Significant wave height, $H_{1/3}$ (m)	Significant wave period, $T_{1/3}$ (s)	Wave steepness in deep wate.	Water depth, h_0 (m)	Water depth at the toe of the dike, h_t (m)	Calculated outflow volume Q_c (m^3/m)
I-1	0.12	2.00	0.0192	-	0.05	0.040
I-2	0.12	2.00	0.0192	-	0.10	0.034
I-3	0.12	2.00	0.0192	-	0.20	0.028
I-4	0.12	1.50	0.0342	-	0.20	0.021
I-5	0.12	2.50	0.0123	-	0.20	0.035

The trends of the outflow volume are the same as those of the hydraulic model and the numerical model; thus, the outflow volume increases when the wave period increases. One reason is that the maximum elapsed time is proportional to the wave period. Thus, even this parameter cannot affect the shear force, the shear resistance, or the maximum outflow rate; when the elapsed time becomes longer, the accumulated outflow rate must become bigger. Another reason is that in the surf zone, the incident wave height becomes higher when the wave period becomes longer (refer to Goda's estimation of wave height in the surf zone diagrams [18]). Thus, the outflow force becomes larger. However, the accuracy is not good when water depth becomes deeper. For the effect of water depth, this parameter affects the maximum return flow velocity, as expressed in

Equation (3.26). However, this formula cannot consider pressure attenuation due to an increase in water depth. Thus, the calculated maximum pore water pressure and the calculated outflow rate must be overestimated when the water becomes deeper. Moreover, since this formula cannot consider the effects of wave breaking types, which have strong effects on the sediment transport in very shallow areas, but the wave period and water depth influence the wave breaking criteria, the accuracy of the formula is lower than expected. The reason that the accuracy of the numerical model is higher than that of the empirical formula is because CADMAS-SURF can simulate wave dynamics with higher accuracy, especially wave breaking and wave motion in front of a structure. Thus, the calculated pressure and velocity must be more accurate than those of the empirical formula, which considers the maximum pressure and the maximum velocity calculated by the empirical equations.

3.5 Applications of the model to field cases

Practical simulations were performed to validate the reliability of the model and examine outflow damage of the target coasts. The outflow damage on the coasts of Hirono, Oarai–Isohama and Ishikawa–Komatsu in Japan, and Khlong Wan, South Patong and Suan Son in Thailand was reproduced. The duration times of these simulations were set to 6 hrs, according to the report of Yamamoto and Minami [5], who mentioned that the duration of strong wind by a typical typhoon is about 10 hrs, which can be separated into 4 hrs of scour and 6 hrs of outflow. Detailed information on each case is given below.

3.5.1 Hirono Coast

The Hirono coast is in Shizuoka Prefecture on the south coast of Japan (the Pacific Ocean side). In 1997, a seawall on the coast was damaged by waves induced by Typhoons. Uda et al. [14] studied the causes of the failure of the seawall. They reported that the seawall was directly destroyed by big waves induced by typhoons, and was indirectly destroyed by seabed erosion. In this research, the author used the wave condition induced by Typhoon no. 18 in 1997 as external force to reproduce the cavity size occurred in the seawall using the proposed outflow model. The simulation

condition, including external force, structural information, the median grain size, mesh sizes, and measured and calculated results is shown in Table 3.9. The simulated result is shown in Figures 3.19–3.20.

The outflow rate seems to be a constant value until the elapsed time became one hour. Then, the rate was significantly decreased because of the empirical equation, Equations (30) and (31). According to the equations, the modification coefficient, C_d, depends on changing the layer thickness of the backfilling materials. At the front of the structure, where $x/x_{max} = 0$, the coefficient is a constant value of 1 when the parameter d/d_{max} is greater than 0.14; when the parameter d/d_{max} is lower than 0.14, the coefficient becomes a varying number from 1 to 0. Thus, when the layer thickness became smaller than 0.14, the simulated pressure was reduced by the equations, and therefore the calculated outflow rate became smaller. Since the calculated result is slightly overestimated, this result can be used to reproduce the formation of the cave and evaluate damage due to the outflow.

Table 3.9. The simulation condition in Hirono Coast.

Significant wave height, $H_{1/3}$ (m)	Significant wave period, $T_{1/3}$ (s)	Front bottom depth, h_t (m)	Tidal level (m)	Median grain size, D_{50} (mm)	Initial backfilling materials volume (m^3/m)	Mesh size in x-direction Δx (m)	Mesh size in z-direction Δz (m)	Measured outflow volume, Q_m (m^3/m)	Calculated outflow volume, Q_c (m^3/m)
4.45	13.9	0	0.70	0.4	74.2	0.3	0.2	28	31.5

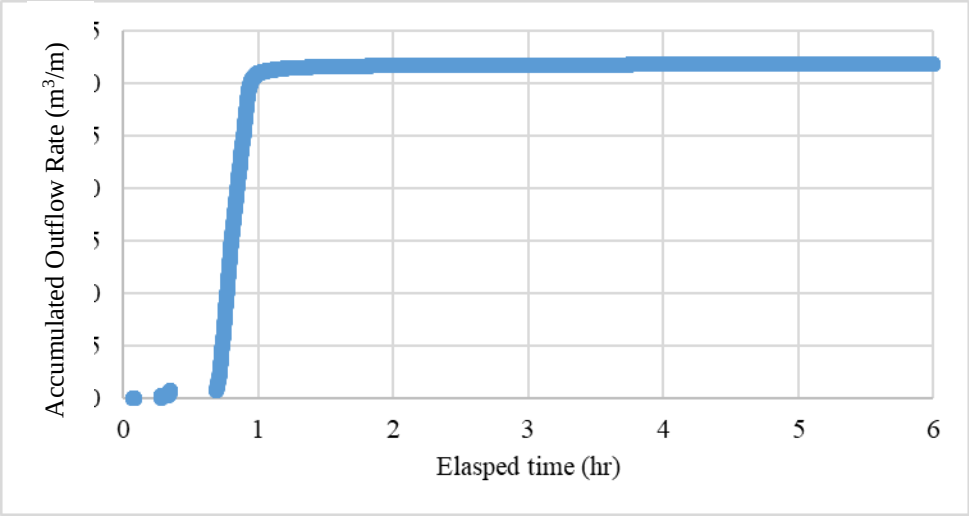

Figure 3.19. The calculated accumulated outflow rates on the Hirono Coast.

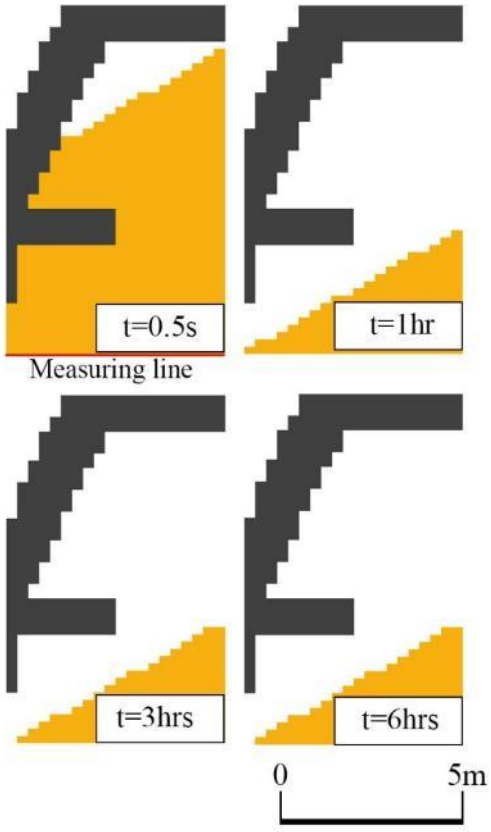

Figure 3.20. Calculated formation of a cave inside the seawall on the Hirono Coast.

3.5.2 Oarai–Isohama Coast

The study case is a seawall constructed in an extended sandy beach in front of Oarai Aquarium located on the Oarai–Isohama coast in Ibaraki Prefecture, Japan (the Pacific Ocean side). This beach has suffered heavy erosion since it was constructed in the 1960s. The seawall has been gradually exposed to waves, and a cavity inside the seawall has formed since October of 2015. In order to calculate the outflow rate, the dimension of the seawall and the wave characteristic of Typhoon No. 23 in 2015 were extracted from the report of Uda et al. [19]. The maximum outflow volume per unit width was estimated from the field survey's photographs. The simulation condition is shown in Table 3.10. The simulated results are shown in Figures 3.21 and 3.22.

The results show that the outflow rates were a constant value, regardless of the simulation time. This is because the total amount of the outflow volume was small compared to its size. As mentioned in the case of the Hirono coast, the coefficient C_d in Equation (3.30) is a constant value of 1 when the parameter d/d_{max} is greater than

0.14. Therefore, since changes in the thickness were small, the coefficient became a constant value, resulting in constant outflow rates.

The calculated volume is underestimated compared to the measured volume because the model cannot consider cracks on the structure. The percentage error is 49.5%. In the field, incident waves infiltrated into the body of the structure through these cracks, resulting in the additional leakage of backfilling materials. Even though the calculated volume is underestimated, since the both of measured and calculated outflow volumes are small compared to the size of the seawall, the results are practical when using the calculated result to examine the degree of damage induced by the outflow. The calculated cave shows that there is no supporting material below the front slope of the seawall. Thus, the calculated results show that the stability of the structure must be weaker than its design value.

Table 3.10. The simulation condition in Oarai–Isohama Coast.

Significant wave height, $H_{1/3}$ (m)	Significant wave period, $T_{1/3}$ (s)	Front bottom depth, h_t (m)	Tidal level (m)	Median grain size, D_{50} (mm)	Initial backfilling materials volume (m^3/m)	Mesh size in x-direction Δx (m)	Mesh size in z-direction Δz (m)	Measured outflow volume, Q_m (m^3/m)	Calculated outflow volume, Q_c (m^3/m)
5.1	10.8	–3.5	0.45	0.2	145	0.4	0.2	20	10.1

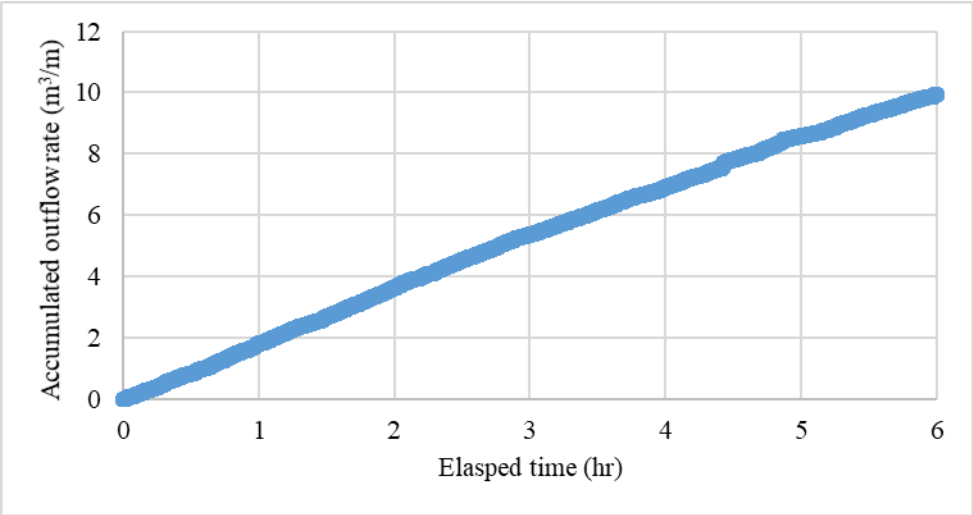

Figure 3.21. The calculated accumulated outflow rates on the Oarai–Isohama Coast.

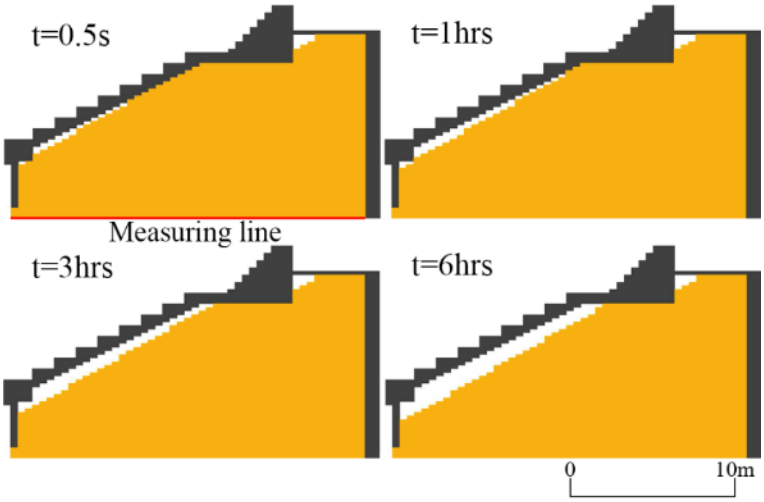

Figure 3.22. Calculated formation of a cave inside the seawall on the Oarai–Isohama Coast.

3.5.3 Ishikawa–Komatsu Coast

This coast is located in Komatsu city, Ishikawa Prefecture, Japan (the Japan Sea side). According to the heavy erosion in the area, the local government decided to construct a concrete dike and detached breakwaters in order to prevent coastal hazards on the seaside. However, the concrete dike was damaged by Typhoon No. 15 in 2001, during which a cavity was found in the body. The dimension of the dike and the wave conditions were extracted from the report of Yamamoto and Minami [5] in order to simulate the outflow. The simulation condition is shown in Table 3.11; the simulated results are shown in Figures 3.23 and 3.24.

The calculated outflow rate was also a constant value for the same reason as the Oarai–Isohama Coast. The calculated result was underestimated because the model cannot consider the effects of cracks. Like the Oarai–Isohama Coast, the calculated outflow rates were large enough to remove the support materials from the front slope of the dike, which has a significant effect on the stability of the dike.

Table 3.11. The simulation condition in Ishikawa–Komatsu Coast.

Significant wave height, $H_{1/3}$ (m)	Significant wave period, $T_{1/3}$ (s)	Front bottom depth, h_t (m)	Tidal level (m)	Median grain size, D_{50} (mm)	Initial backfilling materials volume (m^3/m)	Mesh size in x-direction Δx (m)	Mesh size in z-direction Δz (m)	Measured outflow volume, Q_m (m^3/m)	Calculated outflow volume, Q_c (m^3/m)
6.0	10.5	–2.5	0.58	0.6	71.2	0.3	0.2	16	12.0

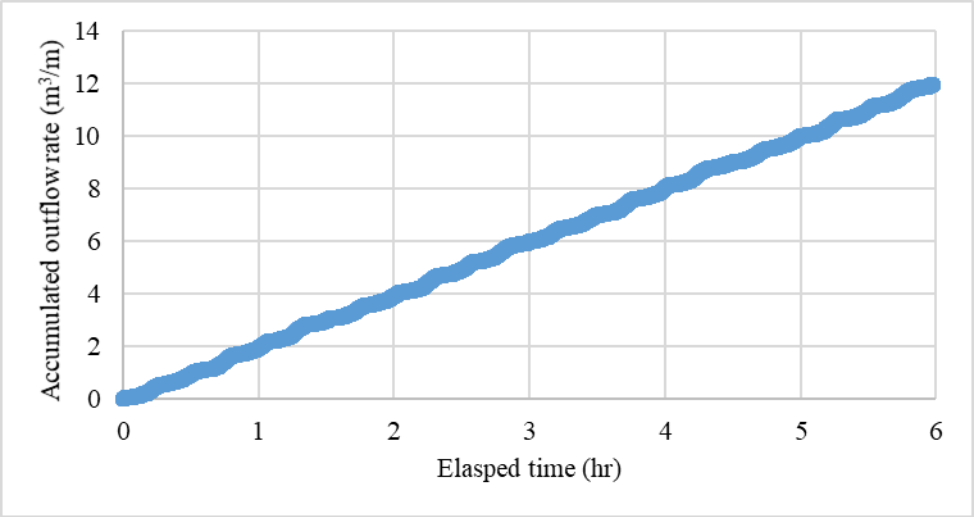

Figure 3.23. The calculated accumulated outflow rates on the Ishikawa–Komatsu Coast.

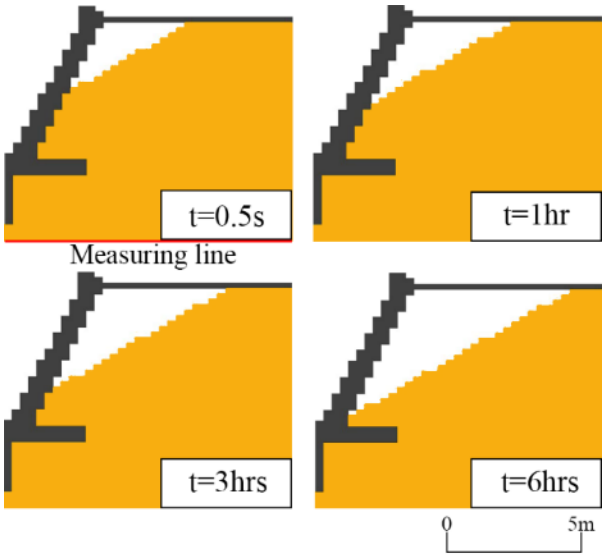

Figure 3.24. Calculated formation of a cave inside the seawall on the Ishikawa–Komatsu Coast.

3.5.4 Khlong Wan Coast

As mentioned in section 2, Khlong Wan Coast was damaged by the outflow of backfilling materials. The wave condition and structural information were extracted from the report of Kuisorn et al. [7]. The simulation condition is shown in Table 3.12; the simulation results are shown in Figures 3.25 and 3.26.

The calculated result is underestimated because the effect of cracks. Even the incident wave height and the calculated outflow rate are pretty small compared to those of Japanese coasts, but when comparing the size between the cave and the dike, damage induced by outflow is also high. At this stage, since there are no supporting materials for the front slope, the dike is more easily to be destroyed by waves smaller than its designed wave.

Table 3.12. The simulation condition in Khlong Wan Coast.

Significant wave height, $H_{1/3}$ (m)	Significant wave period, $T_{1/3}$ (s)	Front bottom depth, h_t (m)	Tidal level (m)	Median grain size, D_{50} (mm)	Initial backfilling materials volume (m^3/m)	Mesh size in x-direction Δx (m)	Mesh size in z-direction Δz (m)	Measured outflow volume, Q_m (m^3/m)	Calculated outflow volume, Q_c (m^3/m)
3.5	6.2	0.1	1.30	2.0	4.5	0.1	0.1	3.5	2.20

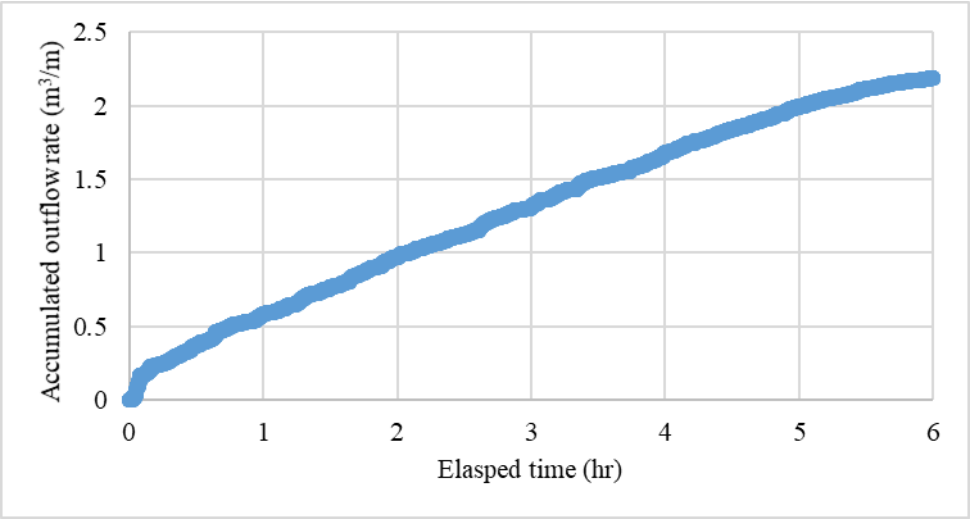

Figure 3.25. The calculated accumulated outflow rates on the Khlong Wan Coast.

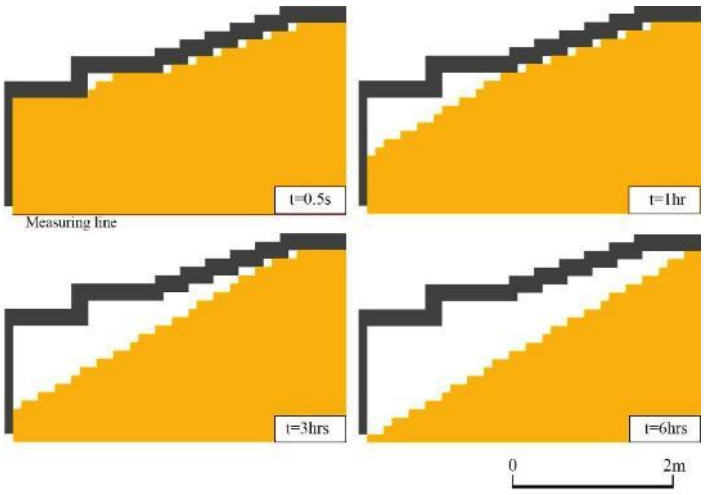

Figure 3.26. Calculated formation of a cave inside the seawall on the Khlong Wan Coast.

3.5.5 South Patong Coast

South Patong Coast is located in Kathu District, Phuket Province, South Part of Thailand (the Andaman sea side). This is one of the most famous attractive beaches for tourists in Thailand; there are many restaurants, hotels, and bars in the area. Since the economic value of this beach is very high, the local government constructed seawalls along the seaside road in order to protect coastal erosion. The study area is the part of the seawalls, which was destroyed by a monsoon in 2011. The external force and structural information are extracted from the report of Kuisorn et al. [7]. The simulation condition is shown in Table 3.13; the simulation results are shown in Figures 3.27 and 3.28.

The simulated results agree with the observed result. From the simulation result, the outflow rate is significantly decreased after the elapsed time of 0.4hr. Since the outflow rate is high and the total volume of backfilling materials is not large, the accumulated outflow rate could reach the middle and the last stages. The model was able to reproduce these stages by using the empirical equations, Equations (3.30)-(3.31); the outflow rate was a constant value until the parameter d/d_{max} became smaller than 0.14, then, the outflow rate become a varying value, which depended on the layer thickness. The calculated results indicate heavy damage to the seawall, in which the supporting materials vanished.

Table 3.13. The simulation condition in South Patong Coast.

Significant wave height, $H_{1/3}$ (m)	Significant wave period, $T_{1/3}$ (s)	Front bottom depth, h_t (m)	Tidal level (m)	Median grain size, D_{50} (mm)	Initial backfilling materials volume (m^3/m)	Mesh size in x-direction Δx (m)	Mesh size in z-direction Δz (m)	Measured outflow volume, Q_m (m^3/m)	Calculated outflow volume, Q_c (m^3/m)
3.5	6.2	0.1	1.30	2.0	4.5	0.1	0.1	3.5	2.20

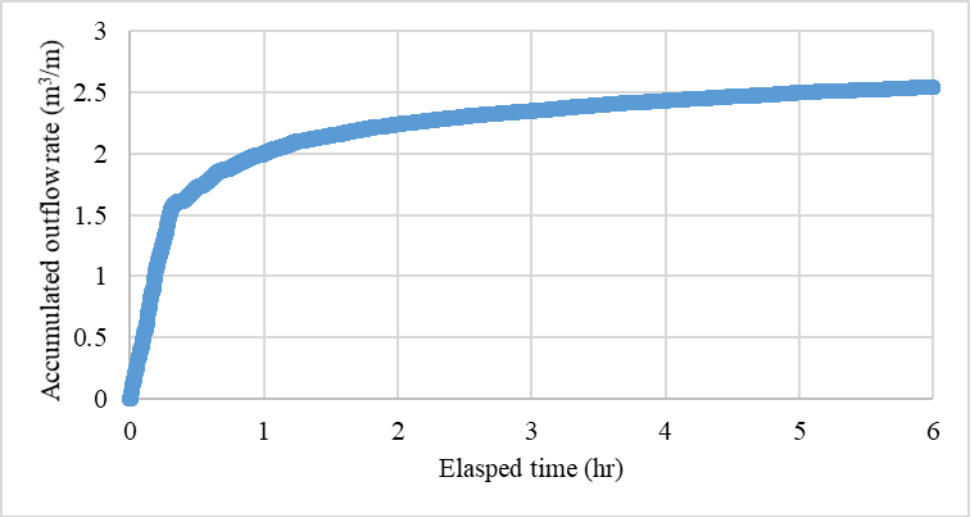

Figure 3.27. The calculated accumulated outflow rates on the South Patong Coast.

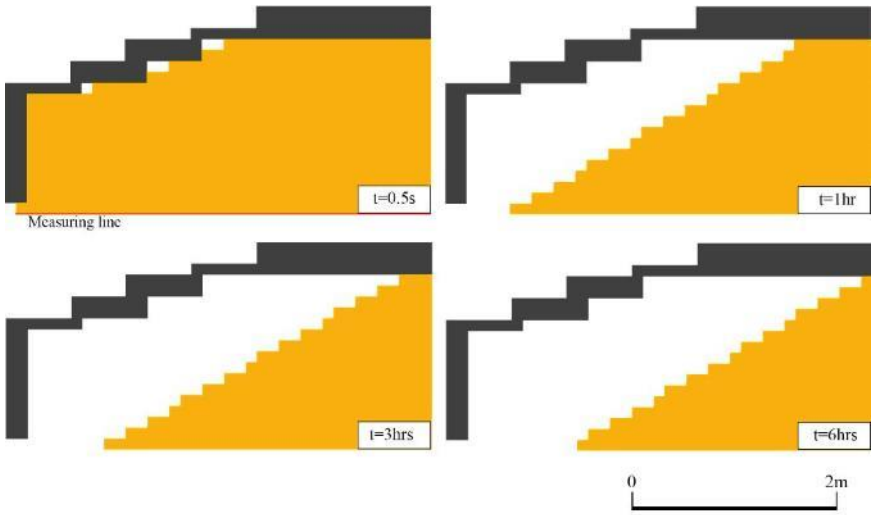

Figure 3.28. Calculated formation of a cave inside the seawall on the South Patong Coast.

3.5.6 Suan Son Coast

The Suan Son Coast is located in Rayong Province, on the eastern portion of the Gulf of Thailand. This coast is a famous beach for tourists and a recreational area for local people due to its wide sandy beach and mild slope. A vertical seawall was constructed by the local government to protect the seaside road and the coastal area of the province. Based on the field surveys of Kuisorn et al. [7], the seawall was damaged by leakage of the backfilling materials induced by wave overtopping and the outflow. The outflow rates were simulated by using the crown height, bottom depth, and wave conditions extracted from their survey report. The simulation condition is shown in Table 3.14; the simulated results are shown in Figures 3.29 and 3.30.

The time series of the accumulated outflow rate shows that there are two stages of the outflow rate, as same as that of the South Patong Coast. According to the same reason of the South Patong Coast: the coefficient C_d in front of the seawall could be changed during the simulation when the parameter d/d_{max} was smaller than 0.14, the outflow rate became a varying value. The simulated results show that a huge amount of the backfilling materials was removed; thus, the possibility that this seawall is destroyed by middle-class waves is high.

Table 3.14. The simulation condition in Suan Son Coast.

Significant wave height, $H_{1/3}$ (m)	Significant wave period, $T_{1/3}$ (s)	Front bottom depth, h_t (m)	Tidal level (m)	Median grain size, D_{50} (mm)	Initial backfilling materials volume (m^3/m)	Mesh size in x-direction Δx (m)	Mesh size in z-direction Δz (m)	Measured outflow volume, Q_m (m^3/m)	Calculated outflow volume, Q_c (m^3/m)
3.0	6.0	–0.3	-	0.2	7.8	0.1	0.1	3.0	3.77

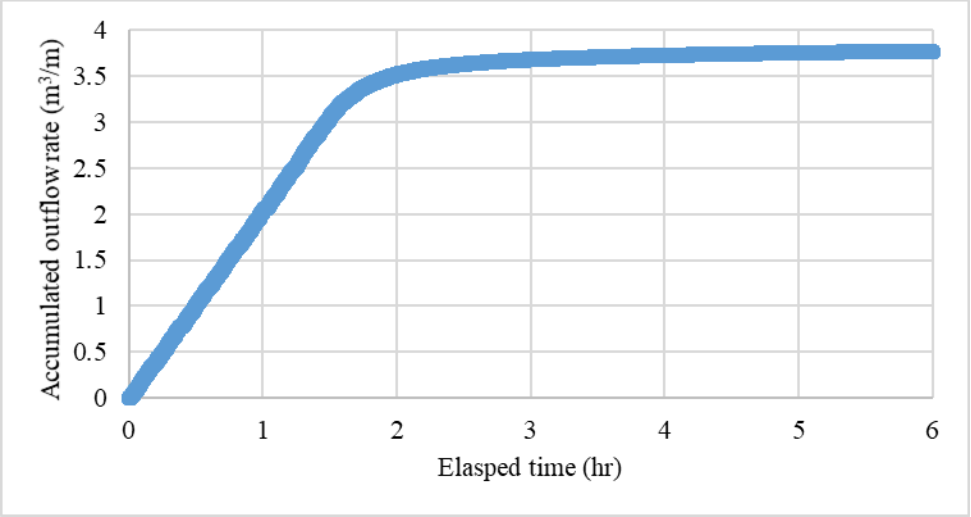

Figure 3.29. The calculated accumulated outflow rates on the Suan Son Coast.

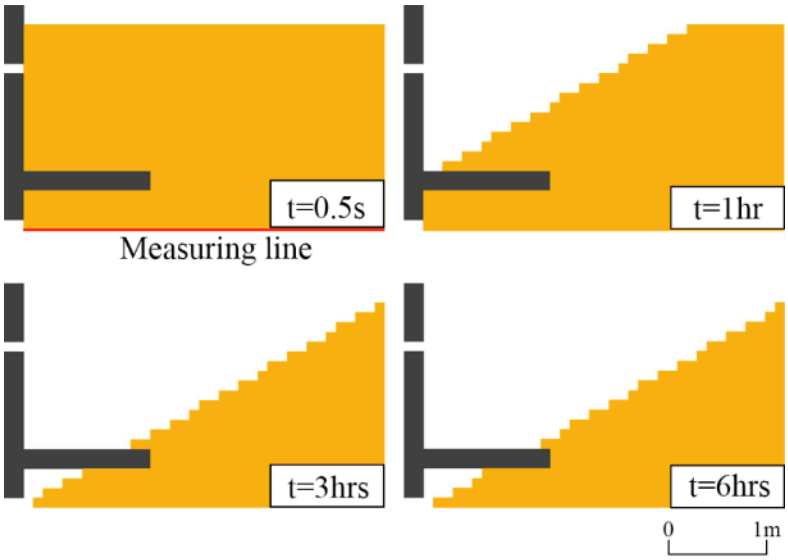

Figure 3.30. Calculated formation of a cave inside the seawall on the Suan Son Coast.

A comparison between the measured accumulated outflow rates and calculated accumulated outflow rates of all cases is shown in Figure 3.31. The accuracy of the calculated results on the Oarai–Isohama Coast is not good. However, the outflow volume of this coast is small when comparing the measured and the initial amount of the backfilling materials. Thus, whether using the calculated results or measured results, the degree of damage is not significantly different. The accuracies on the other coasts seem to be acceptable. Therefore, even though the accuracy is not perfect, since the correlation coefficient is good (R^2 = 0.83), this model can be used to examine the degree of damage induced by the outflow.

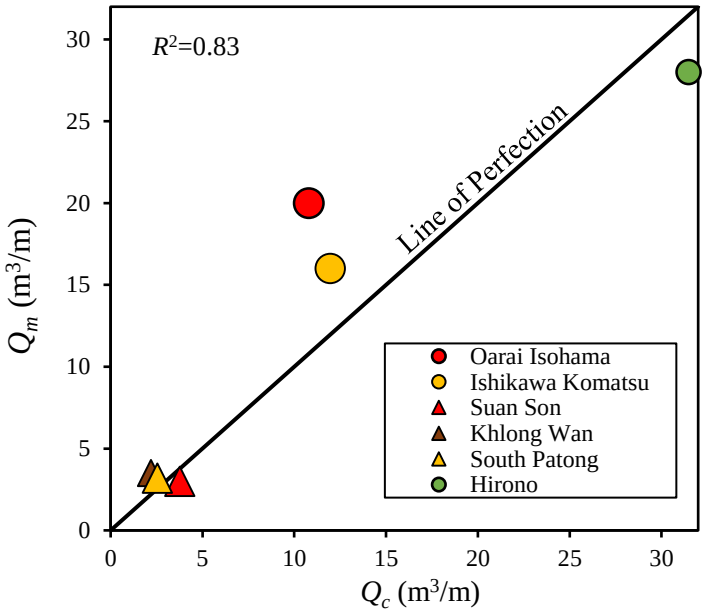

Figure 3.31. The comparison between the measured values and the calculated values.

3.6 Improvement of the design procedure

By combining the outflow rate simulation to the procedure shown in Figure 2.8, the new method was obtained. In this method, the degree of erosion can be determined by analyzing the long-term shoreline changes; the proposed countermeasures can be examined by considering the effects of the wave overtopping, the short-term topographical change, and the outflow. The procedure of the method is as follows:

1) The target area is defined by considering the littoral cell. Then, the target shoreline can be determined.

2) Analyze the shoreline changes in the future by using the one-line simulation model. In this stage, the historical shoreline changes analysis is implemented by using satellite images and aerial photographs. These historical shoreline changes can be used to evaluate the cause(s) of erosion and to calibrate the coefficients of the model. The simulated shoreline changes are used to determined erosion and deposition areas.

3) If there is an erosion area, countermeasures with different scenarios are proposed. These countermeasures must be effective to prevent the wave overtopping (excepted for the zoning). Countermeasures that affect the longshore current must be

evaluated their effects by using the one-line model. The proposed countermeasures are examined their effects to scour induced by big waves by using the topographical change model. Wave condition of typhoon of imposed return period (20-50years is recommended) is used.

4) The outflow on countermeasures filled with granular materials, such as seawalls, dikes, and revetments, is evaluated by the proposed numerical model. If the countermeasures are not able to prevent the outflow, redesigning is needed; in this case, raising the depth of a sheet pile, increasing the size of backfilling materials, and raising the front bottom depth of the countermeasure are recommended.

5) After the evaluations using numerical models, a comprehensive comparison between all countermeasures is implemented. In this comparison, the effects of the countermeasures to the wave overtopping, scour, and environment are compared. Then, the most suitable countermeasure(s) can be proposed.

A flow of the method is shown in Figure 3.32.

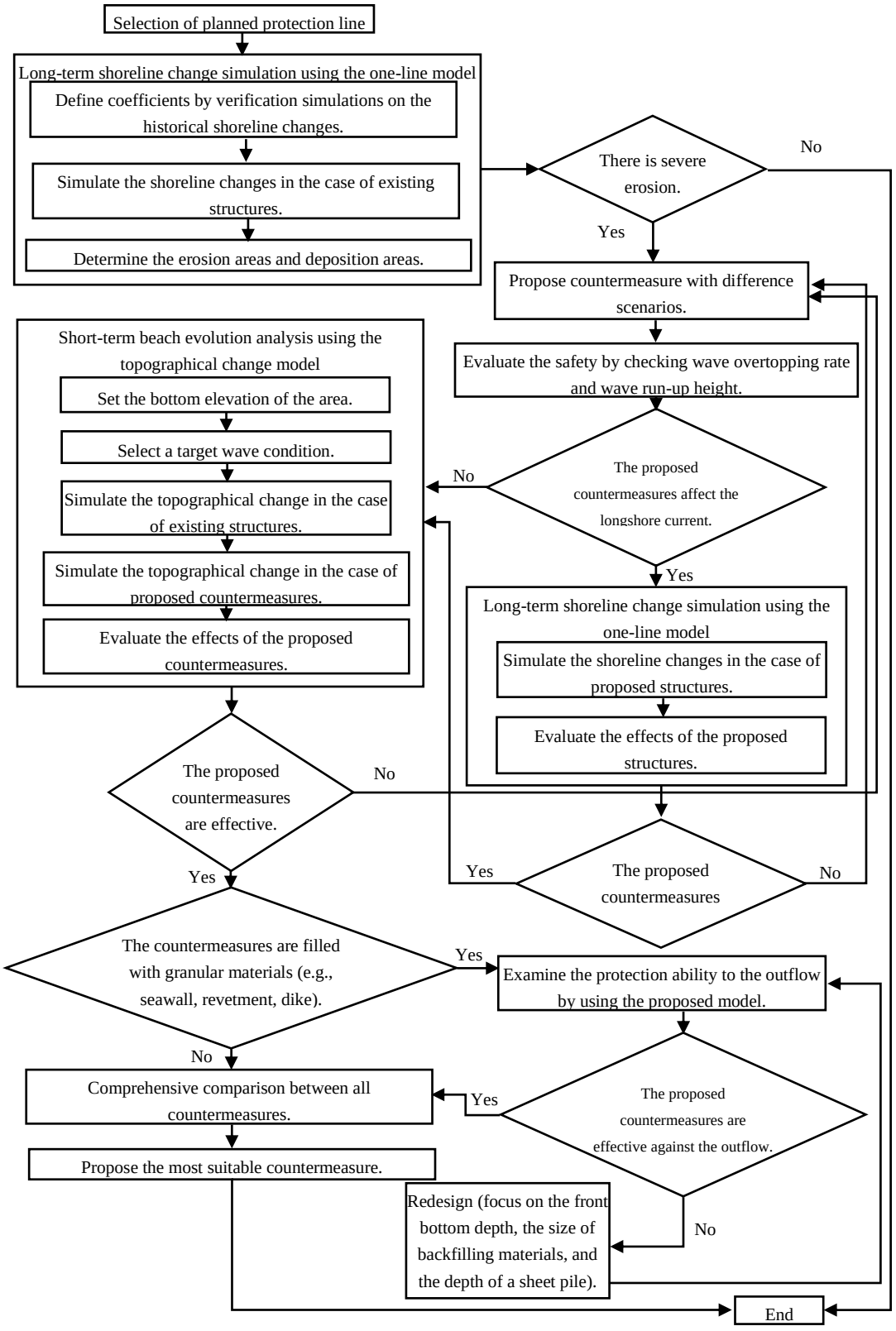

Figure 3.32. The new method for designing a suitable countermeasure using numerical models.

3.7 Conclusions

The outflow of backfilling materials is one of the main causes of the destructions of coastal structures constructed in very shallow areas. The mechanism of outflow was examined by using hydraulic model experiments. Experimental methodologies of Yamamoto and Minami [5] and Ioroi and Yamamoto [6] were applied in this study. The author proposed a numerical consists of CADMAS-SURF [11] and equations—Equations (3.5)–(3.7), (3.11), (3.26)–(3.27), and (3.29)–(3.35), which can be used to simulate the outflow rate changing with elapsed time. The accuracy of the model was confirmed by an experimental result, as shown in Figure 3.12. In addition, the author proposed the effects of water depth and wave periods on the outflow by using hydraulic model experiments. These experiments were performed by varying the water depth in front of the dike and the wave periods, as shown in Table 3.6. The results show that the outflow volume increases when the wave period increases and decreases when the water depth increases. It can be concluded that the outflow must be proportional to the wavelength and inversely proportional to the water depth.

The simulations using the proposed model and the calculations using Ioroi et al.'s formula (with the same conditions as the experiments, as shown in Tables 3.7 and 3.8) were carried out to ensure the reliability of the numerical model and the formula for these effects; the simulated results align well with the experimental results. Even though the accuracies when the total outflow volume is very small were not good, this model can be used to evaluate the relationship between concerned parameters and the outflow. For Ioroi et al.'s formula, the results show the same trend, but the accuracy when the water becomes deeper or when the wave period becomes longer is not good. The reason for this result is that Ioroi et al.'s formula cannot sufficiently account for the effects of these parameters on the pore water pressure and return flow velocity.

The practical applicability of the model is confirmed by comparing these simulated results to the measured values from field cases, that is, the coasts of Hirono, Ishikawa–Komatsu, Oarai–Isohama in Japan, and Khlong Wan, South Patong, Suan Son in Thailand. A correlation graph was created, as shown in Figure 3.31. This graph shows that the model could calculate the outflow rates with acceptable accuracy (R^2 = 0.83). Therefore, this model can be used as a tool for evaluate the safety of coastal structures filled by granular materials.

Finally, the author added the outflow evaluation to the convention procedure, shown in Figure 2.8, and the new designing method is proposed, as shown in Figure 3.32.

References

[1] Silarom, K., Yamamoto, Y., Yoshizawa, S., and Charusrojthanadech, N. (2018). "Development of a numerical simulation model for suction rate using CADMAS-SURF," Proceedings of the 4th International Conference on Engineering, Applied Sciences and Technology, 4-7 July 2018, Phuket, Thailand, 4p. doi: 10.1051/matecconf/201819202063.

[2] Silarom, K., Yamamoto, Y., and Yoshizawa, S. (2019). "Numerical Model for Predicting the Sand Outflow Rate of Backfilling Materials from a Coastal Dike," Journal of Japan Society of Civil Engineers, Vol. 7(1), pp. 63-71. doi:10.2208/journalofjsce.7.1_63.

[3] Silarom, K., and Yamamoto, Y. (2019). "Examinations on Sand Outflow Phenomenon by Using a Numerical Model," Proceedings of the 29th International Ocean and Polar Engineering Conference, 16-21 June 2019, Honolulu, Hawaii, USA, pp. 3783-3790.

[4] Silarom, K., and Yamamoto, Y. (2019). "The Reproduction Ability of a Numerical Model for Simulating the Outflow Rate of Backfilling Materials from a Coastal Structure," Journal of Marine Science and Engineering 2017, 7(12), 447, 17p. doi:10.3390/jmse7120447.

[5] Yamamoto, Y., Minami, N. "Experimental Investigation on Destruction Mechanism of Coastal Dyke due to Big Waves," Journal of Japan Society of Civil Engineers Ser. B2 (Coast. Eng.) (Jpn.) 2009, 65, pp. 901–905, doi:10.2208/kaigan.65.901.

[6] Ioroi, M., Yamamoto, Y. "Formula for Evaluating Suction Rate of Backfilling Materials from a Coastal Dike by Big Waves," Proceedings of the Twenty-Third International Offshore and Polar Engineering Conference, Anchorage, AK, USA, 30 June–5 July 2013; pp. 1210–1216.

[7] Kuisorn, W., Charusrojthanadech, N., and Yamamoto, Y. (2014). "Evaluation Method of Suction Rate of Backfilling Materials from a Coastal Dike or a Seawall," Proceedings of the Twenty-Fourth International Ocean and Polar Engineering Conference, Busan, Korea, 15–20 June 2014; pp. 986–993.

[8] Maeno, S., Kotani, Y., and Hoshiyama, C. (2000). “Outflow Limit of Backfilling Sand of Revetment Under Cyclic Loading of water Pressure,” Annual Journal of Coastal Engineering, JSCE 2000, 47, pp. 926–930. (in Jpn.)

[9] Kotani, Y., Yoshimura, C., Maeno, S., and Nago, H. (2002). “Flow Out of Back-Filling Sand Behind Sea Wall under Cyclic Water Pressure Variation,” Journal of Japan Society of Civil Engineers 2002, pp. 712, 97–106, doi:10.2208/jscej.2002.712_97. (in Jpn.)

[10] Nakamura, T.; Hur, D.S.; Mizutani, N. Suction mechanism of reclaimed sand behind a rubble seawall. J. JSCE Ser. B2 (Coast. Eng.) (Jpn.) 2006, 62, 150–162, doi:10.2208/jscejb.62.150.

[11] Coastal Development Institute of Technology. “CADMAS-SURF,” available online: http://www.cdit.or.jp/program/cadmas-download.html (accessed on 28 June 2019).

[12] Ito, M., and Tsuchiya, Y. (1984). “Scale-Model Relationship of Beach Profile,” Coastal Engineering 1984, pp. 1386–1402, doi:10.1061/9780872624382.096.

[13] Ioroi, M., Yamamoto, Y., and Oshima, Y. (2015). “Improvement of a Suction Rate Formula from the Bottom of the Sheet Pile of a Coastal Dike,” Proceedings of the Twenty-Fifth International Ocean and Polar Engineering Conference, Kona, HI, USA, 21–26 June 2015; pp. 1483–1488.

[14] Yoshizawa, S., Yamamoto, Y., and Kuisorn, W. (2016). “Improvement of Methods for Calculating the Suction Rate from a Coastal Dike or a Seawall,” Journal of Japan Society of Civil Engineers, Vol. 72, No. 2, pp. 1147-1152. (in Jpn).

[15] Yamamoto, Y.; Horikawa, K.; Tanimoto, K. (1996). “Prediction of shoreline change considering cross-shore sediment transport,” Proceedings of the 25th International Conference on Coastal Engineering (ASCE), Orlando, FL, USA, 2–6 September 1996; pp. 3405–3418.

[16] Herbich, J.B., and Ko, S.C. (1968). “Scour of Sand Beaches in Front of Seawalls,”. Coastal Engineering 1968, 1, pp. 622–643, doi:10.9753/icce.v11.40.

[17] Sato, S., Tanaka, N., and Irie, I. (1968). “Study on Scouring at the Foot of Coastal Structures,” Coastal Engineering 1968, 1, pp. 579–598, doi:10.1061/9780872620131.037.

[18] Goda Yoshimi (1985). “Random Seas and Design of Maritime Structures,” 1st ed.; University of Tokyo Press: Tokyo, Japan, 1985; pp. 80–83, ISBN 0-86008-369-1.

[19] Uda, T., Ohishi, M., Itabashi, N., and Arimura, J.I. (1998). “Causes of Damage of Seawall on Hirono Coast in Shizuoka Prefecture,” Proceedings of Civil Engineering in the Ocean, 14, 245–250. doi: 10.2208/prooe.14.245.

IV. Conclusions

From pieces of literature, coastal erosion in Thailand is mainly caused by man-made activities, including mangrove deforestation, inappropriate designs of coastal facilities and land use, etc. Mangroves play an important role to trap sediments and dissipate the incident wave energy. Thus, when mangrove forests are deforested, coastal erosion occurs. Another problem is the inappropriate use of land. Shrimp farms, for example, were the cause of erosion on the Bangkok bay. Farm owners cut mangroves in order to make their farms; then, when there is no natural barrier, it is easy for waves to penetrate the farms and cause erosion. Another cause is the inappropriate design of coastal facilities. Many cases show that countermeasures their self was the cause of erosion.

Since almost all of the coastal erosion countermeasures in Thailand are revetments and seawalls, ground scour in front of the structures and outflow of backfilling materials from their bodies must be a crucial issue that needs to be considered. The causes of coastal erosion on each coast can be evaluated by field surveys, analysis of historical shorelines, and examinations by hydraulic experiments or numerical simulations. For example, the cause of coastal erosion in case studies—Khlong Wan Coast and Chumphon Coast— was analyzed by using historical shorelines analysis and the one-line model. The results conclude that the main cause of coastal erosion is the blockage of soil supply by coastal facilities.

The author introduces a designing method for a suitable countermeasure using numerical models (consisted of the one-line model, the topographical change model of 2D horizontally) and wave overtopping analysis, as shown in Figure 2.8. In this procedure, the long-term shoreline changes, wave overtopping analysis, and the short-term beach evolution are examined. This method was applied to the field cases, Khlong Wan Coast, and Chumphon Beach. The results show that this method can be used to determine the most appropriate countermeasure in the target areas. In addition, since there is no numerical model that can simulate the outflow rates of backfilling materials, which is one of the main causes of the destruction of coastal structures constructed in very shallow areas, the author proposed a numerical model consists of CADMAS-SURF and empirical equation, that can be used to simulate the outflow rate. The applicability of the proposed model was examined by comparing the calculated results to the measured results in field cases in Thailand and Japan.

The author added the outflow evaluation into the method shown in Figure 2.8 and proposed the new designing method shown in Figure 3.32. By using the new method, the physical mechanisms of proposed countermeasures can be examined, and the visual results can be obtained. Thus, this method is a useful tool for designing countermeasures to prevent coastal erosion and damage due to it.

In the future, more experiments using other parameters and conditions such as the uniformity coefficient, dry density, and cracked concrete (or a structure that has voids) should be performed to improve the consideration ability of the model. Additionally, more simulations in field cases with variable conditions (e.g., wave conditions and different shapes of the structures) need to be done to statistically improve the accuracy of the correlation coefficient of the model.

V. Acknowledgements

This study is funded by the Japan International Corporation Agency (JICA) via the AUN/SEED-Net 2017 program and the support of Grants-in-Aid for Scientific Research (c; 18k04667) of the Japan Society for the Promotion of Science (JSPS).

I would like to express my sincere gratitude to Prof. Dr. Yoshimichi Yamamoto, my supervisor, for his guidance through each stage of the process and his benevolence. Thanks also my former advisor when I was a master student, Assoc. Prof. Dr. Nunthawath Charusrojthanadech, King Mongkut's Institute of Technology Ladkrabang, for his always support.

I would like to express my gratitude for Mr. Saburo Matsushima, a senior system analysis, who help me develop the source codes of the model.

I am indebted to Ms. Uba Sirikaew, Assoc. Prof. Wirayut Kuisorn and Ms. Puangpet Rattanarama, King Mongkut's Institute of Technology Ladkrabang, who always support me when I conducted field surveys in Thailand.

I wish to show my gratitude to Mr. Syota Yoshizawa, Mr. Satawat Douangpan, Mr. Ahmadi Sayed Masih, and undergraduate students of Tokai University for helping me conducted experiments and simulations.

And finally, last but not least, I am grateful to my family, my wife, and my friends for their encouragement, moral and emotional support.